Transesterification of Poly(Ethylene Terephthalate) and Bisphenol-A-Polycarbonate

Cannon, Michael J.

Transesterification of Poly(Ethylene Terephthalate) and Bisphenol-A-Polycarbonate

Michael J. Cannon

IRC in Polymer Science and Technology

University of Durham

Durham

DH1 3LE

Acknowledgements

From Invista I should like to express my thanks to Derek Winter for his ongoing support in this project and Mike Gardner and Pete Coleman for their hands on help running extrusion work.

From Sheffield Hallam I must thank Chris Sammon and Deeba Zahoor, Chris for suggesting using Raman in the first place and Deeba for her help acquiring and processing the data.

From Leeds I must thank Peter Hine for what was the most productive day of my three years, put simply there would be no Chapter 4 without him.

From Durham I should like to thank Doug Carswell for his help with the TGA/DSC, Lian Hutchings and Nigel Clarke for their help making dPET and analyzing it by SANS and Stephen Collins and Richard Thompson for their help with the Ion Beam. I am also indebted to Alan Kenright for his help characterizing NMR and Catherine Heffernan for running what must have been hundreds of samples. I should also like to thank all those who have passed through the office during my three years, particularly Randal for starting me on the project, Kim for explaining about neutrons and ions and Matt for our whiteboard moments.

Lastly, I should like to thank Neil for taking on my project midway through and for all his help and advice.

Neil and I are grateful to EPSRC and Invista Process Technologies for their financial support.

Executive Summary

Blends of Poly(ethylene terephthalate) (PET) and bisphenol-A-polycarbonate (PC) have been made by solution and melt blending and these blends were subject to isothermal heating to induce a transesterification reaction. The raw materials and products of this reaction have been studied by a variety of different methods to ascertain the chemical, physical and mechanical properties they possess. The conclusions drawn are listed below.

- PET and PC are immiscible but are compatibilised by transesterification
- Transesterification is a second order reversible process and is fast only when water is present, when absent the rate of transesterification is so slow that little or no reaction is observed in after 60 minutes at 300°C
- When water is present in the blend significant chain scission and degradation takes place, this is not observed in the absence of water
- The material obtained from melt blending has a molecular weight higher than that of commercial PET and it is possible to increase it further by standard solid state polymerization techniques
- The PC concentration in PET is critical to the existence and extent of crystallisation
- PET blends containing 10% PC are not significantly stronger or weaker than commercial PET and perform very similarly to the yield point
- PET blends containing 10% PC are less ductile than commercial PET and will therefore fail sooner when they have yielded under tension
- PET blends containing 10% PC do not injection mould as well as commercial PET under conventional procedures for PET, surface crazing and voiding is observed

Table of Contents

Chapter 1

Background

1.1 Introduction

It is common for polymer chemists to attempt to use blends of known polymers as new materials, rather than design and synthesise a totally novel polymer.[1] This has the advantage of being much cheaper, quicker and the physical properties of a blend of known polymers can be easier to predict than the properties of a completely new polymer.

In the 1970's and 1980's a series of papers were produced documenting the results of miscibility tests carried out on various pairs of polymers.[2-8] Some of the common polymer blends were polyesters (poly(ethylene terephthalate) (PET), Poly(butylene terephthalate) (PBT)) with other polyesters and polyesters with polycarbonates (Polyethylene napthalene-2,6-dicarboxylate (PEN) and bisphenol-A-polycarbonate (PC)). There were initial differences in opinion as to whether these blends were compatible. Cruz and co-workers reported that poly(1,4-cyclohexylenedimethylene succinate) and PC were completely miscible in the amorphous phase[3] and later also that PET and PC were also fully miscible when the blend was more than 70% PC,[4,5] a conclusion supported by Linder and coworkers.[6] Chen and co-workers concluded that the PET/PC system was immiscible over the entire composition range[7] and this was then backed up by Hanrahan et al.[8] These discrepancies were explained by the realisation that the longer one mixed the two in the molten state, the more compatible they became, indicating that there was a reaction going on between the two polymers. Glass transition temperatures (T_g) would merge together and melting points (T_m) would shift and/or disappear altogether.[9] This was shown to be a result of a copolymerization reaction taking place between the

polyester and polyester/polycarbonate, a reaction known as transesterification. Since this discovery many papers and patents have been produced on the subject, explaining the mechanism and kinetics of several blends[10-13] and outlining their uses.[14-17] This indicates the high levels of industrial and academic interest in transesterification. This interest stems from the fact that transesterification can provide novel materials with varying degrees of randomness, composition and physical properties from well known and well documented materials. The product obtained will be a copolymer of the two monomers present, and the properties of this product will be a mixture of the properties of the two initial homopolymers. For example: PC has high impact strength but is soluble in common solvents such as chloroform.[10] PET is less tough but it is only soluble in more aggressive solvents such as trifluoroacetic acid (TFA) and *o*-chlorophenol (OCP). A copolymer made from the two could potentially give a hardwearing polymer, which is resistant to chemical attack. The practical results of this activity have led to many copolymers, produced by transesterification, being used industrially e.g. PET is used in conjunction with various polycarbonates and carbon fillers to form conductive blends so that articles may be electrostatically painted without the application of conductive primers.[18,19]

Transesterification is also a good way to compatibilize two immiscible polymers. In the case of PET and PEN, PET is widely used as a substrate in magnetic tape applications but can be blended with PEN which has superior mechanical properties but is more expensive.[20] In this way the transesterification process keeps down production costs whilst improving the overall product performance. In order to use PET and PC in such a blend, an understanding of the reaction that occurs between them must be reached.

Fundamental to this is determining the reaction products, the reaction mechanism and the kinetics of the reaction. These aspects together with an examination of the influence of transesterification on such aspects as crystallisation rate and mechanical properties have been explored and results and conclusions are presented.

1.1.1 PET

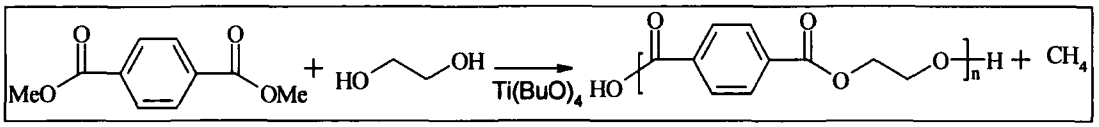

Scheme 1.1 Synthesis of PET

Poly(ethylene terephthalate) (PET) is a thermoplastic, made by melt polymerization, which is heavily used in engineering. It is extensively used in injection moulded and blow moulded bottles, films and extrusions.[21-23] PET is soluble in few solvents, the most effective solvents being TFA and OCP.

PET has a T_g of 67°C when amorphous,[24,25] 81°C when crystalline[25] and 125°C when crystalline and oriented.[26] The equilibrium T_m of PET is 280°C[27] but T_m for commercial PET is between 250°C and 265°C.[28]

1.1.2 PC

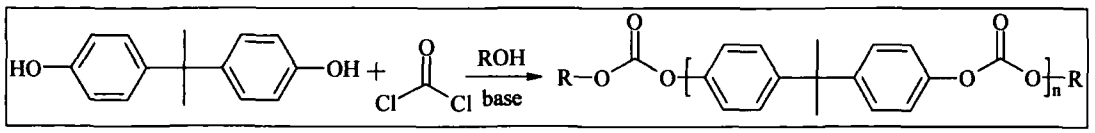

Scheme 1.2 Synthesis of PC

Bisphenol-A-Polycarbonate (PC) is usually made by interfacial polymerization and is used in a variety of forms. Sheets are used in signs, cases and glazing; particularly bullet

proof glass due to its high impact strength.[10] PC is used in films for silk-screen printing, for use in soft-touch controls and resins and injection mouldings are also used extensively. PC is soluble in a large number of solvents, including dichloromethane (DCM), OCP, TFA and chloroform. PC has a T_g of around 145°C and under usual conditions it is amorphous so displays no T_m.

1.1.3 Mechanism of Transesterification

Much work has been carried out on the transesterification of PET and polyethylene naphthalene-2,6-dicarboxylate (PEN) and of polybutylene terephthalate (PBT) and PC. Three distinct mechanisms have been deduced and they are shown below.[29]

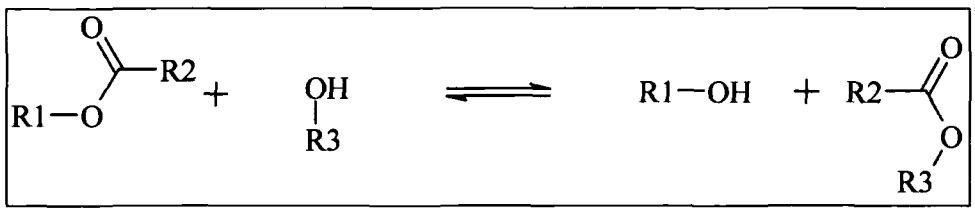

Scheme 1.3 Intermolecular Alcoholysis

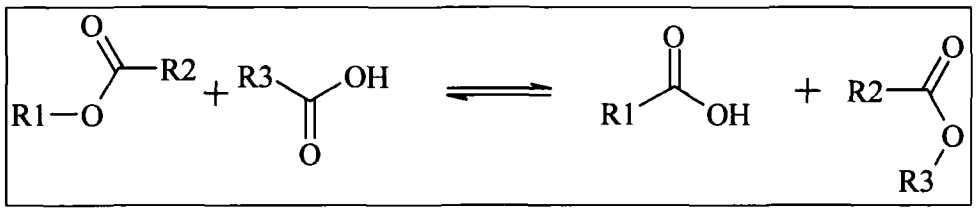

Scheme 1.4 Intermolecular Acidolysis

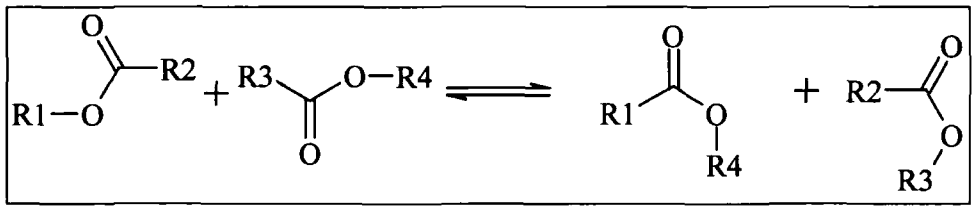

Scheme 1.5 Direct Ester Exchange

It has been shown that in the presence of hydroxyl end groups, intermolecular alcoholysis is the dominant reaction pathway.[30] If the homopolymers do not possess hydroxyl end groups but do possess acid end groups, intermolecular acidolysis is dominant.[31] Direct ester exchange is slow in both cases.[30]

Polymer blends undergoing transesterification initially form block copolymers and then random copolymers. It is this mixing of groups which is responsible for the increased compatibility between the two chains and it is suggested this may in turn lead to increased reaction rates of hitherto unreacted chains.[18]

1.1.4 Side Reactions

Initial work on the transesterification of PET and PC indicates that there may be other reactions at work.[32] Gas is sometimes evolved and yellowing occurs which is not the case in the two more heavily documented reactions, PBT/PC and PET/PEN.[33,34] This can be rationalised by the different linkages present in a polyester and a polycarbonate. Since both the units in a purely polyester transesterification are joined by the same ester links, an exchange of monomers could be expected to have limited effect on the stability of the product formed. In the case of a polyester and polycarbonate such as PET/PC, the product will possess a mixture of carbonate and ester linkages which may be less stable than the starting materials. It is also likely that the ethylene glycol units will become separated from the terephthalate units and lead to a system with three species of monomers and two different ways of linking them together. There is some evidence to suggest that carbonates adjacent to ethylene glycols are not stable and may lead to the evolution of CO_2.[35] This and other proposed side reactions that are believed to occur in transesterification up to 270°C are shown below.[29]

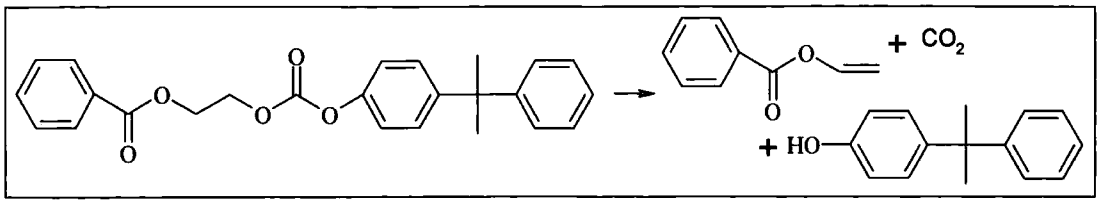

Scheme 1.6 Pyrolysis giving vinyl end groups.

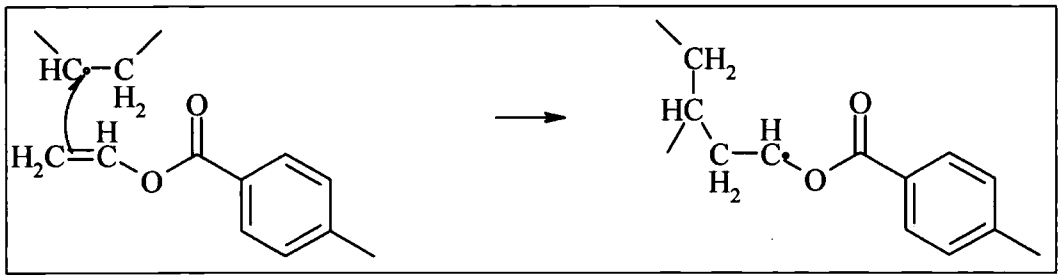

Scheme 1.7 Vinyl Polymerization

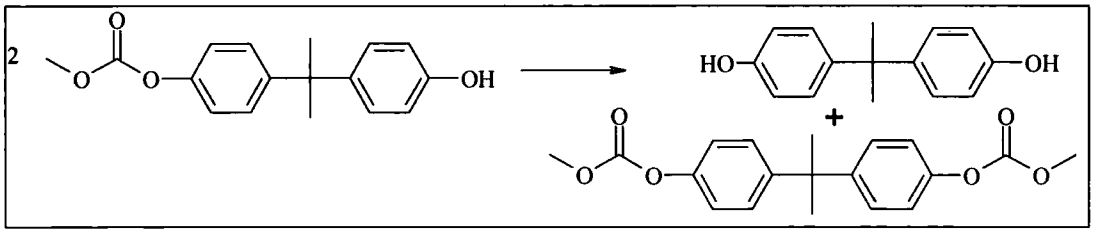

Scheme 1.8 Release of PC units from phenolic end groups

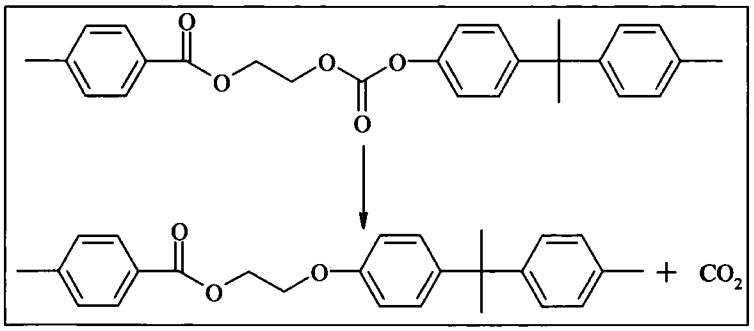

Scheme 1.9 Ethylene carbonate degradation

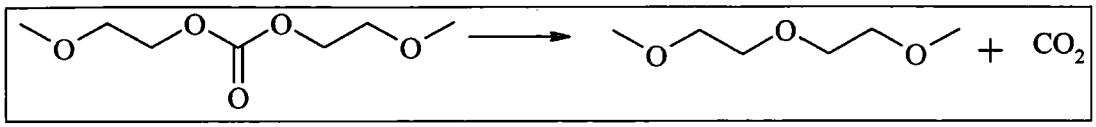

Scheme 1.10 Ethylene carbonate degradation

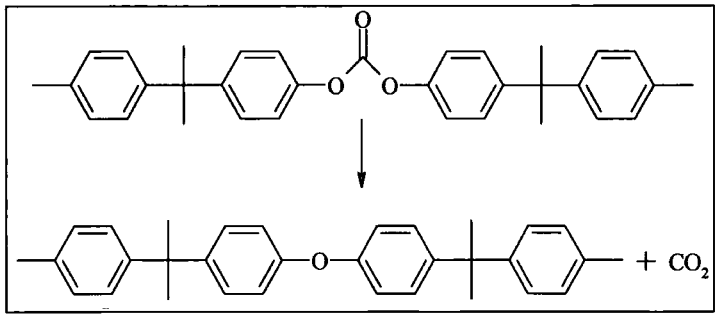

Scheme 1.11 Degradation of PC

There is some evidence to suggest that the major degradation products are dimethyl terephthalate, bisphenol-A-bishydroxy(2-hydroxyethyl) ether, bisphenol-A 2-hydroxyethyl ether and bisphenol-A (shown in below A-D respectively).[36]

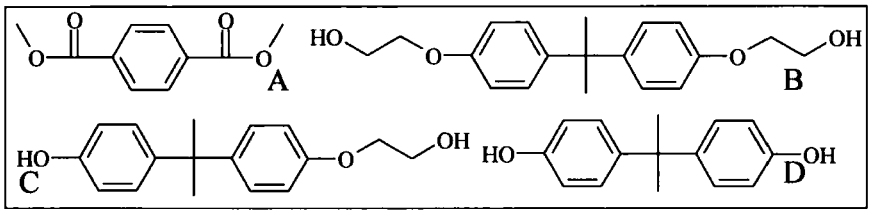

Figure 1.12 Major degradation products of PET/PC transesterification

Another group has reported that bisphenol-A is evolved when PC is heated under reduced pressure to 323°C.[32] It was also noted that random chain scission occurred under the same conditions. Further work by the same group suggests that the carbonate group is the most susceptible part of the polycarbonate chain in the range 300-389°C and that the volatile products included CO_2, CO, CH_4, phenol, diphenyl carbonate and bisphenol-A.[37] A more recent study has used matrix-assisted laser desorption ionization – time of flight

(MALDI-TOF) to study PC which has been degraded at temperatures from 300-450°C.[38] They report that it was possible to obtain surprisingly large amounts of structural information from the data, stating that it was possible to detect degradation including the formation of very low molecular mass oligomers. These were found to include polymer chains containing acetophenone, phenyl-substituted acetone, phenols, benzyl alcohol and biphenyl terminal groups.[39]

PET is known to form carboxyl end groups when molten as part of the following degradation reaction.[40]

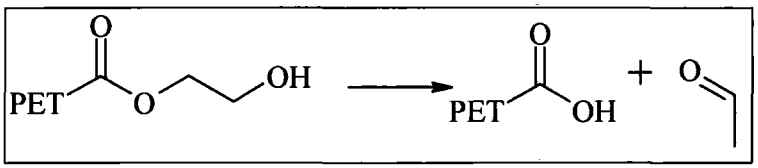

Scheme 1.13 Degradation of molten PET

Evidence of side reactions is discussed in 3.4.6.

1.1.5 Catalysis

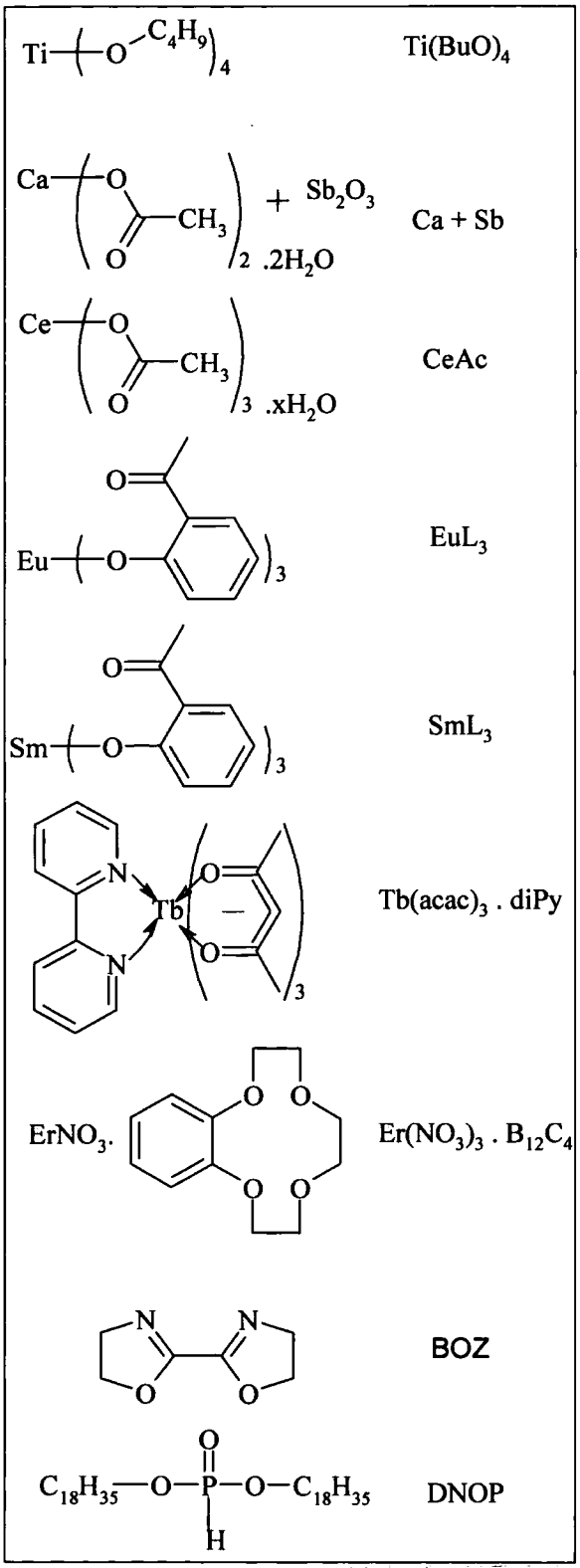

Figure 1.14 Transesterification catalysts and additives

Both transition metals and lanthanides are used to catalyse the copolymerization of ethylene glycol and terephthalic acid and also the polymerisation of bisphenol-A-carbonate. It is well documented that some of the catalysts used in the synthesis of the two homopolymers are also active catalysts for transesterification.[41,42]

A number of catalysts are shown in Figure 1.14. Their order of reactivity has been shown to be:[41] $Ti(BuO)_4$ >> SmL_3 > EuL_3 > Ca + Sb > $CeAc_3$ ≈ $Er(NO_3)_3$. $B_{12}H_4$ > $Tb(Acac)_3$, diPy ≈ 0. Manganese acetate, lead acetate and zinc acetate, $Mn(Ac)_2.4H_2O$, PbAc, $PbAc_2$ and ZnAc, are also known to catalyse transesterification reactions but are easily poisoned by very small amounts of carboxylic end groups.[43] It is also noted that Ca + Sb works in a far more complex way than the other catalysts.[41] 2,2'-bis(1,3-oxazoline) (BOZ) appears to act

to counter the formation of carboxylic end groups by acting as a chain extender between two of them. This increases the molecular weight and also appears to catalyse the transesterification reaction since one group claims the reaction between PET and PEN has an activation energy of 168.9 kJ/mol without BOZ and 94.0 kJ/mol with BOZ.[44]

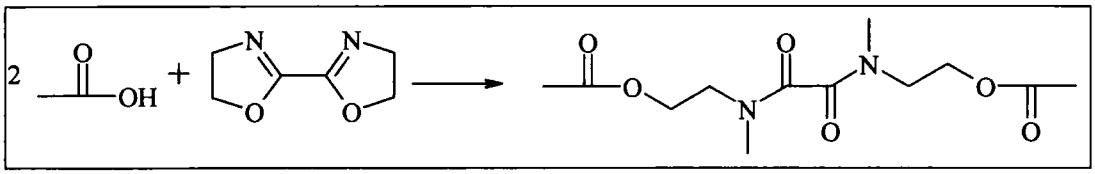

Scheme 1.15 Chain extending activity of BOZ

DNOP appears to act as an inhibitor and it is suggested this activity comes from its ability to co-ordinate to Ti catalyst systems and poisoning them.[29]

Catalysts have not been deliberately used in this work and efforts have been made to remove residual catalyst from both PET and PC during work on the laboratory scale. However in extrusion work this has not been possible and we must assume that catalysts from both the production of PET and PC are present during reactive blending.

1.2 Summary

PET and PC have been examined intermitently for some years as a possible blend but with no consensus as to whether the blend formed is industrially viable. This work aims to understand the PET/PC blend better and establish what chemical, physical and mechanical properties it possess.

1.3 References

(1) Zhang Z.; Xie Y.; Ma D. *J. Polym. Sci: Part A: Polym. Chem.* **2001**, *39*, 232.

(2) Pilati F.; Marianucci E.; Berti C. *J. Appl. Polym. Sci.* **1985**, *30*, 1267.

(3) Cruz C.A.; Barlow J.W.; Paul D.R. *J. Appl. Polym. Sci.* **1980**, *25*, 1549.

(4) Nasser T.R.; Paul D.R.; Barlow J.W. *J. Appl. Polym. Sci.* **1979**, *23*, 85.

(5) Murff S.R.; Barlow J.W.; Paul D.R. *J. Appl. Polym. Sci.* **1984**, *29*, 3288.

(6) Linder H.; Henrichs P.M.; Hewitt J.M.; Massa D.J. *J. Chem. Phys.* **1985**, *82*, 1585.

(7) Chen X.Y.; Birley A.W. *Br. Polym. J.* **1985**, *17*, 347.

(8) Hanrahan B.D.; Angeli S.R.; Runt J. *Polym. Bull.* **1986**, *15*, 455.

(9) Zhang G. Y.; Ma J. W.; Cui B.X.; Luo X. L.; Z., M. D. *Macromol. Chem. Phys.* **2001**, *202*, 604.

(10) Kong Y.; Hay J.N. *Polymer* **2002**, *43*, 1805.

(11) Devaux J.; Godard P.; Mercier J.P. *Polym. Eng. Sci.* **1982**, *22*, 229.

(12) Wilkinson A.N.; Tattum S.B.; Ryan A.J. *Polym. Bull.* **2002**, *48*, 199.

(13) Eguiazabal J.I.; Ucar G.; Cortazar M.; Iruin J.J. *Polymer* **1986**, *27*.

(14) Kruegger P.; Idel K.; Paul F.; Mueller M. *DE Patent 10016190,* **2001**.

(15) Morris J.C.; Bradley J.R.; Scott C.E. *US Patent 6043322,* **2000**.

(16) Onisawa H. *JP Patent 20003128905,* **2003**.

(17) Rauh J.M.; Rauh J.T. *WO Patent 03004561,* **2003**.

(18) Porter R.S.; Wang L.H. *Polymer* **1992**, *33*, 2019.

(19) Cheret E. *WO Patent 0245098* **2002**.

(20) Ihm D.W.; Park S.Y.; Chang C.G.; Kim Y.S. *J. Appl. Polym. Sci: Part A: Phys. Chem.* **1996**, *34*, 2841.

(21) Calvert B.G.; Mulcahy L.T.; Parks J.C. *US Patent 6540862,* **2003**.

(22) Feliks F. *Pl Patent 330773* **2000**.

(23) Gittner F.; Roos U.V. *DE Patent 3908219,* **1990**.

(24) Kolb H J.; Izard E.F. *J. Appl. Phys.* **1949**, *20*, 564.

(25) Edgar O.B.; Hill R. *J. Polym. Sci.* **1952**, *8*, 1.

(26) Woods D.W. *Nature* **1954**, *174*, 753.

(27) Fakirov S.; Fischer E.W.; Schmidt G.H. *Makromol. Chem.* **1975**, *176*, 2459.

(28) Heffelfinger C.J.; Knox K.L. *Sci. Tech. Polym. Films* **1971**, *12*, 587.

(29) Godard P.; Dekoninck J.M.; Devlesaver V.; Devaux J. *J. Polym. Sci.: Part A: Polym. Chem.* **1986**, *24*, 3302.

(30) Collins S.; Peace S.K.; Richards R.W.; MacDonald W.A.; Mills P.; King S.M. *Polymer* **2001**, *42*, 7695.

(31) Kotliar A.M. *J. Polym. Sci. Macro. Rev.* **1981**, *16*, 367.

(32) Davis A.; Golden J.H. *Nature* **1965**, *206*, 397.

(33) Devaux J.; Godard P.; Mercier J.P. *J. Polym. Sci.: Polym. Phys. Ed.* **1982**, *20*, 1901.

(34) Aoki Y.; Li L.; Amari T.; Nishimura K.; Arashiro Y. *Macromolecules* **1999**, *32*, 1923.

(35) Berti C.; Bonora V.; Pilati F. *Makromol. Chem.* **1992**, *193*, 1679.

(36) Berti C.; Bonora V.; F., P. *Makromol. Chem.* **1992**, *193*, 1665.

(37) Davis A.; Golden J.H. *J. Chem. Soc. (B)* **1968**, *1*, 45.

(38) Puglisi C.; Samperi F.; Carroccio S.; Montaudo G. *Macromolecules* **1999**, *32*, 8821.

(39) Carroccio S.; Puglisi C. *Macromolecules* **2002**, *35*, 4297.

(40) Buxbaum L. H. *Angew. Chem.*, **1968**, *80*, 225.

(41) Fiorini M.; Berti C.; Ignatov V.; Toselli M.; Pilati F. *J. Appl. Polym. Sci.* **1995**, *55*, 1157.

(42) Ignatov V.N.; Carraro C.; Tartari V.; Pippa R.; Pilati F.; Berti C.; Toselli M.; Fiorini M. *Polymer* **1996**, *37*, 5883.

(43) Hovenkamp S.G. *J. Polym. Sci.: Part A-1* **1971**, *9*, 3617.

(44) Yang H.; He J.; Liang B. *Journal of Polymer Science: Part B: Polymer Physics* **2001**, *39*, 2607.

Chapter 2

Physical Properties

2.1 Introduction

The physical properties of a polymer dictate its possible uses to a very large extent. The factors affecting the tendency of a polymer to melt, flex, be drawn or resist impact, all have to be taken into account. As mentioned earlier, a large driving force in the PET industry is the wish to improve the O_2 and CO_2 barrier properties of PET by using additives.[1-5] Whilst we do not present data on barrier properties, the work presented in this chapter looks at the physical properties of PET/PC blends and whether they would be practical as PET replacements. If the data from these tests are positive then it is hoped barrier properties testing may be carried out in the future. To that end the desirable properties for a PET/PC blend are:

Controllable Crystallinity

PET is highly crystalline and some crystallinity can improve structural and thermal properties. Too much crystallinity can reduce transparency, something that is undesirable for many brands. It is therefore important that the PET/PC blend be flexible in the amount of crystallinity it exhibits and that this crystallinity is controllable.

Practical Melting Point

For an easy change over to PET/PC the blend must have similar extrusion and injection blow mould behaviour. It would be most convenient if the melting point (T_m) of the blend was around 250°C in order to minimise the work needed to adapt equipment.

High Glass Transition

The glass transition (T_g) is the temperature below which a material acts brittle and above which it behaves like a rubber. Once an item is formed from a polymer, it is desirable that it retain that shape throughout its working life. The higher the T_g of a polymer, the higher the operational temperature to which the item can be exposed without a drop in performance. At the very least, PET/PC ought to have a T_g no lower than that of PET.

Stability

Polymers must be stable in the environment in which they are moulded and in the environment in which they must operate. The majority of polymer applications are under ambient conditions; however thermoplastics are necessarily moulded at high temperatures. If PET/PC blends are to be used they must be able to be blended in the melt and injection moulded without side reactions leading to serious discolouration or formation of undesirable byproducts.

Molecular Weight

Three commonly used measures of molecular weight are $\overline{M}_n$, $\overline{M}_w$ and $\overline{M}_z$. The three are defined in equations 2.1, 2.2 and 2.3.

$$\overline{M}_n = \frac{\sum_i N_i M_i}{\sum_i N_i} \quad \textbf{Equation 2.1}$$

$$\overline{M}_w = \frac{\sum_i N_i M_i^2}{\sum_i N_i M_i} \quad \textbf{Equation 2.2}$$

$$\overline{M}_z = \frac{\sum_i N_i M_i^3}{\sum_i N_i M_i^2}$$ **Equation 2.3**

In themselves the $\overline{M}_n$, $\overline{M}_w$ or $\overline{M}_z$ values are not very important but a high molecular weight tends to give better mechanical properties and it will also affect the thermal properties. Any reactive blending of PET and PC could be expected to produce material which has a higher average molar mass than either PET or PC but the properties of the product will depend on how much degradation occurs in the reaction. It is desirable that the molecular weight of the blend can be tailored in order that properties can be optimised.

2.2 Theory

2.2.1 Crystallization

Crystallization can play a large role in determining the macroscopic properties of a material. Crystalline materials may have different thermal, mechanical and chemical properties to their amorphous analogues. In the case of injection moulded PET, high levels of crystallinity can lead to clouding which is undesirable for many commercial applications. Control of crystallinity is very important; to manufacture a product via any automated process requires that every item is identical within certain parameters. Since crystallization is so influential it is necessary that the crystallization process is understood.

PET is semi-crystalline so contains crystalline regions and amorphous regions. When melted at around 250°C all crystallinity is broken and the material becomes molten. If a sample of molten PET is suddenly cooled (in liquid N_2 for example) the amorphous character is frozen in. No crystallization will be possible as long as the PET is held below its T_g. Above this point, some molecular movement is possible and the polymer chains will fold back on themselves to maximise the favourable inter-repeat unit forces. In the case of PET it is known that this crystallization process is largely controlled by molecular orientation.[6] A high degree of orientation allows favourable interactions to be maximised with long straight parallel sections which, as they grow, form crystals. A perfectly ordered crystal would take in all of one or more polymer chains, however, entropy and branching points in the chains mean that some chains may bridge more than one domain and that chains may leave one crystal and re-enter at a later point. The

idealised model is referred to as the regular folding array; the less ordered state is known as the switchboard model. Both are shown below.

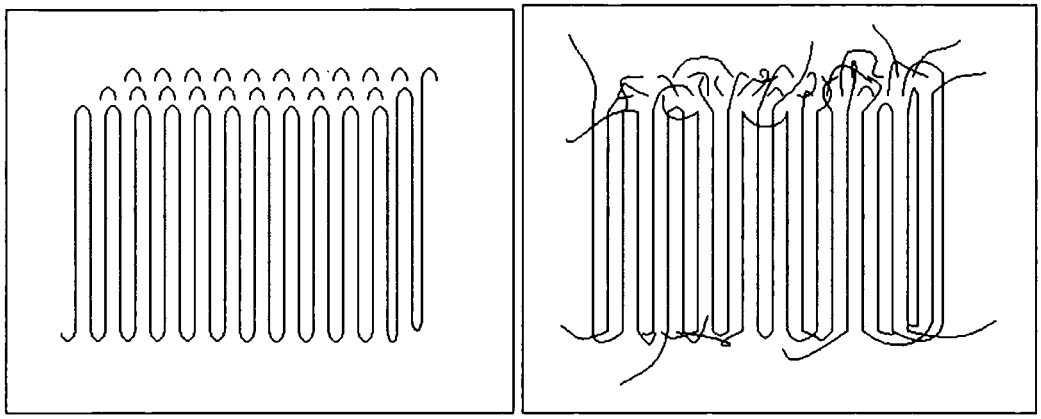

Figure 2.4 Illustrations of the regular folding array and switchboard model

As crystallization continues the disordered sections above and below the crystals give way to ordered regions adjacent to them; that is to say, above and below the original crystal. In this way, three dimensional lamellae form; this is illustrated below.

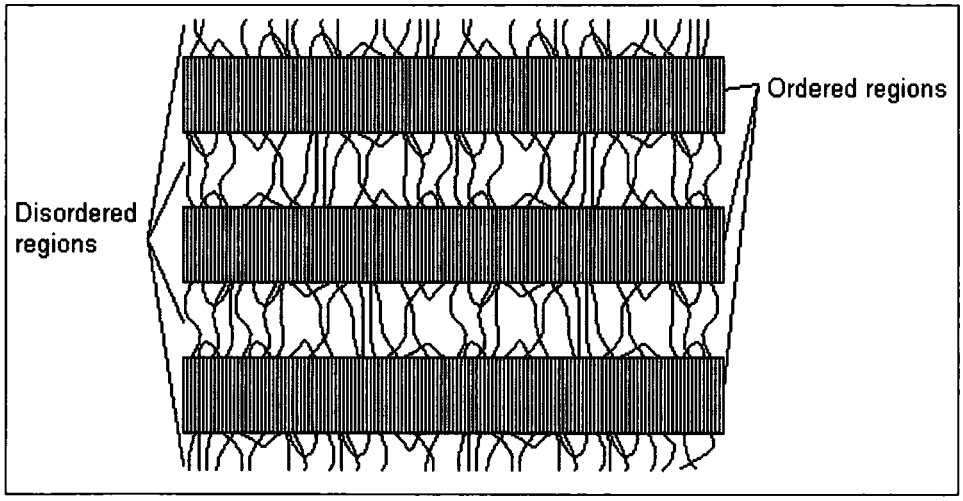

Figure 2.5 Lamellae formation in polymers

As crystallization proceeds the crystallites take on a spherical morphology. The centres of these regions, known as spherulites, are the starting point of the crystallinity, from here fibrous lamellae form in a radial orientation to fill all the space contained within the

growing spherulites. These spherulites start through either random fluctuations in the structure of the polymer or impurities which nucleate growth. These spherulites will expand and impinge on one another until they are no longer distinct in their own right. In Figure 2.6 below the spherulites marked "A" are distinct and can thus be measured.

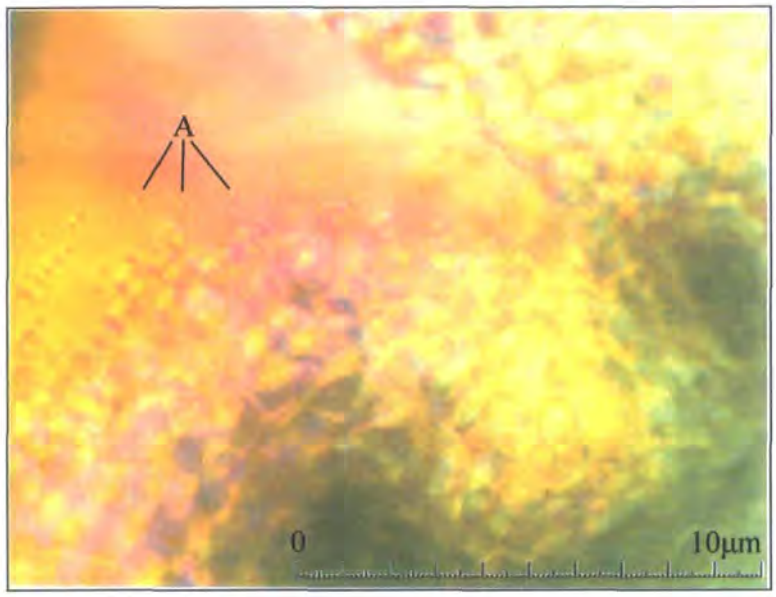

Figure 2.6 Spherulitic crystallization in a 50/50 PET/PC sample transesterified at 290°C for 15 minutes

The rate of spherulitic growth is described by the Avrami equation[7,8]:

$$\frac{w_L}{w_0} = \exp(-kt^n) \quad \textbf{Equation 2.7}$$

Where k is the rate constant, w_L and w_0 are the masses of the melt or amorphous polymer after time t and at time zero. The exponent n is the Avrami exponent and is an integer which varies according to the type of crystallization. In the case of spherulites forming from sporadically occurring nucleation sites the exponent takes the value 4, in the case of simultaneous nucleation the value is 3. Experimentally, radial growth rates have been observed to be linear with respect to time.[9]

In high temperature crystallizations, the rapid tumbling of the polymer chains means fewer nucleation points form giving large spherulites. In low temperature crystallizations, many more nucleation points develop and the morphology is very different with far more, smaller domains making up the crystalline regions.

The higher the temperature, the more mobile are the chains and the faster is the crystallization process. There will be a limiting temperature where the amount of thermal motion starts to disrupt the ordering, above this is the melting point which removes all ordering altogether. The properties of a polymer depend on the thermal history, for example the extent of crystallinity will depend on the amount of time that the sample has spent between 80°C and 250°C since it was last molten.

Optical clarity is very important in the PET bottle sector in particular. It is desirable to produce PET bottles which are transparent and this is achieved by annealing the finished item for sufficient time to initiate crystallization but not so long that crystallites are visible. When this happens, the bottle becomes cloudy and is therefore less desirable from a marketing point of view. To this end, additives are used to break up crystallinity and reduce the rate of crystallization to a level which can be controlled. Di-ethylene glycol sequences are used, as are some *meta* substituted phthalate units, known as isophthalates, shown in Scheme 2.8.

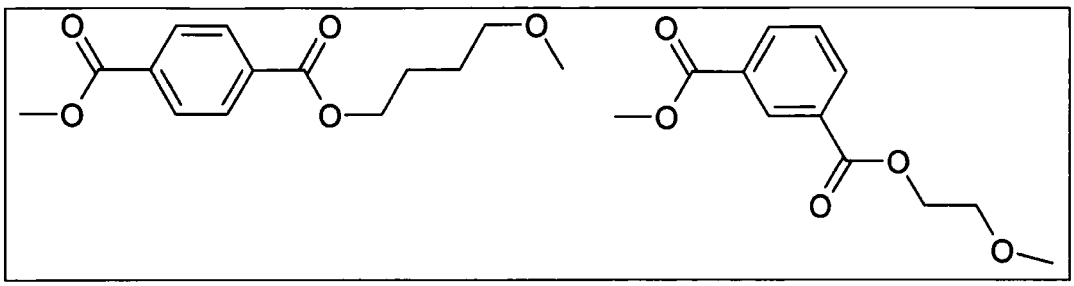

Scheme 2.8 Di-ethylene glycol (left) and *meta* substituted phthalate incorporation (right)

2.2.2 Optical Microscopy

As stated above, PET is semi-crystalline and as such it is possible to follow the rate of crystallization by optical microscopy (OM). Using a hot stage and microscope, it is possible to observe the growth of individual spherulites until they start to impinge on one another. Carrying out this technique on a series of samples that have been transesterified for different lengths of time and at different temperatures can reveal the effect that reaction has on the physical properties of the blend. Whilst this will not explain the crystallization in terms of the Avrami equation it will provide a radial growth rate and some qualitative information as to the crystallization in different blends which have been annealed for different lengths of time and at different temperatures.

2.2.3 Extent of Mixing

Another factor that will affect the crystallinity in an annealed PET/PC sample will be the amount of inter-diffusion which has occurred in the sample during heating. The two polymers are of course immiscible but reaction is known to compatibilise the two.[10] The transesterification reaction will necessarily involve PET moving into the PC regions and

vice versa, however the relationship between reaction and diffusion could take on a number of forms:

1. Diffusion only

The two polymers diffuse into one another, PET diffuses into PC only or PC diffuses into PET only. Here, large degrees of mixing may be observed however there would be no transesterification evident.

2. Diffusion followed by reaction

Diffusion of one or both components occurs faster than reaction. Here, a large amount of exchange may exist without a large extent of transesterification.

3. Reaction limited by rate of diffusion

Reaction may be faster than diffusion in which case any mixing would be a direct indication of transesterification.

Whilst OM will show us qualitatively how quickly crystallinity is suppressed it will not give us information on the rate of diffusion or the composition of the amorphous and crystalline areas. Two tools which are able to help with this are Nuclear Reaction Analysis and Raman Mapping.

2.2.4 Nuclear Reaction Analysis

Nuclear Reaction Analysis (NRA) falls under the heading Ion Beam Analysis, a term for a range of techniques which use a beam of ions to probe materials. NRA effectively gives

a depth profile of any deuterium in the sample, meaning a sample consisting of one deuterated species and one hydrogenous substance can show the dispersion of the one in the other. Given a series of samples over time, NRA can show how one substance diffuses into another.

NRA uses a beam of ^{3}He nuclei to interact with any deuterium present in the sample. This is described in Equation 2.9.

$$ {}^{3}_{2}He + {}^{2}_{1}H \rightarrow {}^{5}_{3}Li \rightarrow {}^{4}_{2}He + {}^{1}_{1}H \quad \textbf{Equation 2.9} $$

The ^{3}He nuclei react with deuterium to form an unstable ^{5}Li ion; this then decays rapidly to form a helium atom and a proton. The energy of the incident beam is normally of the order of 0.7-1.0 MeV but the reaction is so exothermic that both particles produced have much higher energies than this, some 18 MeV in total. Both the proton and ^{4}He produced can be detected and the energy measured but the proton interacts far less with the sample and is therefore used to observe the reaction. The heat produced is enough to damage the sample but since the beam is around 1mm in diameter the same sample can be studied at a number of locations and all the results added together to increase the size of the data set and minimise any statistical abnormalities.

The depth of the deuterium in the sample is calculated by studying the energy of the proton detected and working out how much energy must have been lost due to the beam interacting with the sample on the way in and the proton interacting with the sample on the way out. This is related to the angle of incidence as shown in Figure 2.10.

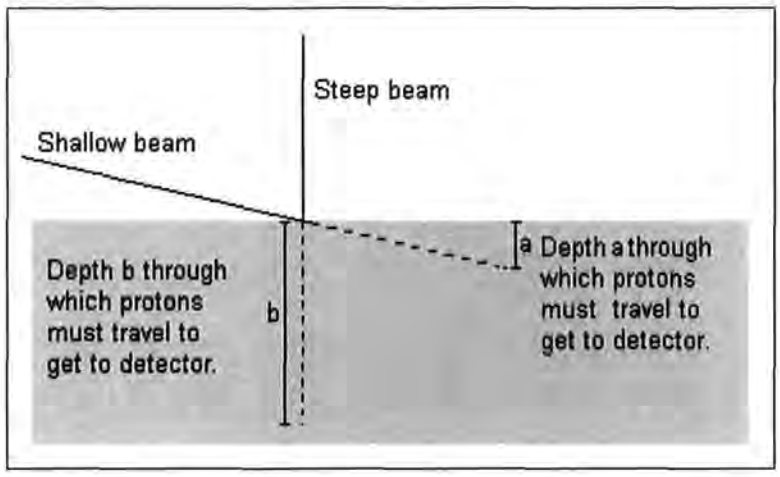

Figure 2.10 Illustration of the effect of changing the angle of incidence in NRA experiments

The angle of incidence also affects the quality of the data to a very large extent. A shallow angle does not probe very deeply whereas a steep angle gives poor resolution as the extra depth attained means the protons on the way out of the sample experience more inelastic collisions with the sample introducing greater statistical error and smearing of data. Very shallow incident beams accentuate surface imperfections in the sample so are potentially a source of statistical error in an uneven sample.

The energies of the protons detected can then be converted into depth if the stopping power of a sample is known. This can be determined theoretically based on the density and chemical composition of the sample or found experimentally by analyzing a very thick sample of the deuterated material in the ion beam.

2.2.5 Raman Mapping

Raman mapping allows us to target specific areas of a sample and obtain information on the Raman allowed stretches, vibrations and bends present. The sample must be translucent in order to resolve it under a microscope, a laser is then focused on the sample

and the Raman spectrum of that area obtained. With a two component system such as ours it should be possible to identify peaks in the spectra produced by pure PET and pure PC and in each location establish the concentration of each component. It ought to be possible to find out the critical level of PC required to prevent crystallization and get a qualitative idea for the speed of diffusion in the sample.

The sample can either be mapped automatically using a motorised sample stage or manually looking at areas of interest. The former has the potential to provide a lot more data but it takes longer and could ultimately produce much more data than is necessary.

2.2.6 Melting Point and Glass Transition Temperature

Crucial to the behaviour of a polymer is the temperature at which it melts. Not only does this limit the operational temperature to which it can be exposed but it also dictates how it may be shaped. The T_m can be found using differential scanning calorimetry (DSC - see below for explanation). It is possible to find out the size of the melting endotherm and the temperature at which it starts and finishes. Unlike crystalline solids, which have a very narrow melting point, most polymers are polydisperse and so melting takes place over a broad range of temperatures.

Even highly crystalline polymers have an amorphous component to them. The crystalline regions will keep their structure as they are heated, until the amount of energy gained through heating is enough to break the inter-molecular bonds and the material will melt like any other crystalline solid. In contrast, the molecules in the amorphous region will

move more and more as the temperature increases and so by definition there is no T_m. There is however a physical change associated with these amorphous regions called the glass transition temperature (T_g). This corresponds to the point when all motion is frozen out of the amorphous regions on cooling and instead of acting as a rubber these areas will become rigid and brittle like a glass.

2.2.7 Differential Scanning Calorimetry

A differential scanning calorimeter (DSC) requires two samples; the first is an empty reference sample pan, the other is a sample of the material under investigation contained in an identical pan. The two pans are kept in separate chambers which are initially held at the same temperature, and then the temperature is increased or decreased at a desired rate (measured in ^{o}C/min). The DSC measures the amount of energy required to maintain the two pans at the same temperature. This gives thermal information on the contents of the sample pan only. The trace produced is thus a trace of the heat flow to or from the sample as a function of temperature and can be interpreted as described below.

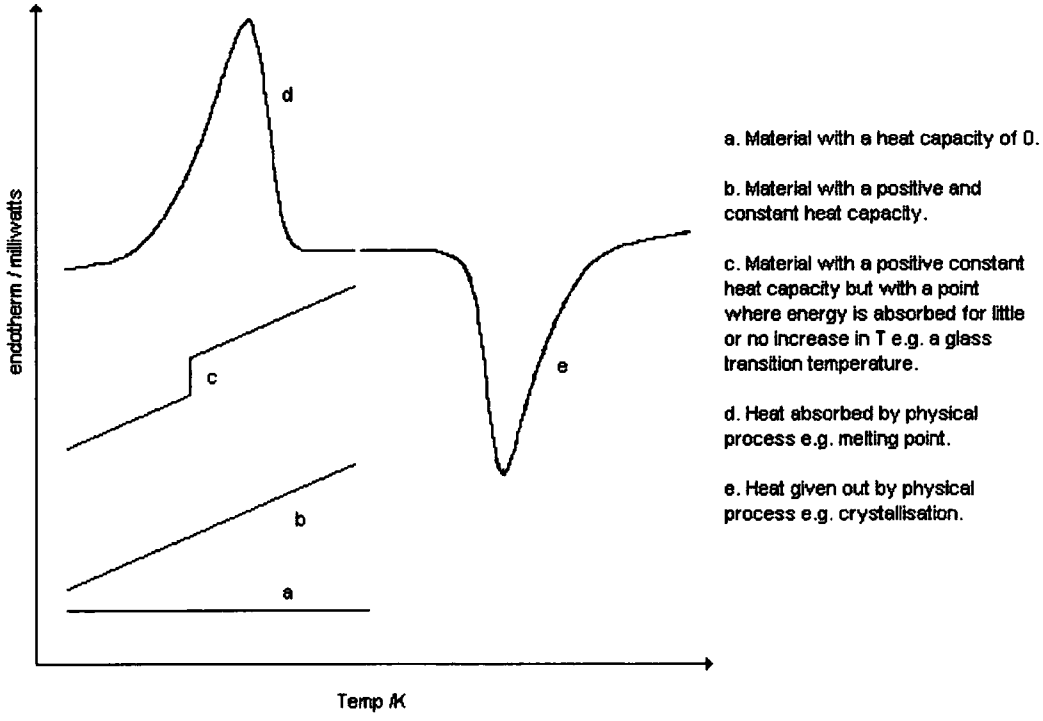

Figure 2.11 Explanation of common phenomena on DSC traces

2.2.8 Glass Transition Temperatures

PET is semi-crystalline and PC amorphous under normal conditions and so both will exhibit a T_g, PET at 80°C, PC at 140°C (data shown in Table 2.12). When the two are mixed physically the T_g values are unchanged and visible in a DSC trace. As reaction proceeds, the two polymers exchange units and as they do so the amount of PET character in the PC chains increases and vice versa.[11] This means the two T_g values start to move towards each other.

Table 2.12 Literature values for the T_g of PET and PC

Polymer	T_g /°C	References
Amorphous PET	67	12,13
Crystalline PET	81	13
Crystalline and Orientated PET	125	14
PC	140	15-17

After a sufficient time the mixture becomes a compositionally homogeneous random copolymer and only one T_g is associated with this new polymer. The Fox equation[18] can be used to predict the T_g of a copolymer where the T_g values of the initial homopolymers and the weight fractions of both are known. In the formula below, w_i is the weight fraction of polymer *i* and T_{gi} is the glass transition temperature of polymer *i*.

$$\frac{1}{T_g} = \frac{w_1}{T_{g1}} + \frac{w_2}{T_{g2}} \quad \textbf{Equation 2.13}$$

Using Equation 2.13 the calculated T_g values predicted are shown in Table 2.14. These values assume the two components have formed a statistical copolymer.

Table 2.14 Calculated T_g values for fully transesterified PET/PC samples of varying compositions

% PET	% PC	T_g /°C
100	0	80
90	10	85
75	25	93
60	40	102
50	50	108
40	60	114
25	75	123
10	90	133
0	100	140

2.2.9 Melting Point

As stated above, the Fox equation predicts that the presence of amorphous material in the PET will affect these regions and make them more similar to PC. The Fox equation looks only at the effect on the T_g but it could be predicted that this reaction would have a similar effect on the melting point. Since these reactions occur in the melt there are no crystalline regions at the time of reaction therefore all areas of the PET will be equally susceptible to reaction. The system also phase separates since the PET and PC are not miscible so inhomogeneity exists in the reaction medium and can therefore be expected in the product. Areas of PET with a high extent of reaction would contain more amorphous character than those with low levels and it is likely that crystallinity will be less prevalent in the transesterified blend than the pure PET. This extent of crystallinity can be probed by DSC, giving not only the start of any melting in the material but also the total amount in the sample and, if the weight of the sample is known, the proportion of crystallization relative to pure PET and that expected from a purely physical blend of PET and PC given their relative amounts.

2.2.10 Molecular Weight

Since transesterification is a co-polymerization reaction which is mainly catalysed by end groups, it could be expected that transesterification between two polymers of molecular weight M_1 and M_2 would yield a product with a molecular weight approaching M_1+M_2. However, both PET and PC can absorb water and PET in particular is vulnerable to hydrolysis. Given that the reaction temperatures are of the order of 250°C or higher, it could be expected that if there is a way for gas to escape from the reaction that any water

would be removed rather quickly. However, even in this short space of time water can do a large amount of damage. If the reaction is carried out in a closed environment such as a screw extruder there is essentially nowhere for the water to go and it is thus trapped at super critical temperatures. Hydrolysis is known to be a rapid reaction at elevated temperatures[19] causing chain scission and therefore a drop in molecular weight. To counter this, both polymers must be rigorously dried before use and stored under an inert atmosphere. Even so, some water can be expected to get into the system or other mechanisms may cause chain scission.

A standard practice in the PET industry is to build the molecular mass of the PET using a process known as solid state polymerization (SSP). SSP, as the name suggests, involves heating PET polymer chips below the T_m, specifically around 170-210°C. This process removes volatiles from the chips and reactive end groups can join up to raise $\overline{M}_n$ and $\overline{M}_w$. Since the process takes place above the T_g of PET, it is necessary to keep the chips moving to prevent them sticking to one another. The whole process is therefore carried out on a fluidised bed of dry nitrogen. As part of this work, SSP will be carried out on one of the blends to see if the process works on the blend and what sort of weights are obtainable. The molecular weight of the PET/PC will be followed using size exclusion chromatography (SEC).

2.2.11 Size Exclusion Chromatography

SEC, like any chromatography technique, separates the different components of a mixture and quantifies each. SEC relies on the principle that molecules cannot pass through channels narrower than their hydrodynamic diameter. SEC uses a column

packed with porous polymer particles, the voids between which create many channels of differing dimensions for the polymer solution to pass through. The material under investigation is dissolved in a good solvent and a sample of the solution is pumped through the column. The largest molecules in the solution will not be able to enter the small channels, many of which are dead ends, and as a result the first material to pass through the column is the highest molecular weight polymer with the lower molecular weight material following it. The speed at which the material passes through the column is determined by the interaction between the solute and the column. This is corrected for by using a standard of known mass, ideally of a similar chemical nature to the material under investigation and the results of the SEC carried out are quoted in reference to the standard. Even if a close chemical match cannot be found for SEC in a case such as SSP, when a series of samples of the same material can be removed at different times, it is possible to say whether the molar mass of the PET/PC is increasing or not even if the absolute values of the molar mass are not known.

2.3 Experimental

2.3.1 Materials

The PET used in this work is manufactured by DuPont and marketed as Melinar®. The two grades used have intrinsic viscosities of 0.5 and 0.8 dL g^{-1} and are referred to as *Base* and *Laser* respectively. Using the intrinsic viscosity[20] and the equation below, the number average molecular mass ($\overline{M}_n$) for *Base* has been calculated as 12,750 g mol^{-1} and 22,600 g mol^{-1} for *Laser*.

$$[\eta] = 2.15\times10^{-4}\times\overline{M}_n^{\,0.82} \quad \textbf{Equation 2.15}^{(21)}$$

Three grades of PC were used in this work; they are all produced by Bayer and marketed as Makrolon® *1239*, *2605* and *2205*. *1239* is the highest viscosity grade and is used for injection blow moulding of water bottles, *2605* and *2205* are the medium and lowest viscosity grades respectively and are both used for injection moulding, as such they include a release agent to help remove moulded articles from the mould. Documentation from Bayer gives the following values for the melt volume flow rate of the Makrolon® used.

Table 2.16 Melt mass-flow rate of PC grades used[22]

Grade	Melt mass-flow rate /g/10min
1239	3
2605	13
2205	38

All three grades were analysed by SEC against polystyrene standards and the masses obtained were as follows.

Table 2.17 Molecular weight data from SEC

Grade	$\overline{M}_n$	$\overline{M}_w$	PDI
1239	11,900	35,400	3.0
2605	10,500	28,300	2.7
2205	8,500	20,800	2.4

Dichloromethane (DCM), *o*-chlorophenol (OCP) and methanol were used in small scale work. The suppliers and purities are summarised in Table 2.18.

Table 2.18 Solvent suppliers and purity for solvents used in blend preparation

Chemical	Supplier	Purity
DCM	Fischer	99.5%
OCP	Aldrich	99%
Methanol	Fischer	99.0%

The cover slips used in OM were supplied by BDH and were 16 μm thick and 16 mm in diameter.

NRA was carried out using d_4-PET of $\overline{M}_v$ 78,800 supplied by Polymer Source Inc; the formula is shown below.

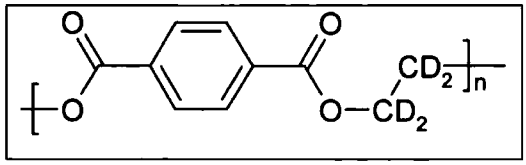

Figure 2.19 Structure of dPET used for NRA

The solvents used in the preparation of NRA samples were 1,1,1,3,3,3-hexafluoro isopropanol (HFIPA) and chloroform. The suppliers and purities are summarised in Table 2.20.

Table 2.20 Solvent suppliers and purity for solvents used in NRA sample preparation

Chemical	Supplier	Purity
HFIPA	Aldrich	99%
Chloroform	Fischer	99.5%

Samples were prepared using 76x52x1 mm glass slides supplied by Fischer and 76mm diameter polished silicon wafers supplied by Compart Technology Ltd.

2.3.2 Large Scale Work

In extrusion/melt work the material was dried overnight at 160°C and stored under N_2 during use. The chips were then weighed out as needed for each blend (shown in Table 2.21) and poured into a hopper which was kept under N_2 also. This fed into a Haake Fisons Rheocord (shown in Figure 2.22) with a general purpose screw. The temperature of the barrel was set to between 280 and 295°C depending on the behaviour of the material being processed and the material was processed at a typical rate of some 150 g min^{-1}. The lace from the die was cooled in a water bath and fed into a chipper.

Table 2.21 Weight composition of blends made, blends in bold used for moulding and physical testing

	% PET		% PC		
Blend	Laser	Base	2605	1239	2205
1		**90**	**10**		
2		75	25		
3		60	40		
4		50	50		
5		10	90		
6		90		10	
7		90			10
8		75			25
9		50			50
10	**90**			**10**	
11	75			25	
12	50			50	
13	90				10
14	90		10		
15	75		25		

Figure 2.22 Haake Rheocord used for melt blending PET and PC on kilo scale

3 kg of *Base* plus 10% *2605* (blend 1) were taken for solid state polymerization (rig shown in Figure 2.23). The material was allowed to crystallize at 160°C in a fluidised air bed (500 L min^{-1}) for ten minutes then dried at 210°C for 30 minutes under fluidised N_2

(150 L min^{-1}). After this, the material was held at 210°C for 10 hours and samples were removed after 0, 1, 2, 3, 4, 5, 6, 7 and 10 hours.

Figure 2.23 SSP rig, material fed in at "A"

DSC analysis was carried out on samples of extruded material as described below in section 2.35.

2.3.3 Small Scale Work

In small scale work, samples of pure PET were obtained by dissolution in OCP (10 g in 150 ml) and precipitated by pouring the PET solution into excess methanol and filtered using a glass sinter. The OCP still in the precipitated polymer was then solvent extracted using 200 ml of methanol per 10 g of dry polymer for at least 24 hours before filtering

and removing the methanol that persisted by drying the polymer *in vacuo* at 60°C for at least 24 hours.

Samples of pure PC were obtained by the same procedure with DCM in the place of OCP, which made the solvent extraction step unnecessary.

All polymer blends were prepared by first weighing the required amounts of the dry polymer and then dissolving the two components in OCP (10 g in 150 ml). The subsequent isolation was identical to the preparation of pure PET, outlined above.

Transesterification of the 50:50 *Base/2605* blend was carried out on a Perkin Elmer Pyris 1 TGA. 5-10 mg samples of the material were sealed in Perkin-Elmer aluminium pans. These pans are supplied with circular aluminium lids and when full were sealed shut using a Perkin Elmer press. Before filling, both the lid and pan to be used were placed on a Perkin-Elmer AD4 Autobalance, and the apparatus was tared. The sealed, full pan was then reweighed and the mass of polymer obtained to the nearest μg. Samples were then placed in the furnace of a Perkin Elmer Pyris 1 TGA for annealing; the furnace was purged with nitrogen at a rate of 20 ml min^{-1} during the procedure. The furnace temperature was then increased to the reaction temperature at 100 °C min^{-1} and held there for the desired time. Timing was started from the moment the temperature reached 10°C below the desired reaction temperature and the furnace opened automatically when the time had elapsed. After this, the samples were rapidly cooled to ambient temperature by removing the sample from the furnace.

2.3.4 TGA

Samples of pure PET or PC and solution blended 50:50 blends of the two were subjected to thermo-gravimetric analysis on the same Perkin Elmer Pyris 1 TGA used to anneal samples but the polymer was not encapsulated in pans in order to facilitate the speedy removal of volatiles. Instead it was placed in an open steel pan which was heated to the desired temperature at 100°C min^{-1} and maintained at that temperature for the desired time. TGA was carried out under nitrogen flowing at 20 ml min^{-1}.

2.3.5 DSC

Transesterified samples were then analysed by differential scanning calorimetry using a Perkin Elmer Pyris 1 DSC. Samples were analysed at a heating rate of 20°C min^{-1} from ambient temperature to 300°C and then cooled at 200°C min^{-1} back to ambient temperature. The sample and reference pans were purged with helium at a rate of 20ml/min. Analysis of the DSC traces was carried out using automatic software to record the onset of any melting endotherms and their magnitudes. The mid-point of any T_g features was also recorded.

2.3.6 Optical Microscopy

A small sample of the 50:50 *Base/2605* blend (around $1mm^3$) was placed between two glass cover slips The sample was annealed in a THM 600 Linkam hot stage (shown in Figure 2.24) for various times at or above 270°C before rapid cooling using a CS196 Linkam cooling system to below 80°C (the T_g of PET). During heating, the sample hot stage was kept under nitrogen. Once the sample had been quenched to below 80°C, the

sample was then rapidly heated up to 150°C where it was re-crystallized. Whilst being held at this temperature, the sample was observed for any signs of spherulite formation using 300 × magnification. When one or more isolated spherulites were found they were photographed periodically using an Olympus BH-2 Microscope with JVC KY-F30E Video Camera and the image printed using a Sony UP-5000P Colour Video Printer. This was continued until all the spherulite(s) shown in the photographs had impinged on neighbouring spherulites.

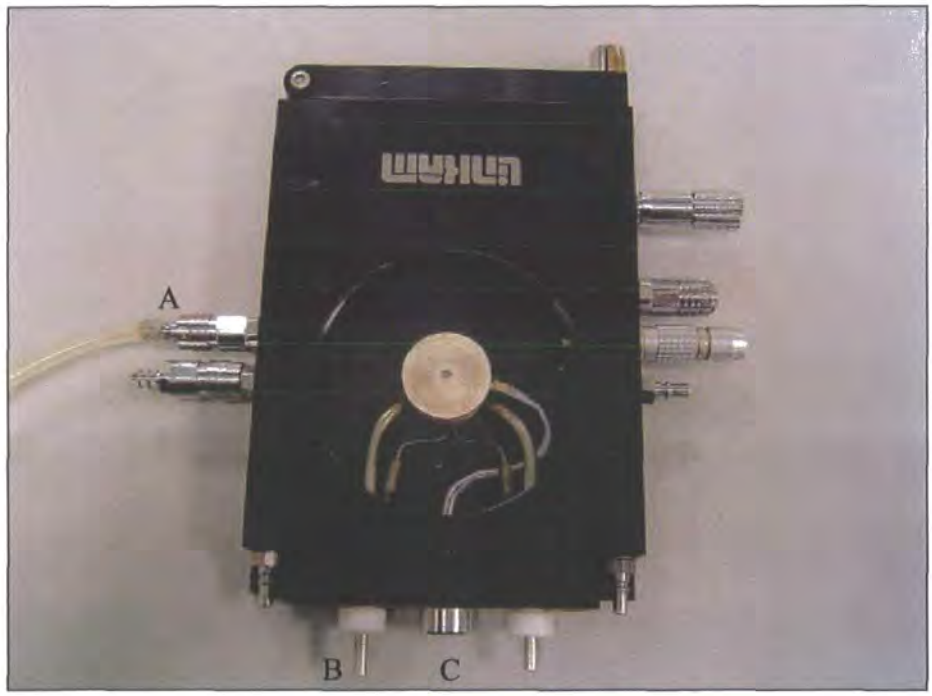

Figure 2.24 Linkam hot stage used for OM, N_2 (g) supplied via "A", cold N_2 (g) supplied via "B", power supplied via "C"

2.3.7 NRA Sample Preparation

0.1g of d_4-PET was dissolved in 10 ml of (HFIPA). An excess of the solution was pipetted onto a 76mm radius polished silicon wafer which was spun in air at 2000 rpm for 30 sec yielding a thin PET film on the surface which was brown in appearance. Two

films were spun and the thickness of the resulting films was confirmed by ellipsometry as 56 ± 1nm using a Sentech SE400 ellipsometer. Once the films had been cast they were on were kept sealed until needed.

0.6g of *2605* was dissolved in 10 ml of chloroform, 0.5 ml of this solution was discarded and the solution made back up to 10 ml with toluene. An excess of this was then pipetted onto the surface of a 76x52 mm glass slide. The slide was then spun at 2000 rpm in air for 30 sec. Once cast, the edges of the glass slide were roughened using the edge of another glass slide. The PC film was then floated off in a bath of high purity water. A silicon wafer was then immersed in the bath and raised up so the PC film was smoothly stretched across the surface of it. This was repeated with the second wafer and both were then placed in an oven at 60°C for three hours at atmospheric pressure to remove any water.

After annealing, the total thickness of the polymer was determined by reflectivity as 658 ± 15nm using an FTP500 optical reflectometer built into the Sentech ellipsometer. Subtracting the thickness of the PET layer, this gave a PC layer of 602 ± 16 nm. The wafers were then scored on the sample surface with a glass cutter and up to fourteen samples were obtained from each disk. Seventeen large pieces were selected and numbered on the reverse from 0-16. Sixteen of the samples were heated in an oven for times between 5 and 60 minutes at temperatures between 270 and 300°C. The sample labeled "0" was left unannealed.

2.3.8 Nuclear Reaction Analysis

NRA was carried out on an NEC 5SDH Pelletron accelerator using a 0.9 MeV ^{3}He beam at an angle of incidence of 45°. Each sample was analysed at several spots, each amounting to 5 μC of beam and the data added together to minimise the effect of beam damage.

2.3.9 Raman Mapping

The same samples used for OM were also used for Raman mapping. The machine was first calibrated using industrial PET and PC samples. The blend samples were studied under a microscope for a PC domain which had a region of crystalline PET nearby. The laser was focused via the microscope so this was focused on spherulites adjacent to a PC domain. The sample was then moved so the beam was over the centre of the PC domain and a sequence of 10 spectra was obtained sampling the Raman features inside the PC domain, in the PET just outside of the PC domain, in the region on the edge of the crystallites and then finally in the crystallites themselves. Each Raman spectrum was obtained between 1100 and 400 cm^{-1}. The acquisition time varied from 10 to 60 sec, typically PC gave a lower return and so allowed for longer exposure, PET tended to saturate the detector within 20 sec. The equipment used is shown below.

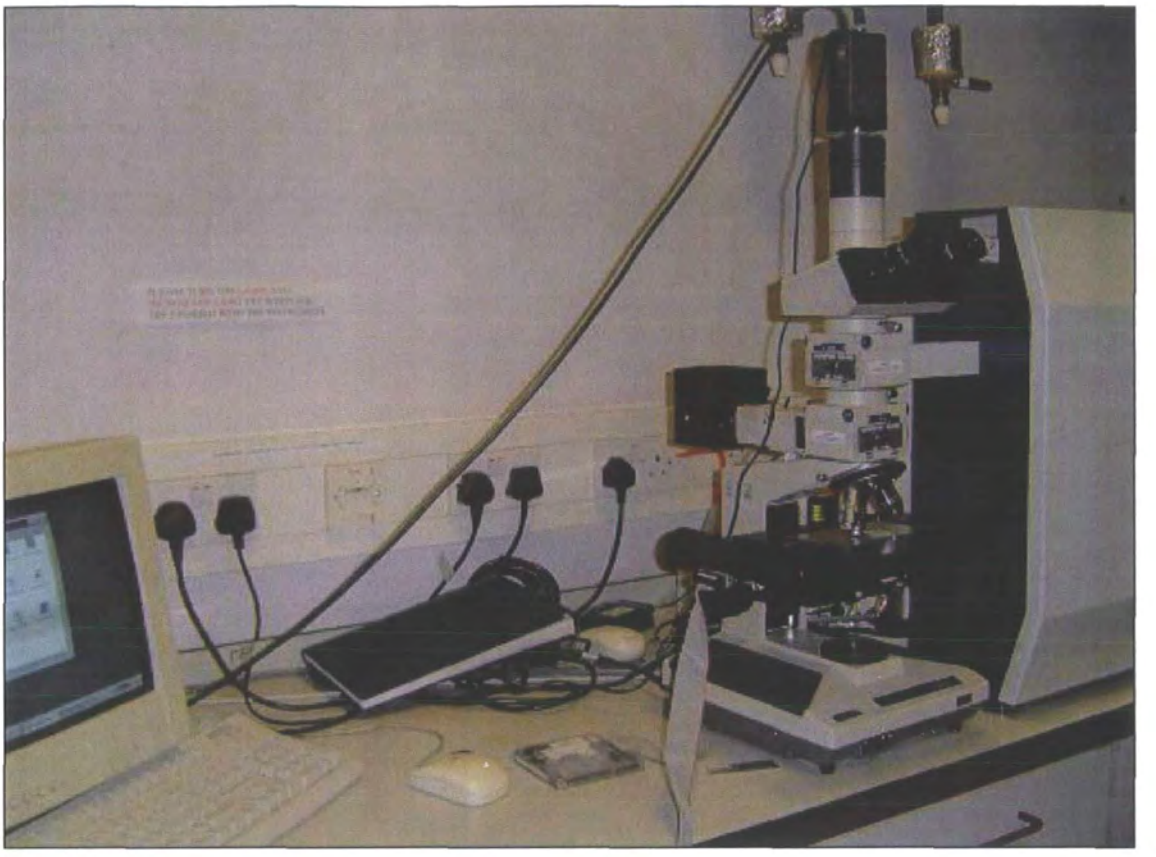

Figure 2.25 Setup used for Raman work

2.4 Results and Discussion

2.4.1 TGA

The following traces were obtained for samples of pure PET, pure PC and a 50:50 blend of the two.

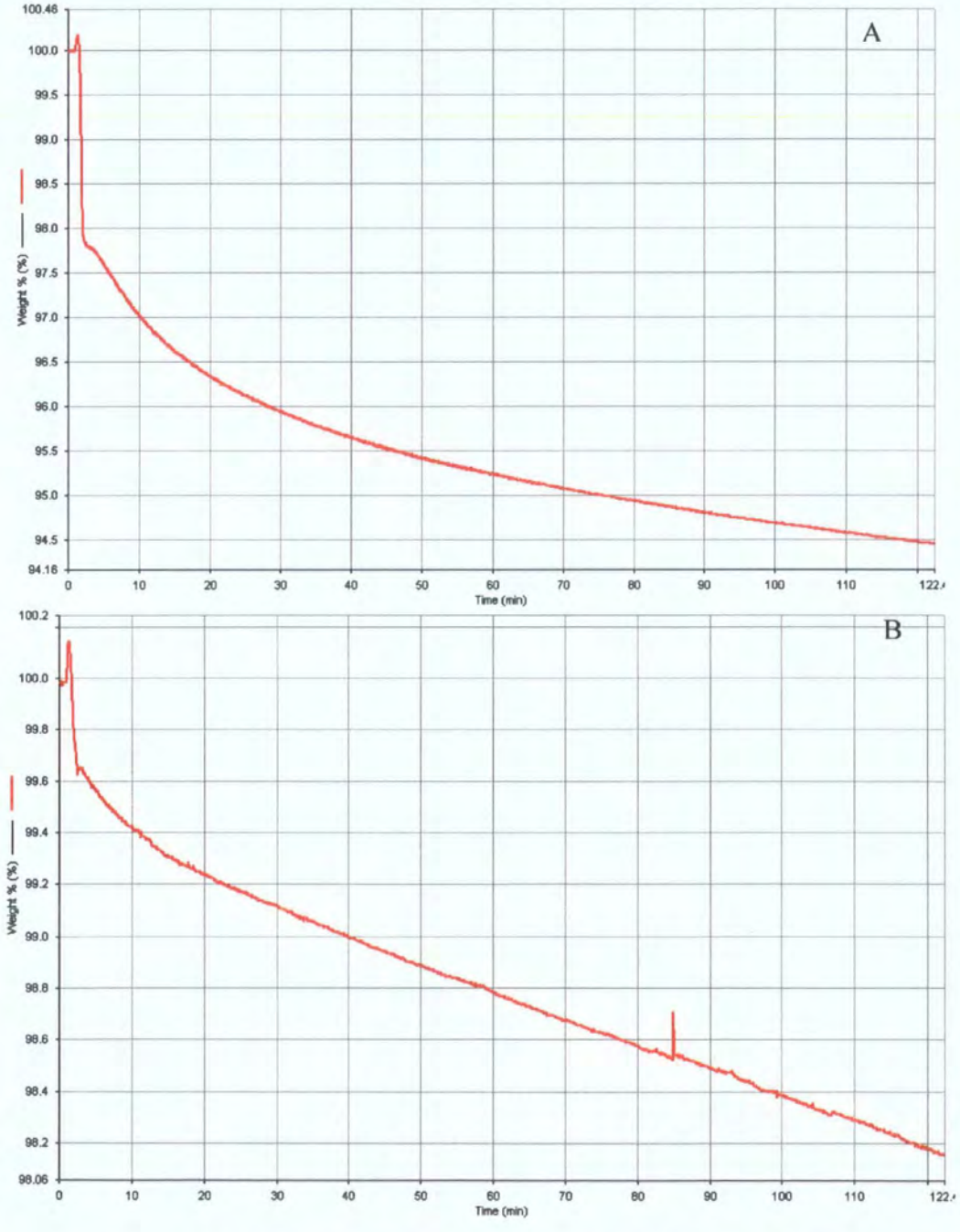

Figure 2.26 The weight of PC (A) and PET (B) annealed at 300°C, as analysed by TGA, expressed as a percentage of the original weight

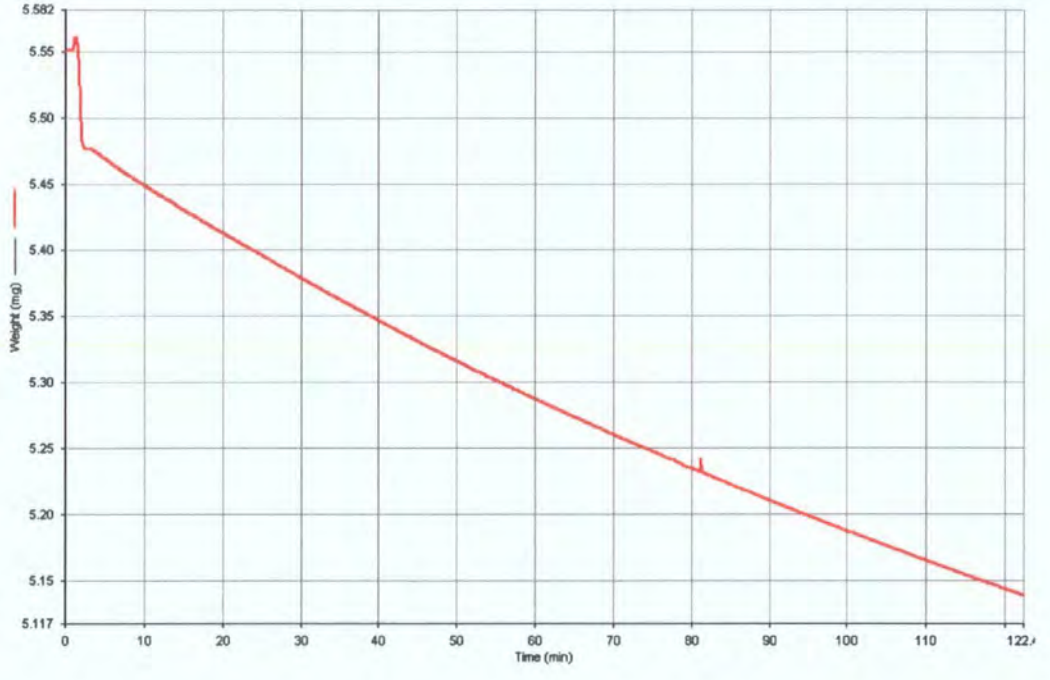

Figure 2.27 The weight of a sample of the 50:50 polymer blend annealed at 300°C as analysed by TGA expressed in mg

Table 2.28 Decomposition data for PC, PET and 50:50 PET/PC

	% Loss		
Sample	In heating	In hold	Total
BPA	2.39	3.39	5.78
PET	0.35	1.6	1.95
Average	1.37	2.495	3.87
50:50 mix	1.26	6.13	7.39

From the data in Table 2.28 a 50:50 w/w mix of PET and PC would be expected to lose less than 4% over two hours at 300°C in nitrogen. However, due to the reaction between the two the mixture loses nearly 7.4%, almost double the expected amount. There must therefore be some weight loss attributed to the formation of products which are less stable than either starting material. This suggests complications may occur during high temperature extrusion and low molecular weight material is likely to be produced.

2.4.2 DSC

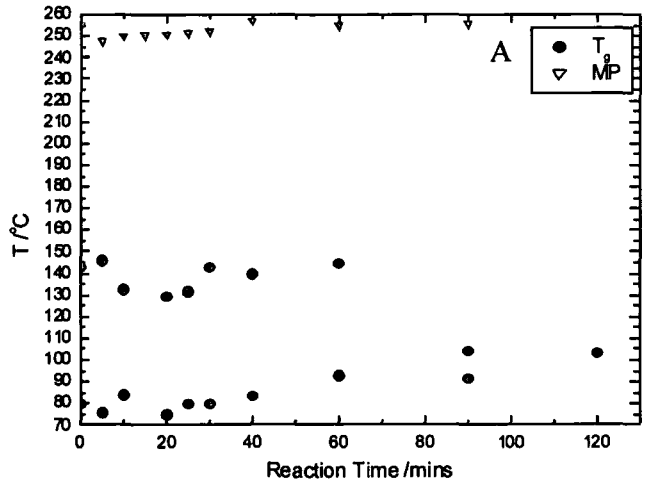

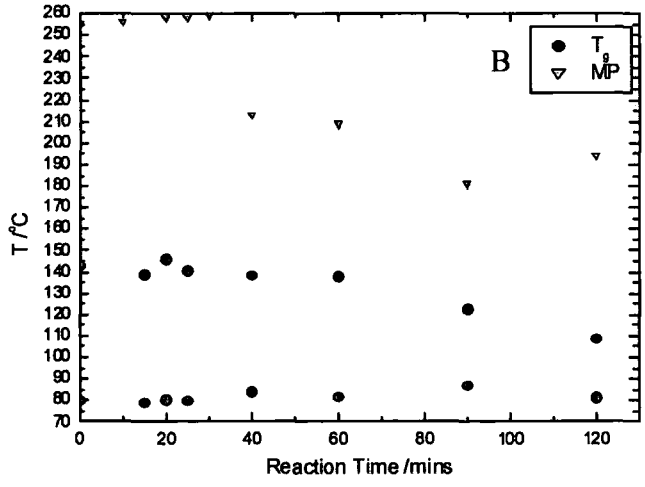

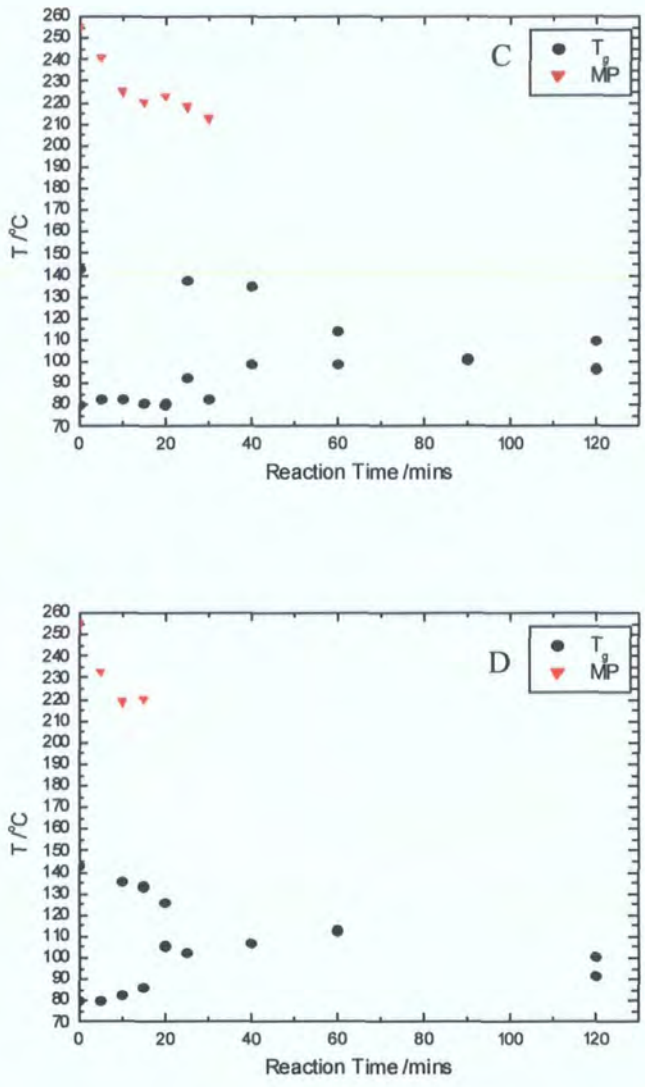

Figure 2.29 Values of T_g and T_m observed in samples of 50:50 PET/PC after transesterification for different times at 270°C (A), 280°C (B), 290°C (C) and 300°C (D).

Data obtained by DSC from solution blended material are tabulated in the Appendix, Table I. Figure 2.29 shows the two T_g values and T_m visible on DSC traces of samples of 50:50 PET/PC transesterified for a time at one of the four temperatures under investigation. It can be noted that T_m tends to fall with increased reaction time and there

is a time applicable to each temperature, after which no T_m is visible. The T_m endotherm becomes wider and decreases in area with increasing reaction time, eventually becoming so long and flat that it cannot be distinguished from the base line.

Figure 2.30 is a plot of the enthalpy of fusion determined from all of the DSC traces which display a visible melting point endotherm. The data show that reaction for short periods of time at the higher reaction temperatures causes extensive crystallization inhibition. Conversely reaction at 270°C can be carried out for up to an hour with little effect. Inhibition is believed to be due to disruption of ordering by the amorphous bisphenol-A units. As such, inhibition is an indication of blending thought to only occur after some amount of reaction has occurred.[11] The lack of effect of reaction time on the extent of crystallinity is an indicator that very little reaction occurs after up to an hour at 270°C.

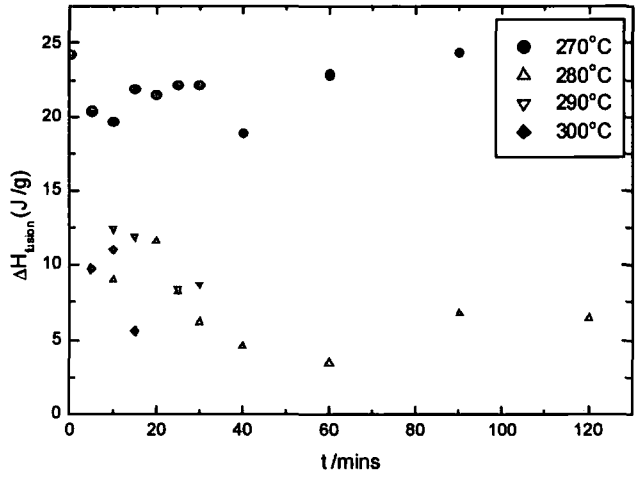

Figure 2.30 Enthalpy of fusion for samples of 50:50 PET/PC transesterified for different times at the four temperatures under investigation

Figure 2.30 shows little evidence of reaction during heating for up to an hour at 270°C but all other temperatures show inhibition of crystallinity. Total inhibition is achieved in shorter reaction times as the reaction temperature increases. As expected, the onset of melting occurs earlier with increased reaction whilst, simultaneously, the extent of melting decreases. It is impossible to say from these data alone whether PC reacts with PET and disrupts the crystallization or whether simple diffusion is occurring. Data on the kinetics of the reaction in Chapter 3 and Raman mapping below look into this question in further detail.

Data collected from melt blended material are presented below. The raw data are tabulated in the Appendix, Table II.

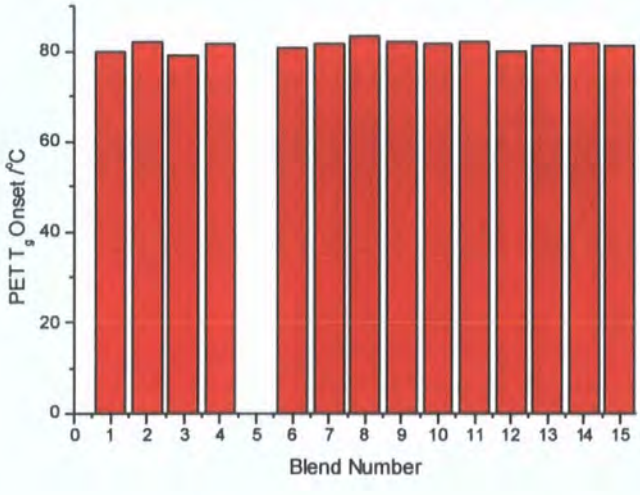

	% PET		% PC		
Blend	Laser	Base	2605	1239	2205
1		**90**	**10**		
2		75	25		
3		60	40		
4		50	50		
5		10	90		
6		90		10	
7		90			10
8		75			25
9		50			50
10	**90**			**10**	
11	75			25	
12	50			50	
13	90				10
14	90		10		
15	75		25		

Figure 2.31 T_g values identified in DSC traces of melt blending experimentation

Figure 2.31 shows the T_g values visible in DSC traces, no T_g is visible in the 140°C region since that region is occupied by the crystallization exotherm. This is caused by the

ordering of crystallizable material which did not order between the extrusion of the molten material and the point at which the blend lace cooled to below 80°C. The T_g values are all very similar regardless of blend; no PET T_g is detected for blend 5 since this is only 10% PET so the feature is very weak.

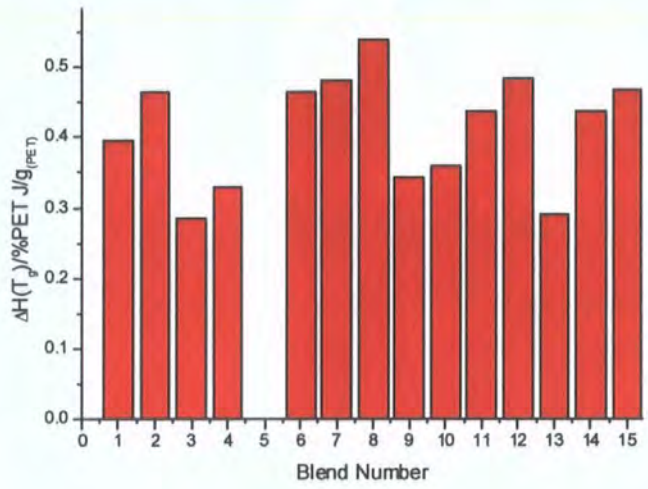

	% PET		% PC		
Blend	Laser	Base	2605	1239	2205
1		**90**	**10**		
2		75	25		
3		60	40		
4		50	50		
5		10	90		
6		90		10	
7		90			10
8		75			25
9		50			50
10	**90**			**10**	
11	75			25	
12	50			50	
13	90				10
14	90		10		
15	75		25		

Figure 2.32 Enthalpy of T_g adjusted for amount of PET

Figure 2.32 shows the enthalpy for the T_g, shown adjusted for the amount of PET (ΔH/weight fraction of PET). There appears to be no trend in the endotherms shown, either in the Base blends from 1-9 or the *Laser* blends.

It appears, on the strength of these data, that the material produced in the melt has been transesterified to a much lower extent than the material produced in small scale experiments. The melt reactions effectively heat the sample at between 280 and 290°C for 5 minutes with mixing, this would suggest that the mixing is not crucial and that good transport occurs in static solution blended systems.

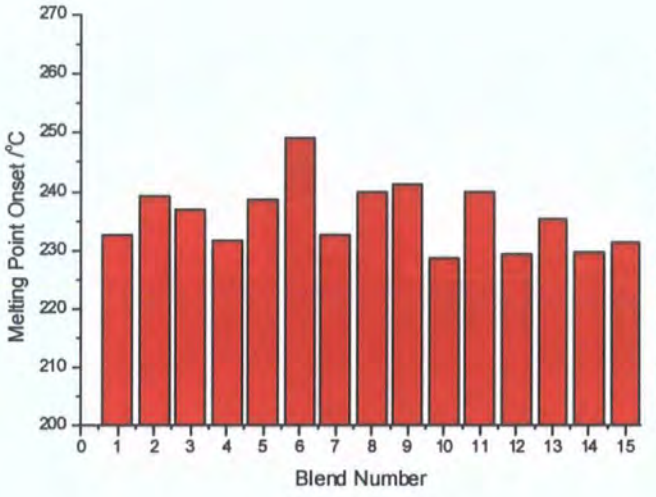

	% PET		% PC		
Blend	Laser	Base	2605	1239	2205
1		**90**	**10**		
2		75	25		
3		60	40		
4		50	50		
5		10	90		
6		90		10	
7		90			10
8		75			25
9		50			50
10	**90**			**10**	
11	75			25	
12	50			50	
13	90				10
14	90		10		
15	75		25		

Figure 2.33 Onset of melting endotherm in melt blended material

All samples show a crystallization endotherm in much the same way as do all of the 270°C solution blended samples. However, there is significant variation in the onset of the endotherm (Figure 2.33) suggesting there is similarity between this process and reactions at 280°C. This in itself is not surprising since the extruder screw was heated to 285°C in most cases, higher only for the samples made up of 40% or more PC. The size of the melting endotherm does not relate simply to the thermal history of the blending and cooling process, a large degree of ordering takes place during heating in the DSC. To obtain the extent of crystallinity it is necessary to deduct the crystallization exotherm from the melting point endotherm, this is presented below adjusted for the weight % of the sample which is made up of PET.

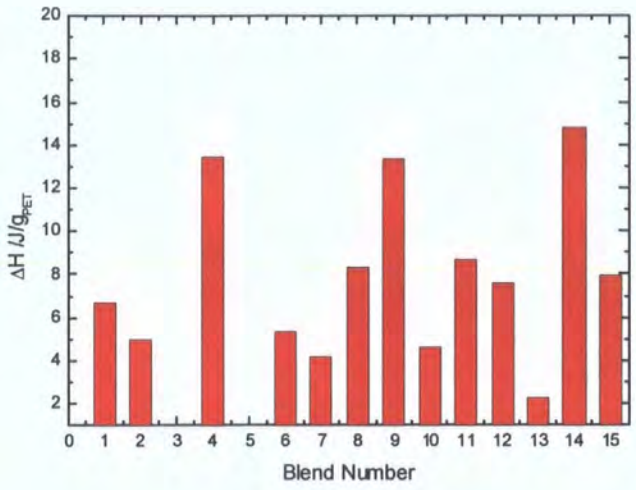

	% PET		% PC		
Blend	Laser	Base	2605	1239	2205
1		**90**	**10**		
2		75	25		
3		60	40		
4		50	50		
5		10	90		
6		90		10	
7		90			10
8		75			25
9		50			50
10	**90**			**10**	
11	75			25	
12	50			50	
13	90				10
14	90		10		
15	75		25		

Figure 2.34 ΔH_{melt} %PET for melt blended PET/PC obtained by DSC

There are no data for blend 5 because there is no crystallization endotherm and none for blend 3 because it was not possible to collect some information on the crystallization exotherm. There is no trend visible in the remaining samples, blends 4, 9 and 14 show high levels of crystallinity but whilst two of these samples are 50% PC, the third is only 10%. To get an idea of the relative rate of crystallization it is necessary to compare these data with the total potential crystallization. This is presented below, again adjusted for the proportion of PET in each sample.

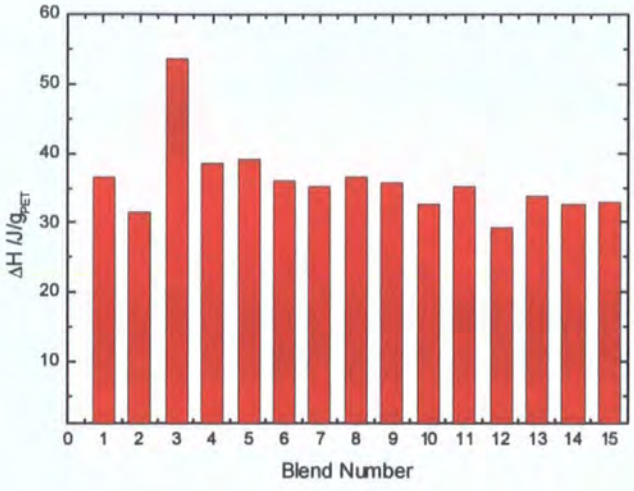

	% PET		% PC		
Blend	Laser	Base	2605	1239	2205
1		**90**	**10**		
2		75	25		
3		60	40		
4		50	50		
5		10	90		
6		90		10	
7		90			10
8		75			25
9		50			50
10	**90**			**10**	
11	75			25	
12	50			50	
13	90				10
14	90		10		
15	75		25		

Figure 2.35 Maximum crystallization possible in blends 1-15

There is very little deviation in the crystallization exhibited in the melt blended material. This suggests that the variation shown in the crystallinity of the melt blended material is either due to differences in the rate of growth of crystallites or in the length of time the lace takes to cool. This is dictated by the torque in the screw extruder. One way of measuring the proportion of crystallinity in a sample, relative to the maximum possible is shown in Equation 2.36.

$$\frac{\Delta H_t}{\Delta H_\infty} = X_t \quad \textbf{Equation 2.36}$$

X_t is known as the fractional crystallinity, ΔH_t is the enthalpy of crystallization of the sample crystallized for time t and ΔH_∞ is the enthalpy of crystallization of the sample having been annealed to full crystallinity.

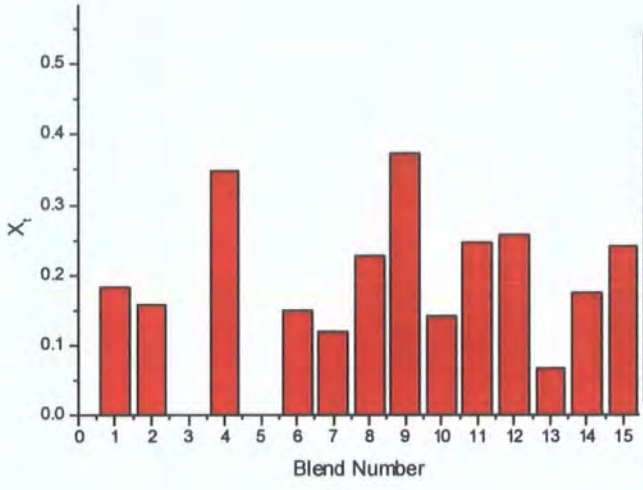

	% PET		% PC		
Blend	Laser	Base	2605	1239	2205
1		**90**	**10**		
2		75	25		
3		60	40		
4		50	50		
5		10	90		
6		90		10	
7		90			10
8		75			25
9		50			50
10	**90**			**10**	
11	75			25	
12	50			50	
13	90				10
14	90		10		
15	75		25		

Figure 2.37 Extent of crystallization

No trends are evident in Figure 2.37, this is understandable since no attempt was made in the manufacture of the blends to give all of the blends the same crystallization conditions. What can be concluded is that achievable crystallinity of a PET/PC blend can be varied over a large range. It is not clear which conditions are necessary to achieve a particular level of crystallinity but we propose that it should be possible to control crystallinity by changing the time the blend spends in the screw extruder. Longer periods of heating should lead to samples with a lower tendency to crystallize although the optimum time would depend on the desired properties of the final product and would have to be experimentally determined.

More telling therefore is the maximum potential crystallinity per gram of blend since this is the limiting value of what would be exhibited by the blend in a real application.

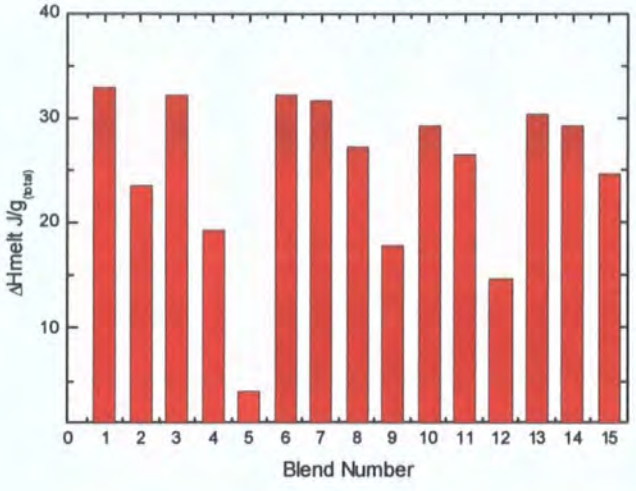

	% PET		% PC		
Blend	Laser	Base	2605	1239	2205
1		**90**	**10**		
2		75	25		
3		60	40		
4		50	50		
5		10	90		
6		90		10	
7		90			10
8		75			25
9		50			50
10	**90**			**10**	
11	75			25	
12	50			50	
13	90				10
14	90		10		
15	75		25		

Figure 2.38 Maximum crystallinity of each blend

Figure 2.38 is effectively Figure 2.35 but without the adjustment for PET concentration. The result is that since the crystallization per gramme of PET is stable, the maximum extent of crystallization is dictated largely by the concentration of PET in the blend. This may seem obvious but it suggests a low extent of reaction in the samples, a high extent of reaction would have inhibited crystallization. Because the different blends are all treated similarly, the DSC results would have shown up any differences in the blends tendency to react. Since PET and PC are immiscible, it would be expected that the rate of reaction would be affected significantly by the interfacial area – in turn dictated by morphology. These results tell us that the morphology of blends containing from 10% up to 50% PC are all very similar. This can be understood by considering the volume percentage of PET and PC in a 50:50 blend. Because PC has a much higher molecular weight, a 50:50 blend by mass will equate to a 57:43 mole blend with an excess of PET. This means that in the melt the PC is suspended in an excess of PET and the morphology will reflect this.

It is only at the 50:50 volume blend that a bi-continuous structure of the two might be predicted. Below this, the PC will be surrounded by PET and seek to minimise these interactions. The minimum interfacial area is therefore achieved by forming macroscopic spheres. By decreasing the amount of PC in a blend from 50% w/w the number and frequency of these pockets will reduce but they will remain large in order to minimise the unfavourable interactions between the two polymers. This means that the effective surface area over which reaction or diffusion can occur remains roughly constant meaning the rate of reaction also does. This can be seen in greater detail in 2.4.4 where OM results are discussed.

2.4.3 Solid State Polymerization

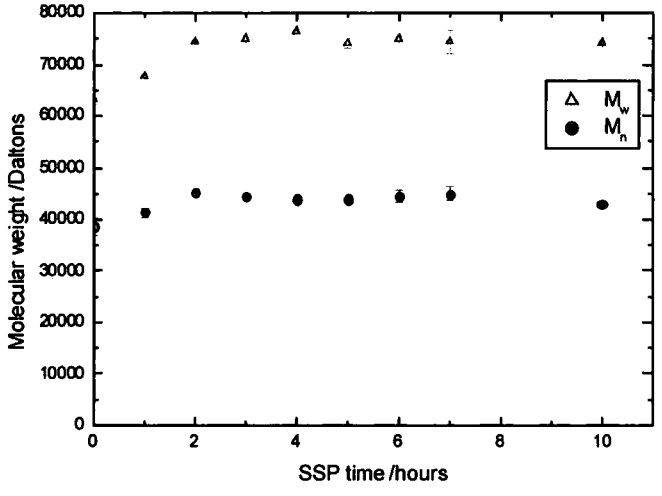

Figure 2.39 $\overline{M}_n$ and $\overline{M}_w$ of blend 1 during SSP

Data for the molecular weight of material that has undergone SSP is in the Appendix, Table III. Figure 2.39 shows that both the $\overline{M}_n$ and $\overline{M}_w$ rise during the first 2 hours of SSP. This rise appears to be roughly linear. After two hours the molecular weight of the blend plateaus.

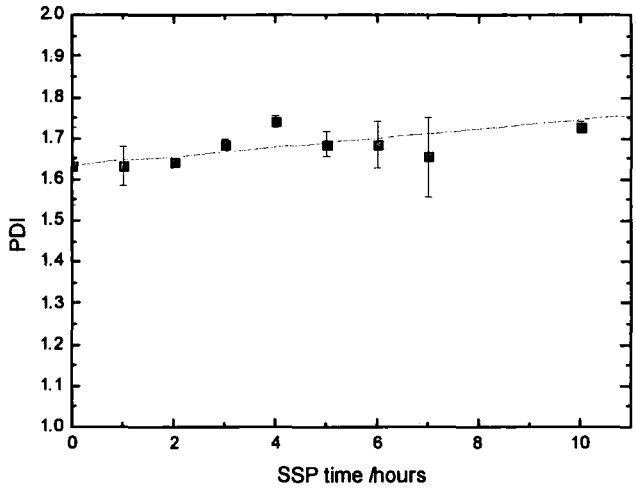

Figure 2.40 PDI of blend 1 during SSP

The conclusion we draw is that during the first two hours of SSP volatiles are removed and the molecular weight rises. After this, the blend is in equilibrium and there is no further significant molecular weight increase. It can be concluded that SSP of blend 1 is possible and under the conditions used can increase $\overline{M}_n$ to around 45,000 Daltons and $\overline{M}_w$ to around 75,000 Daltons within two hours.

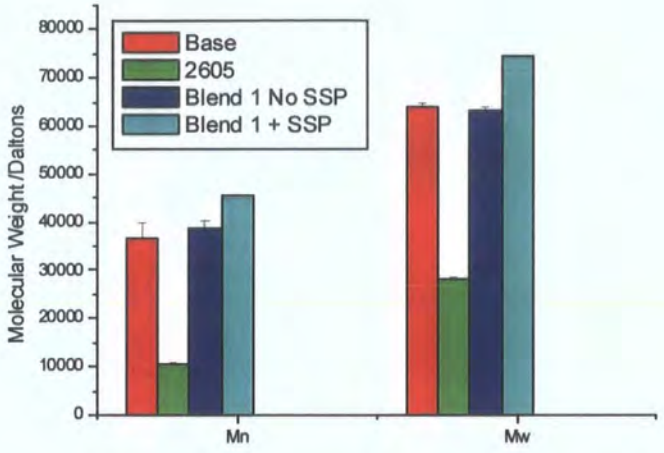

Figure 2.41 $\overline{M}_n$ and $\overline{M}_w$ blend 1 before and after SSP compared with *Base* and *2605*

Figure 2.41 shows that blend 1 has higher molecular weight than either of the raw materials before SSP so it may be that SSP would be unnecessary in industrial applications.

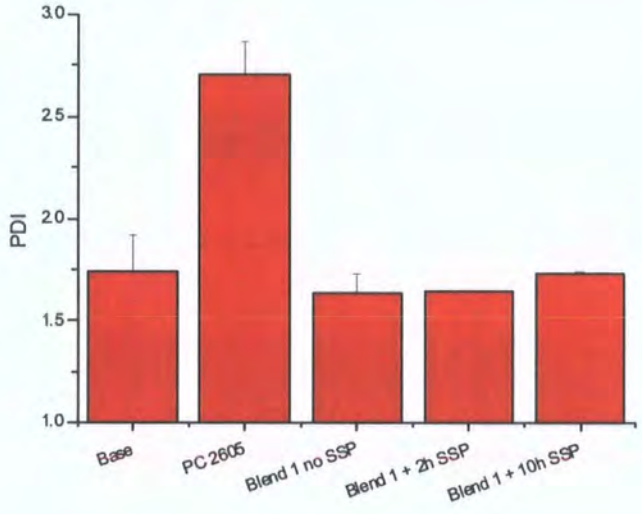

Figure 2.42 PDI of blend 1 before, during and after SSP compared with *Base* and *2605*

In Figure 2.42 it can be seen that blend 1 is less polydisperse than both raw materials before SSP and after the optimum 2 hours SSP treatment. The PDI after 10 hours is

around the PDI of *Base* PET so if high polydispersity is desirable then it can be achieved also.

2.4.4 Optical Microscopy

As described in 2.2.1, spherulites in PET are known to grow radially at a constant rate. The rate can be derived as follows:

$$G = \frac{(D_2 - D_1)}{\Delta t} \quad \textbf{Equation 2.43}$$

where D_1 and D_2 are the diameter of the spherulite at two different times and Δt is the time elapsed between the two measurements. Graphs of the spherulite growth rate observed for samples transesterified for different lengths of time are shown in Figure 2.43 A-D. Data is listed in the Appendix Table IV.

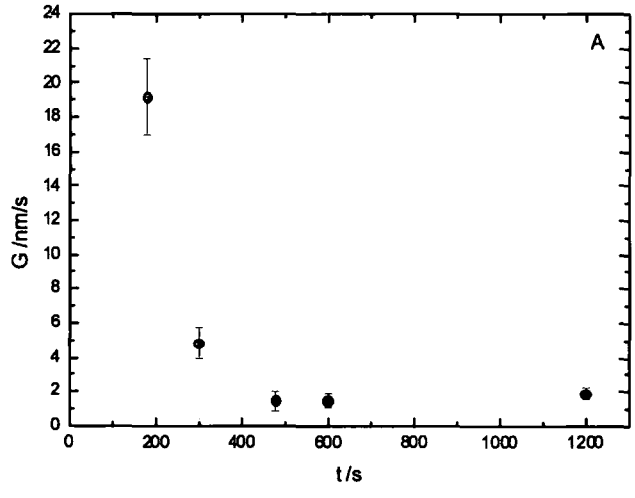

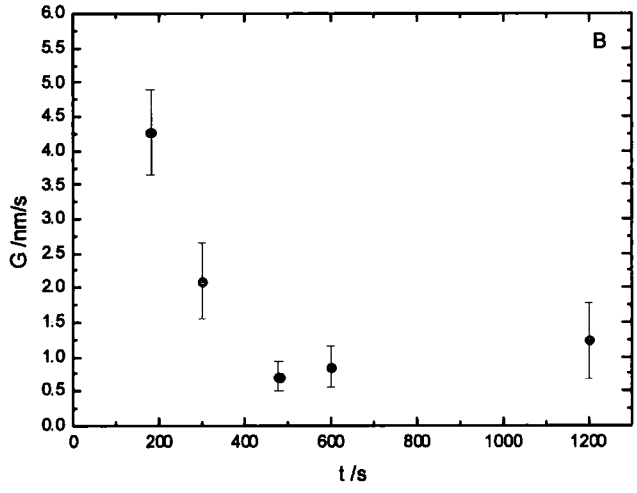
B
G /nm/s
t /s
0.0
0.5
1.0
1.5
2.0
2.5
3.0
3.5
4.0
4.5
5.0
5.5
6.0
0
200
400
600
800
1000
1200

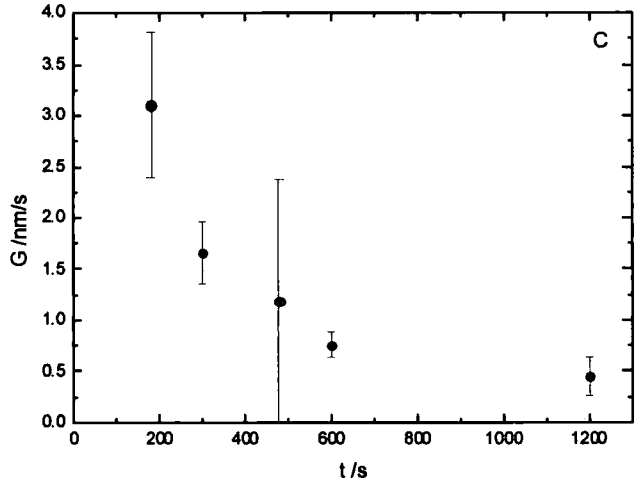
C
G /nm/s
t /s
0.0
0.5
1.0
1.5
2.0
2.5
3.0
3.5
4.0
0
200
400
600
800
1000
1200

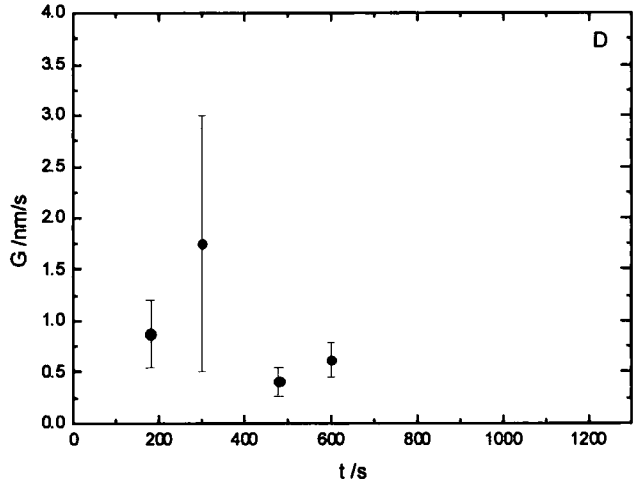

Figure 2.43 Rate of spherulite growth of PET/PC blends which have been transesterified for different times at 270°C (A), 280°C (B), 290°C (C) and 300°C (D)

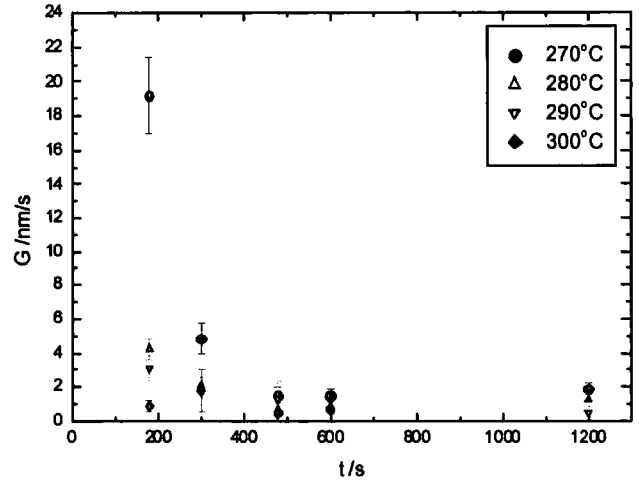

Figure 2.44 G values from Figure 2.44 A-D shown on the same axes

Treating the results of the blend held at 270°C as an exponential decay curve it is possible to extrapolate back to the origin to obtain a value for the rate of crystallization of pure

PET. The value obtained is 67.3 ± 13.0 nm s^{-1} which is plotted in Figure 2.45 with literature values for the crystallization of PET (see Appendix Table V). The results presented here are in rough agreement with literature, therefore our treatment of the data would appear to be supported.[23]

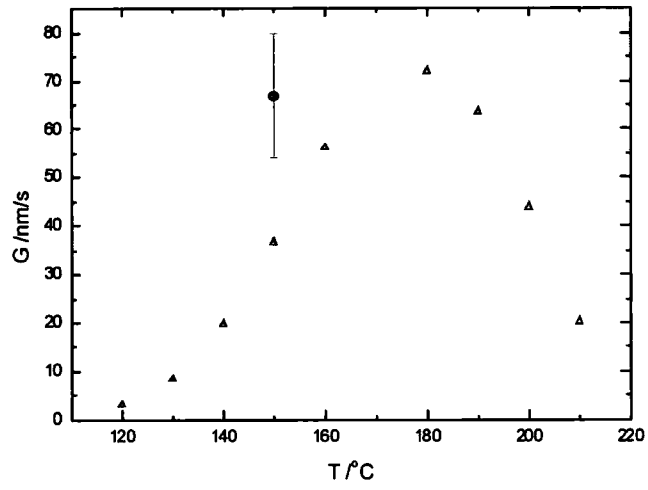

Table 2.45 Spherulite growth rates of PET at various temperatures as reported in the literature (red) plotted with the rate found by extrapolating Figure 2.44 A (black)

The effect of transesterification temperature on the crystallization rate of PET is significant. After just three minutes at 300°C the rate observed is 0.88 ± 0.32 nm s^{-1} whereas after three minutes at 270°C the rate is observed to be 19 ± 2 nm s^{-1}. The fact that there is any crystallization at all at relatively high conversion appears to be related to the reaction conditions. The sample under examination was not stirred during the annealing process and so the rate and extent of transesterification is controlled largely by diffusion. This is illustrated by the distribution of areas of crystallinity within samples with different extents of transesterification. In cases where the extent of reaction is very

low, spherulites are found throughout the PET phase. In cases where the extent of reaction is much higher, spherulites are found only in areas of the sample far from areas of PC. Two examples are shown in Figure 2.46.

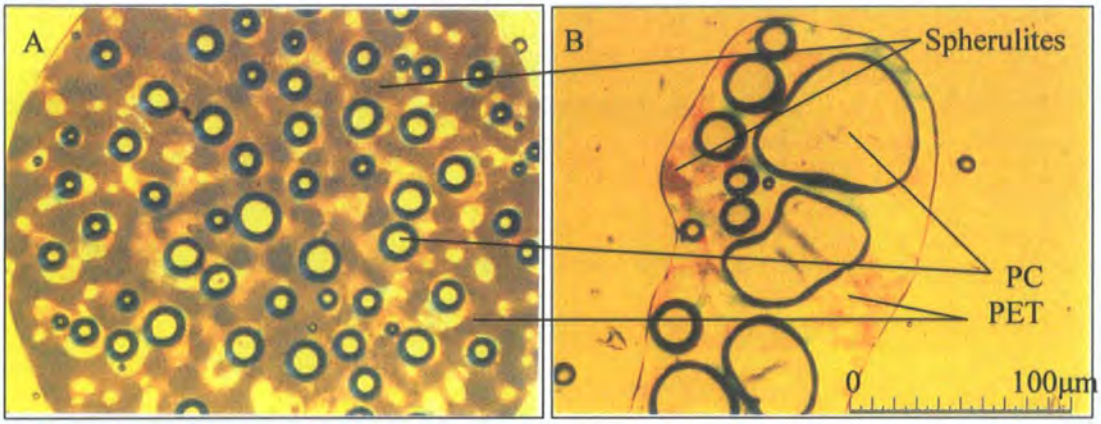

Figure 2.46 Images of PET/PC that have been annealed for 5 minutes at 270°C (A) and 300°C for 30 minutes (B) and then crystallized at 150°C

The brown areas in the two photos above are areas of crystallization within the PET phase, the "bubbles" in the photos are areas of PC that are immiscible with the PET phase. Samples transesterified under the same conditions as those shown in Figure 2.46 have been analysed by ^{1}H NMR and the randomness of both samples has been shown to be equal to 0 (see Chapter 3), i.e. the extent of transesterification is negligible in both cases. Evidently some changes have occurred because the extent of crystallization differs by several orders of magnitude based on the area of crystalline regions. Also, where the sample is transesterified at the lowest temperature, the PET crystallizes twenty times faster than that reacted at the highest temperature. This illustrates the fact that ^{1}H NMR is able to probe the bulk effects of transesterification on the sample whereas microscopy only allows the analysis of local effects which may or may not be part of a larger trend.

It is not possible to plot the ^{1}H NMR data against the spherulite data since the reaction times do not overlap sufficiently.

It has been shown in the literature that PET and PC, along with other polymer blends, become miscible after annealing above the T_m for some time.[24-28] From microscopy it appears this process involves reaction at the interface of the amorphous and crystalline regions and when co-polymer is produced it is retained in the amorphous areas, making these areas appear to expand and consume the regions which originally contained PET. Below is an image of a sample that has been reacted for an hour at 300°C.

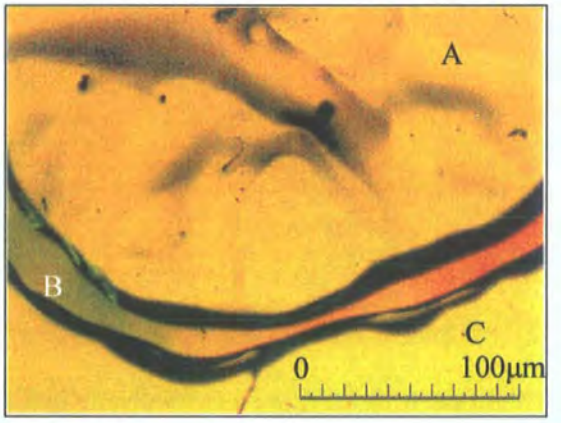

Figure 2.47 A photo of a sample of PET/PC that has been annealed for 60 min at 300°C and then annealed at 150°C for 30 min.

It is clear that two phases still exist in the photo above. The outer corona is the PET phase (B), which has been steadily consumed by the expanding areas of amorphous polymer, originally PC phases. These areas expand to such a point that eventually just one amorphous region exists as all of them combine (A). The area labelled C is a view through the two cover slips which sandwich the polymer, no sample is present in this area.

It must also be the case that some PC character enters the crystalline regions since the crystallinity in these regions is disrupted very rapidly. If all copolymer was located in the phase which originally contains pure PC then reaction would have no effect on the rate of crystallization in the crystalline regions. There must presumably be some critical point in the reaction where the interface between the amorphous and crystalline regions breaks down as the two areas become more homogeneous or, alternatively, when the originally crystalline areas are consumed totally by the amorphous areas. This is discussed further in 2.4.6 in the context of Raman mapping.

2.4.5 Nuclear Reaction Analysis

NRA results are shown below as overlays of the data from samples heated at the same temperature. The scatter plots should map out a Gaussian distribution of the actual profile so the curves do not necessarily signify a gradual concentration gradient.

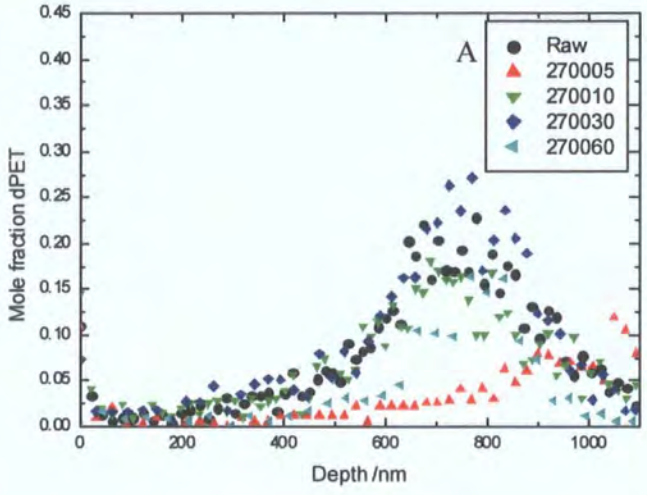

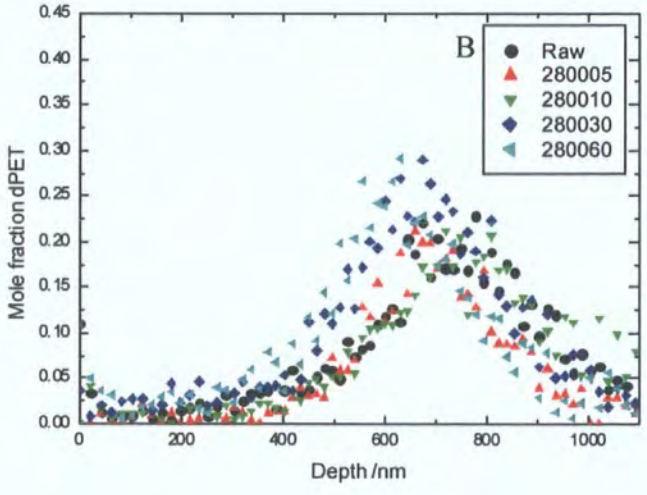

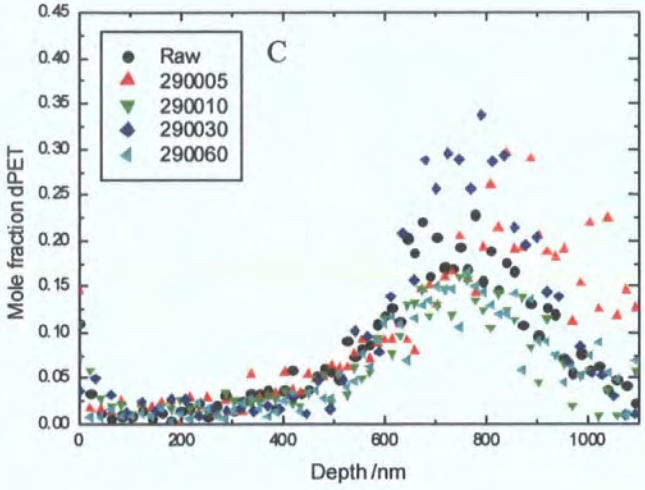

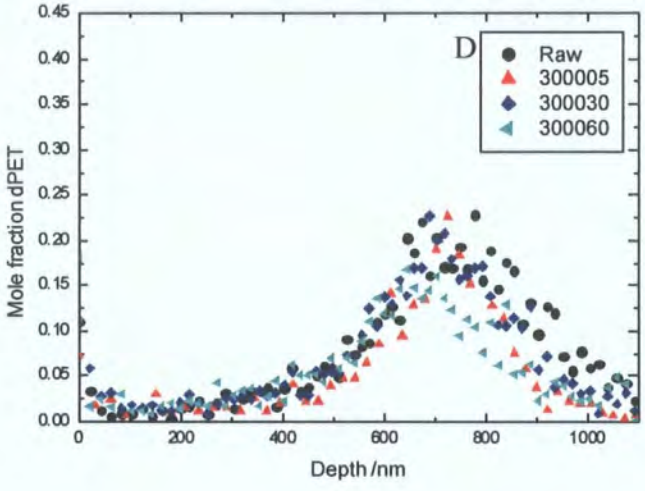

Figure 2.48 Depth profiles of the mole fraction of dPET for samples annealed at 270°C (A), 280°C (B), 290°C and 300°C (D)

The results shown above do not show particularly large scale movement, even after 60 min at 300°C very little movement is observed, certainly not enough to show clear change beyond the effect of background noise. It is known that PET and PC are immiscible in one another but even so some compatibilisation would be expected. It is

possible that the strict bi-layer nature of the samples inhibits diffusion, a spherical morphology which is seen in blends up to and including 50% PC in PET would have a much greater surface area to volume ratio and thus higher levels of diffusion could be expected. The samples used were dried very thoroughly and it is suggested from NMR data in Chapter 3 that if this is the case that the PET/PC reaction can proceed very slowly. This is discussed further in the conclusions in both Chapters 2 and 3.

2.4.6 Raman Mapping

Shown below are composite photos of the points where Raman spectra were collected. Below each photo is the corresponding plot of PET and PC repeat unit concentration. In generating the concentration plots the amount of PET present was taken as equal to the area of the Raman peak at 855 cm^{-1}, the peak used for PC was the one at 720 cm^{-1}. Some points are omitted because neither peak was detected.

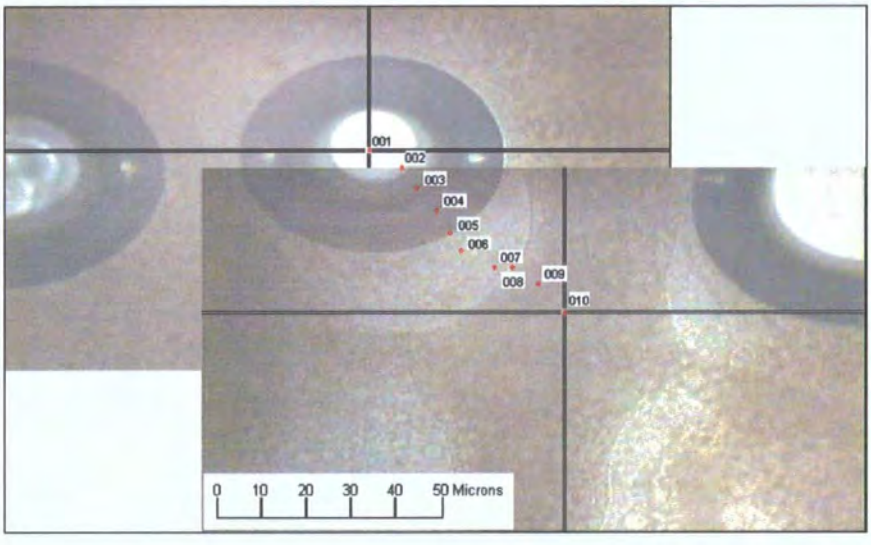

Figure 2.49 Schematic of points used for 270005 sample

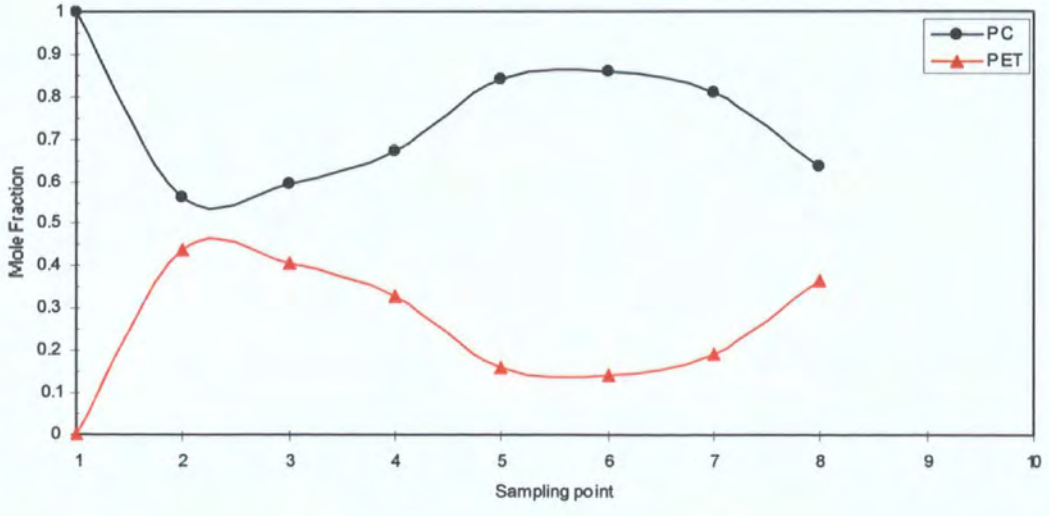

Figure 2.50 PC/PET molar concentration plot for 270005 sample

Figure 2.50 shows significant agreement with the position of the sampling points in Figure 2.49 above. Because the spectra taken at points nine and ten could not be processed, there are no data points taken presented in Figure 2.50 for crystalline PET. This is indicated by the PC concentration being constantly higher than that of PET. As the sample is probed from the amorphous area to the crystallization boundary the proportion of PET increases, this is to be expected. What is interesting is that the amorphous region outside of the original PC "bubble" is predominantly PC. The PC has not diffused from out of its bubble and broken down crystallinity - rather it has diffused out displacing the PET for the most part but absorbing a small amount of it.

Figure 2.50 shows a large amount of PET within the PC bubble. This may be due to focusing, the Raman was focused on the crystallites in the PET and they were assumed to be equatorial with respect to the bubble. It appears that the first point is focused correctly; this is most likely since the bubble is thickest at this point so there is a greater chance of focusing entirely within it.

Point 8 on the interface between the amorphous and crystalline phases shows that the material is less than 40% PET.

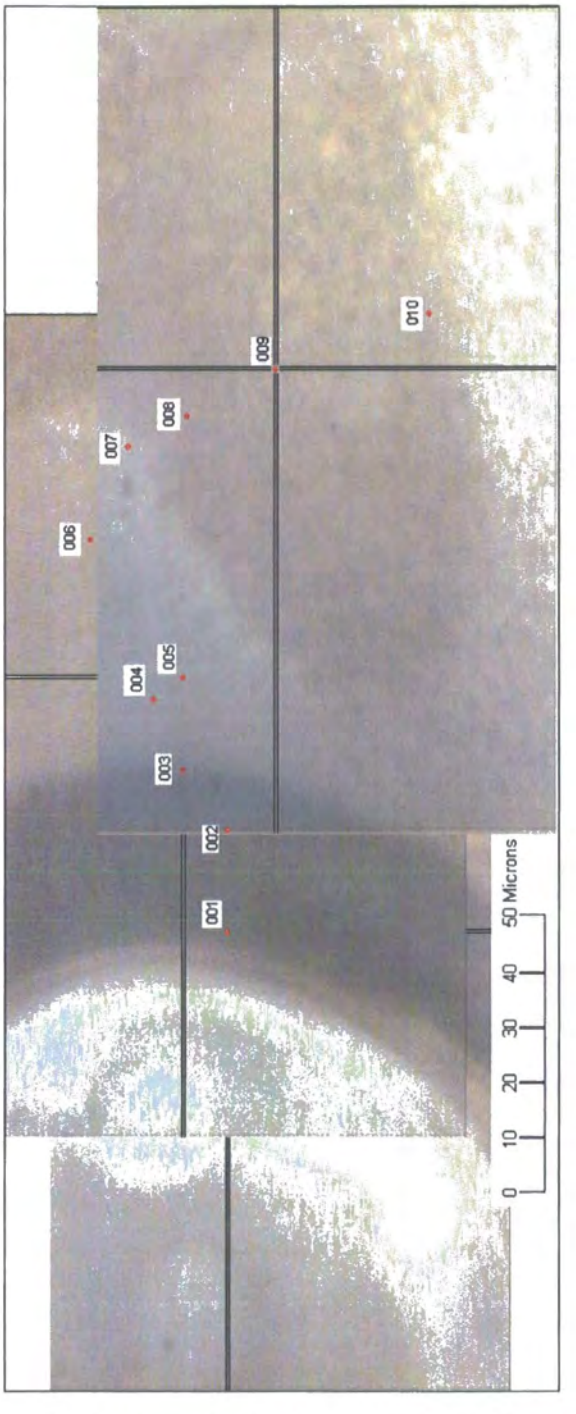

Figure 2.51 Schematic of points used for 270010 sample

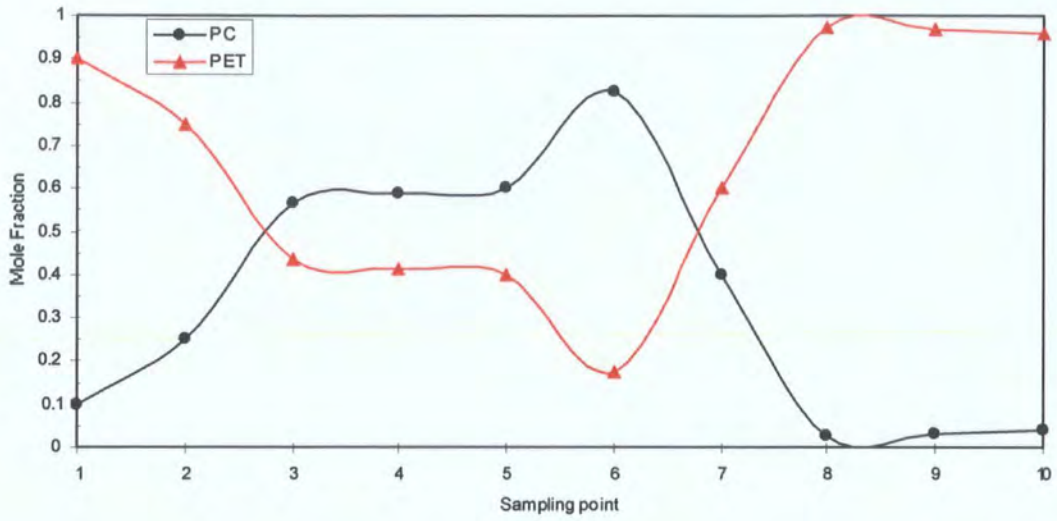

Figure 2.52 PC/PET molar concentration plot for 270010 sample

Figure 2.52 shows high levels of PET within the PC bubble just as points 2 and 3 for Figure 2.50 do. This may again be due to focusing. Points 4 and onwards however show the transition from amorphous phase to crystalline phase very clearly and point 7, shown in Figure 2.51 to be on the interface, is around 60% PET.

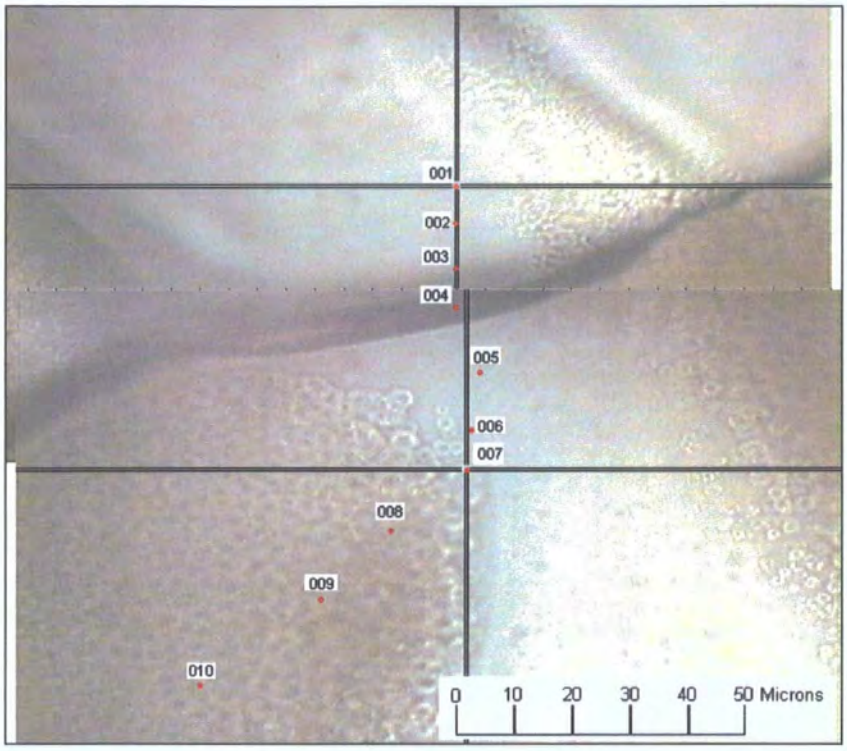

Figure 2.53 Schematic of points used for 270030 sample

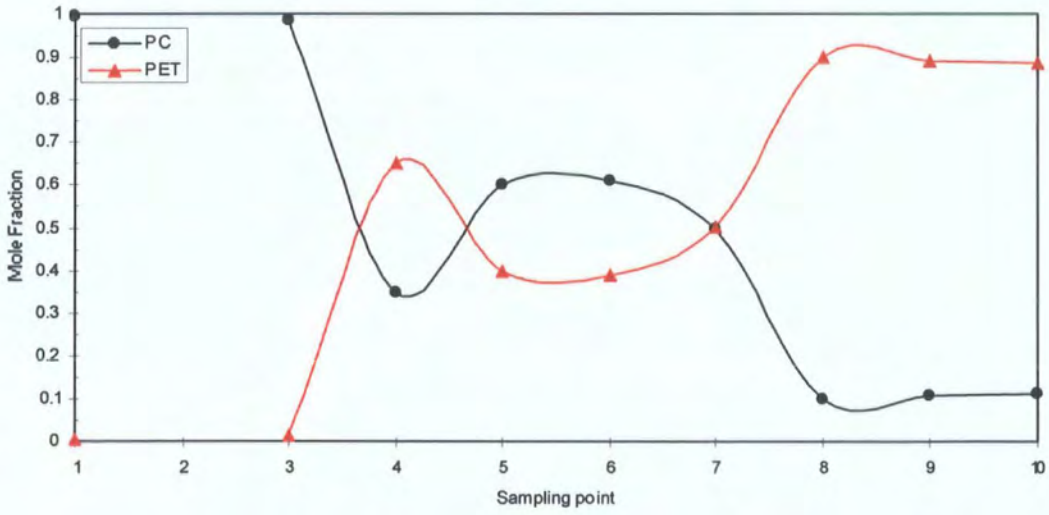

Figure 2.54 PC/PET molar concentration plot for 270030 sample

The sample shown in Figure 2.53 appears to be well focused and points one and three show 100% PC content which is understandable with point two being ambiguously positioned so it could well be outside of the bubble. In either case the amorphous region

outside of the bubble has a PET content between 40 and 65% with the content at the interface with the spherulites being 50%. The PET content within the spherulites is 90% so some contamination is clearly tolerable without total inhibition.

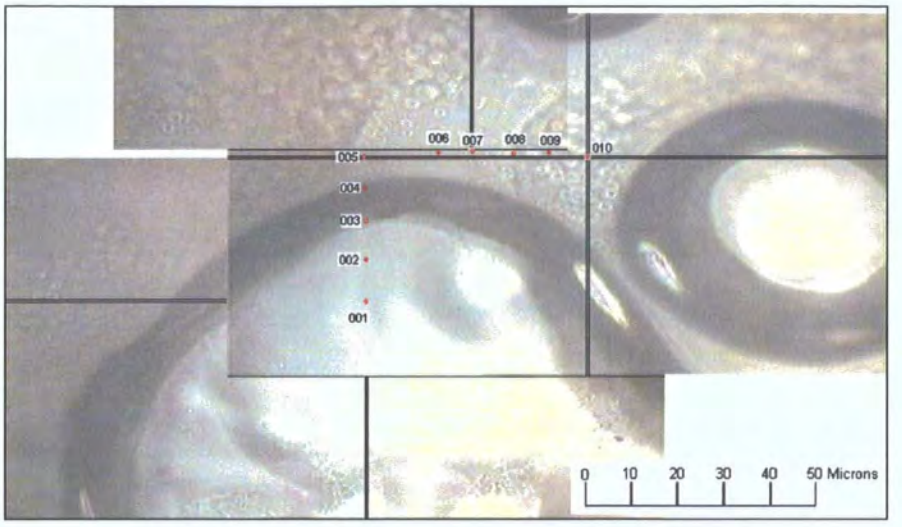

Figure 2.55 Schematic of points used for 300005 sample

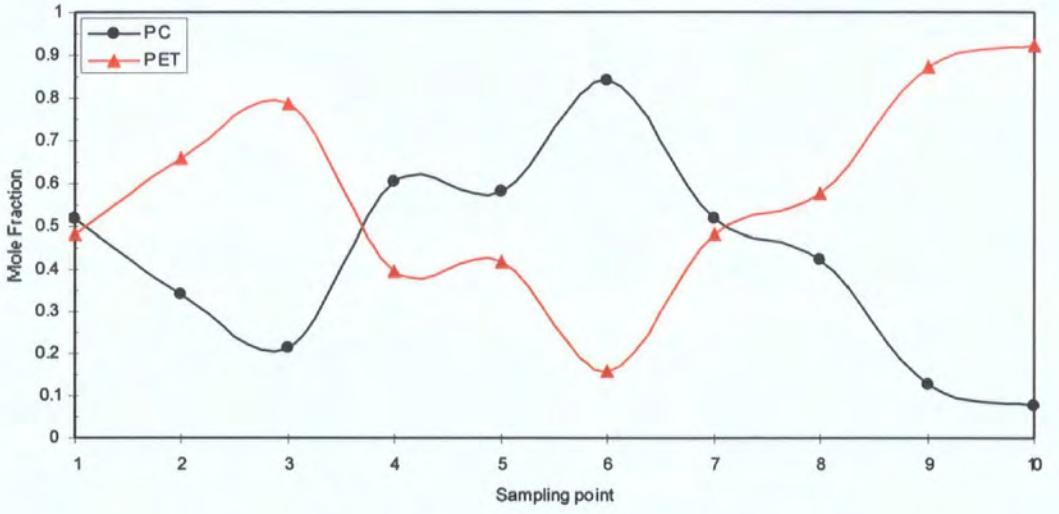

Figure 2.56 PC/PET molar concentration plot for 300005 sample

Figure 2.56 suggests that Figure 2.55 is not focused such that points 1-3 are inside the PC bubble. Points 4-7 show a range of between 17 and 50% PET and point 8 shows nearly 60% PET at the interface. The crystalline region shows up to 12% PC content.

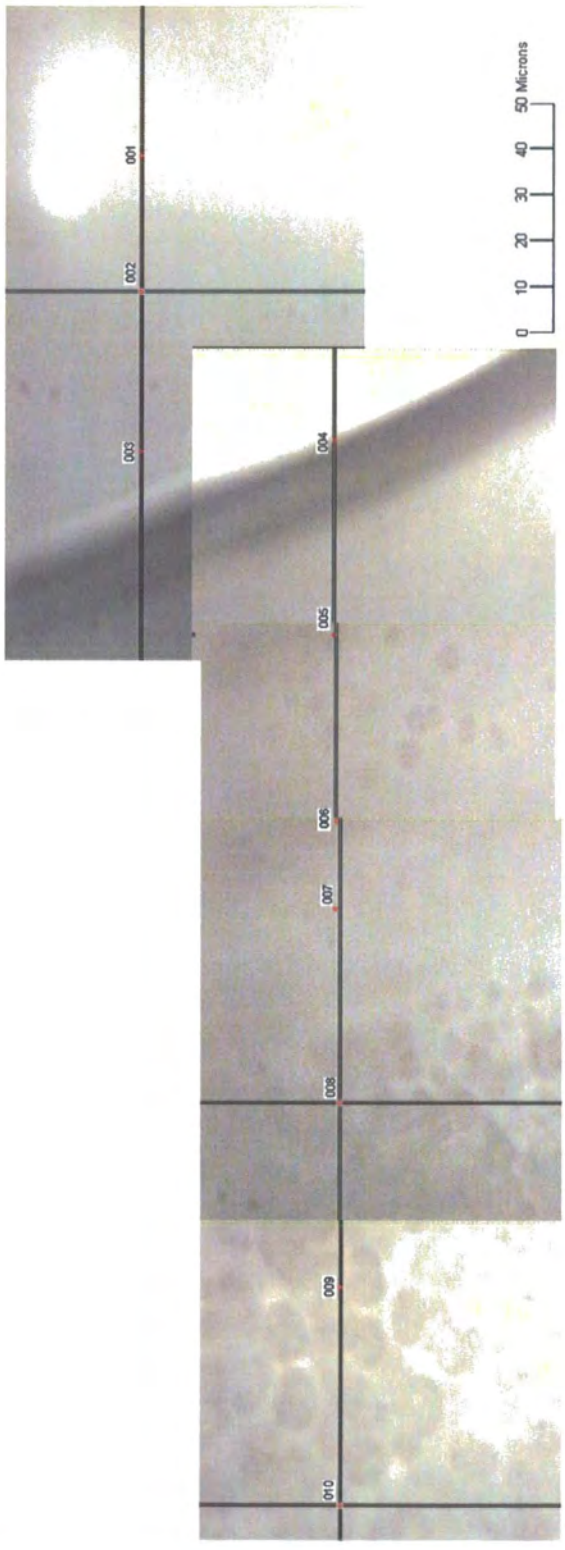

Figure 2.57 Schematic of points used for sample 300010

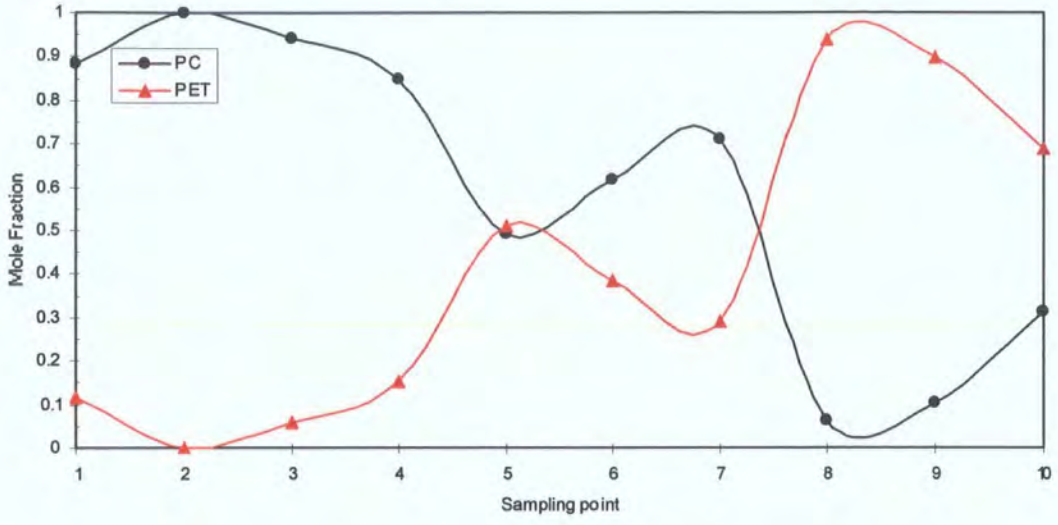

Figure 2.58 PC/PET molar concentration plot for 300010 sample

Figure 2.57 shows a very different type of crystallinity to the previous composite images, the spherulites are separated by amorphous regions giving them a cloudy appearance. Figure 2.58 seems to show that Figure 2.59 is focused such that points 1-10 all lie in the PC bubble (1-4), amorphous region (5-7) and crystalline PET (8-10). The data indicate that the amorphous region outside of the bubble can vary from under 30% to over 50% and that the crystalline region can be made of up to 30% PC in this expanded form.

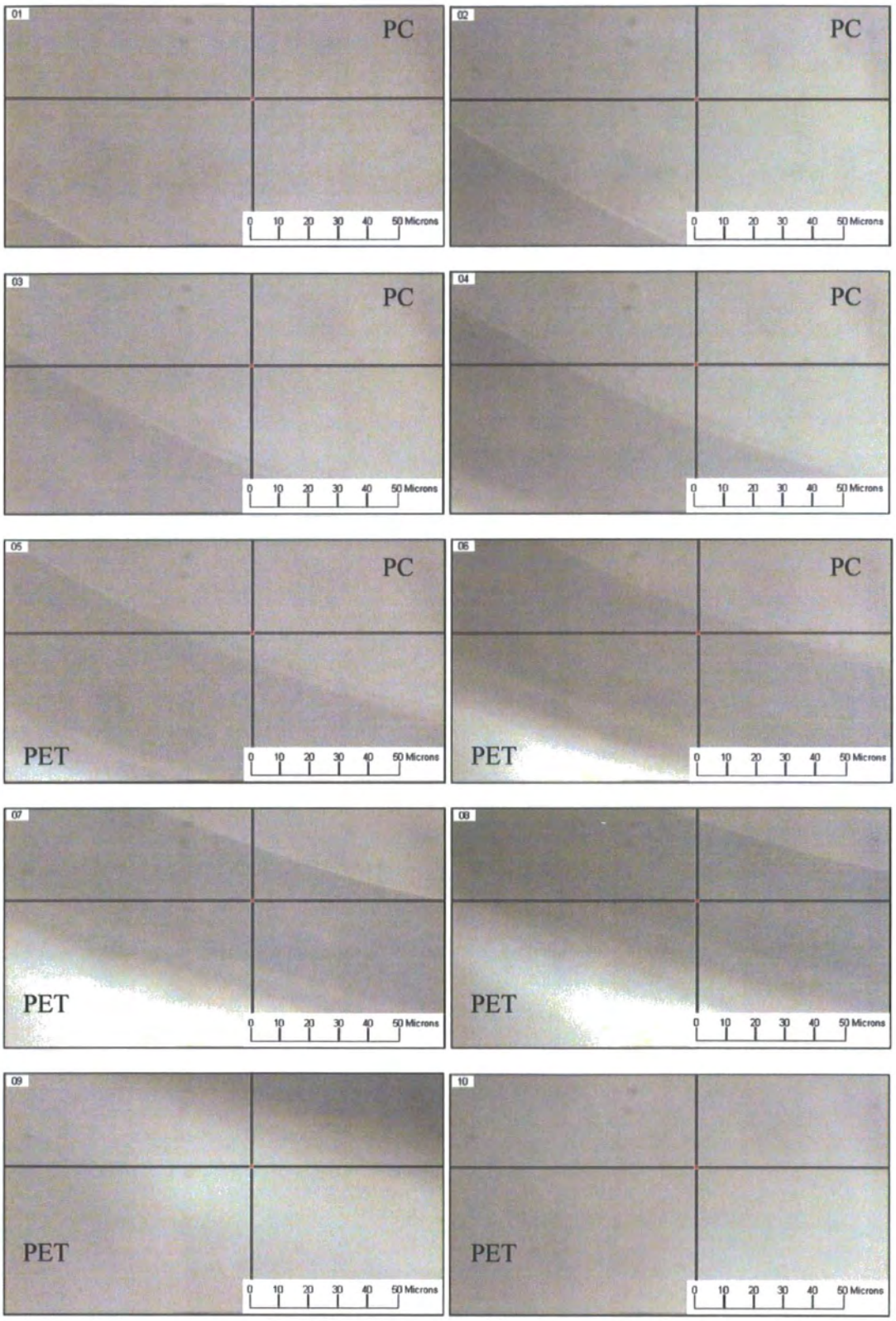

Figure 2.59 Schematic of the points used for 300030

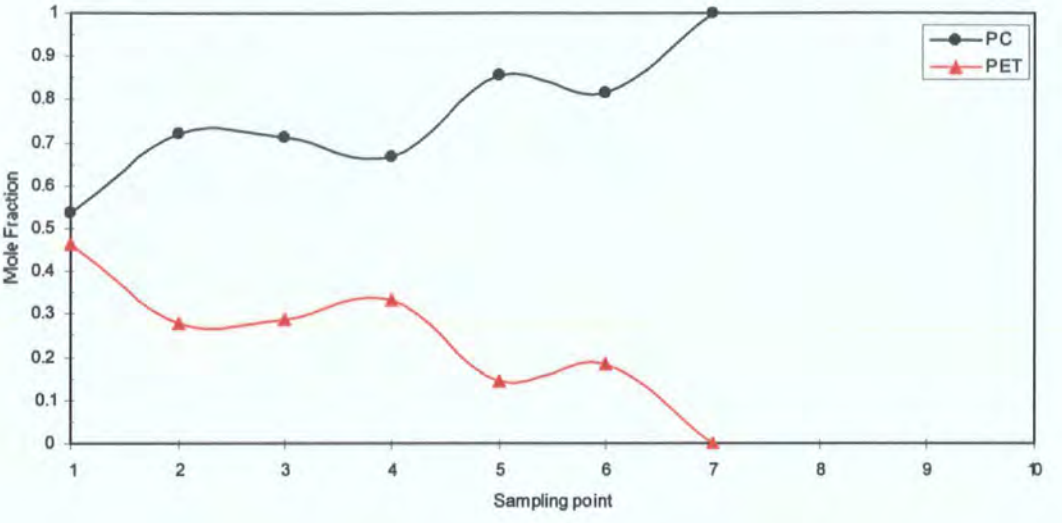

Figure 2.60 PC/PET molar concentration plot for 300030 sample

The 300030 sample contained no crystallites of any kind and as such there was nothing to accurately focus on. Figure 2.60 suggests that the microscope was not focused on the PC bubble and as such the plot is of little practical use. It is interesting to note that on what is effectively a random walk through amorphous copolymer large variations are visible (points 6-10). It was not possible to generate a composite image for Figure 2.59 because there are too few features to correlate.

The Raman results show that crystallization can occur in material made up of up to 30% PC if in a cloudy morphology but only up to 10% in a more densely packed form. The Raman data also suggest that in the early stages of annealing, little PET moves into the PC bubbles but instead PC leaks out of these areas into the surrounding PET. The pictures obtained in both the OM and Raman show that these areas are not uniform around PC bubbles so it may well be that they are highly susceptible to surface tension between the two polymers. It is understandable that PC would be more mobile in the

melt than PET since PC is effectively molten from when PET passes its glass transition temperature (140°C) whereas PET is only molten past 250°C.

2.5 Conclusions

Reaction of PET and PC leads to increased degradation compared with the pure homopolymers, particularly in the presence of low levels of water. In initial studies reaction of solution blended material at 270°C is undetectable by DSC, reaction proceeds quickly at 300°C and best control over crystallinity is achieved when reacting between 280°C and 290°C where reaction proceeds at an appreciable but controllable rate. In later work where water is excluded from the reaction far more thoroughly very little reaction was observed even after the longest holds at the highest temperatures. When using powdered PET/PC it is essential to assume that it is not dry unless it has been stored *in vacuo* since being dried. Given the surface area to volume ratio of a powder such as this it is best to produce samples for testing and then dry them afterwards.

Reaction of melt blended material with a heating time of up to five minutes at a temperature of 285°C or higher causes little reaction and the maximum crystallinity is dictated more or less solely by the proportion of PET in the blend. Solid state polymerization is possible resulting in modest increases in molecular weight but the material produced direct from the extruder is of a comparable molecular weight to PET in most applications.

PET crystallization is inhibited when PC makes up 10% of the blend and crystallization is stopped altogether when PC makes up 30% of the blend. In less strict drying conditions PC is seen to be more mobile than PET and therefore have a greater effect on crystallinity. In strict drying conditions very little movement is observed.

2.6 References

(1) Ravi R. *WO Patent 0192007* **2003.**

(2) Gianni M.; Roberta P. *US Patent 2005171229* **2005.**

(3) Peter F.; Norio K.; Hiroaki O. *US Patent 6872459* **2005.**

(4) Mehta S.; Liu Z.; Huang X.; Schiraldi D. *WO Patent 2005023530* **2005.**

(5) Schiraldi D.; Sekelik D.; Smith B. *Eur Patent 1283234* **2003.**

(6) Smith F. S.; Steward R. D. *Polymer* **1974**, *15*, 283.

(7) Avrami, M. *J. Chem. Phys.* **1939**, *9*, 177.

(8) Evans U. R. *Trans. Faraday Soc.* **1945**, *41*, 365.

(9) Palys L.H.; Phillips P.J. *J. Polym. Sci.: Polym. Phys. Ed.* **1980**, *18*, 829.

(10) Zhang G. Y.; Ma J. W.; Cui B.X.; Luo X. L.; Ma D. Z. *Macromol. Chem. Phys.* **2001**, *202*, 604.

(11) Henrichs P.M.; Tribone J.; Massa D.J.; Hewitt J.M. *Macromolecules* **1988**, *21*, 1282.

(12) Kolb H J.; Izard E.F. *J. Appl. Phys.* **1949**, *20*, 564.

(13) Edgar O.B.; Hill R. *J. Polym. Sci.* **1952**, *8*, 1.

(14) Woods D.W. *Nature* **1954**, *174*, 753.

(15) Progany G.A. *Polymer* **1970**, *11*, 66.

(16) Temin S.C. *J. Polym. Sci.* **1965**, *9*, 471.

(17) Allen G.; McAinsh J.; Jeffs G.M. *Polymer* **1971**, *12*, 85.

(18) Fox T.G. *Bull. Am. Phys. Soc.* **1952**, *1*, 123.

(19) Mishra S.; Zope V.S.; Goje A.S. *J. Appl. Polym. Sci.* **2003**, *90*, 3305.

(20) Alexandrova L.; Cabrera A.; Hernandez M.A.; Cruz M.J.; Abadie M.J.M.; Manero O.; Likhatchev D. *Polymer* **2002**, *43*, 5397.

(21) Devaux J.; Godard P.; Mercier J.P. *Makromol. Chem.* **1978**, *179*, 2201.

(22) Bayer *Makrolon (PC) Product Range, Typical Properties* **2001-06**, 12,19.

(23) Wilkinson A.N.; Tattum S.B.; Ryan A.J. *Polymer* **1997**, *38*, 1923.

(24) Zhang G.Y.; Ma J.W.; Cui B.X.; Luo X.L.; Ma D.Z. *Macromol. Chem. Phys.* **2001**, *202*, 604.

(25) Kong Y.; Hay J.N. *Polymer* **2002**, *43*, 1805.

(26) Zhang Z.; Xie Y.; Ma D. *Eur Polym. J.* **2001**, *37*, 1961.

(27) Ma D.; Zhang G.; He Y.; Ma J.; Luo X. *J. Polym. Sci: Part B: Polym. Phys.* **1999**, *37*, 2960.

(28) Ihm D.W.; Park S.Y.; Chang C.G.; Kim Y.S. *J. Appl. Polym. Sci: Part A: Phys. Chem.* **1996**, *34*, 2841.

Chapter 3

Chemical Properties

3.1 Introduction

As discussed in Chapters 2 and 4, the physical and mechanical properties of a material determine its uses. In a sense, the chemistry is irrelevant as long as the desired macroscopic properties can be achieved. However, PET/PC is produced via a transesterification reaction, one which in other systems has been shown to be mainly end group catalysed.[1] In order to optimise this process and produce a copolymer with the best possible properties it is necessary to understand how this reaction proceeds and to that end the chemistry is essential.

Parameters that need to be known include:

Reaction Kinetics

The level of co-polymerization will affect the T_g and crystallisation of the product and as a result the reaction conditions required to obtain a particular degree of co-polymerization are highly important. If the transesterification reaction is indeed end group catalyzed as reported[2] then some characterisation of the end groups will be necessary. Once a mechanism is established the speed of reaction and how much reactive blending is required to affect the extent of reaction required is necessary also.

Randomness

A high degree of randomness implies a high degree of reaction. This would be ideal if high levels of homogeneity were desirable, for example a homogeneous PET/PC sample would lead to a polymer with a single T_g and no crystallisation. Whilst this might be desirable in materials required to operate above 80°C, this would be undesirable for

materials required to operate at 105°C and above since, with no crystallisation, the sample would become molten. It is desirable to understand the extent of randomness in samples of real material and to correlate these to mechanical properties.

3.2 Theory

3.2.1 Reaction Kinetics

Transesterification reactions have been kinetically analysed in a quantitative fashion using ^{1}H [3-6] and ^{13}C NMR.[4,6-8] NMR is a very powerful tool because it can provide information on the amount of the two monomers present and whether they are in their original environment (within sequences of homopolymer) or a new environment (adjacent to the other monomer unit). The steric and electronic properties of the two homopolymers and the cross product are different and this will have an effect on the degree of electron shielding around the nuclei in the two different environments. Not all the atoms in a given repeat unit will have their electronic structure altered significantly by the change in neighbouring unit, but those that do will produce additional resonances in an NMR spectrum. The intensities of these peaks will be related to the relative number of those units in the different environments. Below is a simple schematic showing the type of reaction that could be expected to occur, followed by the mathematical interpretation of the resulting NMR spectra.

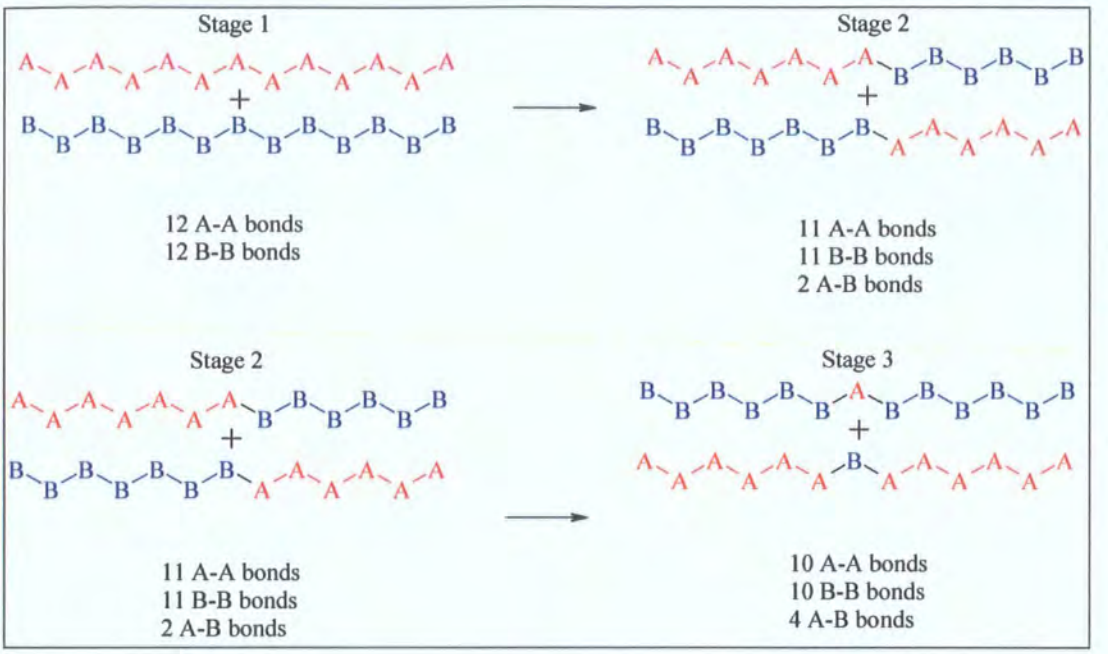

Scheme 3.1 Likely steps in the early stages of a transesterification

If a signal in the NMR spectrum is attributed to an A group next to an adjacent A group then this signal will be seen to diminish over the course of a reaction. Likewise if a signal is attributed to a B group adjacent to another B group it too will reduce in intensity. There must therefore be a signal present for an A group adjacent to a B group which will increase over the course of the reaction. If this is the case then the following will be observed.

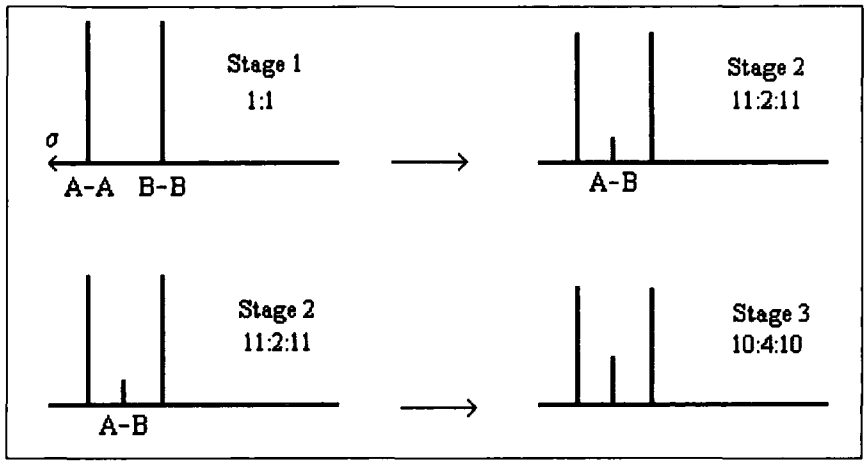

Scheme 3.2 Possible NMR spectra using Fig. 13 as a model

The reaction can be followed simply by using the integrals of the A-A and B-B peaks as measures of the amount of reactant left and the A-B integral as a measure of product.

If the relative integration of A-A bonds and B-B bonds present at t = 0 are *a* and *b* respectively and the integration of A-B bonds at time t is taken as *2x* then the integration of A-A and B-B bonds at time t are *a-x* and *b-x* respectively. This is summarised below.

PET—PET	+	BPA—BPA	⇌	PET—BPA	+	BPA—PET
t = 0 a		b		0		0
t > 0 a-x		b-x		x		x

Scheme 3.3 Mole fractions of reactants and products in transesterification

3.2.2 First Order in PET-PET

If the reaction proceeds at a rate proportional to the concentration of PET-PET bonds still in the system then the integrated rate equation can be derived thus:

$$-\frac{d[A-A]}{dt} = k[A-A]$$

$$-\int_{t=0}^{t=t} \frac{d[A-A]}{[A-A]} = k\int_{0}^{t} dt$$

$$\left[-\ln[A-A]\right]_{t=0}^{t=t} = kt$$

$$t=0, [A-A] = a$$

$$t=t, [A-A] = (a-x)$$

$$-\ln(a-x) - (-\ln a) = kt$$

$$\ln\frac{a}{a-x} = kt \qquad \textbf{Equation 3.4}$$

So a plot of the $\ln(a/(a\text{-}x))$ verses t will be a straight line if indeed the reaction is first order in PET-PET bonds.

3.2.3 First Order in PC-PC

This is effectively the same as for the PET-PET case therefore:

$$\ln(\frac{b}{b-x}) = kt \quad \textbf{Equation 3.5}$$

in the case of a reaction which is first order in PC-PC bonds. A plot of $\ln(b/(b\text{-}x))$ against t will be a straight line if the reaction is first order in PC-PC bonds.

3.2.4 Irreversible Second Order

In this case the reaction is first order in both reactants meaning it is second order overall. If this is irreversible the integrated rate equation can be obtained thus:

$$\frac{dx}{dt} = k_1[A-A][B-B]$$

$$\frac{dx}{dt} = k_1(a-x)(b-x)$$

$$\int_{t=0}^{t=t} \frac{dx}{(a-x)(b-x)} = k_1 \int_0^t dt$$

This is a standard integral which yields,

$$\frac{1}{(b-a)} \ln \frac{[b\times(a-x)]}{[a\times(b-x)]} = k_1 t \quad \textbf{Equation 3.6}$$

So a plot of the left hand side of Equation 2.19 against time will yield a straight line, the gradient of which is k_1 if the reaction is irreversible and first order in PC-PC bonds and PET-PET bonds.

3.2.5 Reversible Second Order[9]

The reaction may also be reversible and first order in both reactants. In this case the integrated rate equation can be obtained by the following method.

$$\frac{dx}{dt} = k_1[A-A][B-B] - k_{-1}[A-B]^2$$

$$\frac{dx}{dt} = k_1(a-x)(b-x) - k_{-1}x^2$$

At equilibrium:

$$\frac{dx}{dt} = 0$$

$$\Rightarrow k_1(a-x_{eq})(b-x_{eq}) = k_{-1}x_{eq}^2$$

$$k_1[ab-(a+b)x_{eq}+x_{eq}{}^2] = k_{-1}x_{eq}^2$$

Equating polynomial terms:

$$k_1 x_{eq}{}^2 = k_{-1} x_{eq}^2$$
$$\Rightarrow k_1 = k_{-1}$$

This can be substituted into the original equation:

$$\frac{dx}{dt} = k_1(a-x)(b-x) - k_1 x^2$$
$$\frac{dx}{dt} = k_1(ab-(a+b)x+x^2) - k_1 x^2$$
$$\frac{dx}{dt} = k_1(ab-(a+b)x)$$

a and b are the mole fractions of PET and PC at $t = 0$ therefore,

$$a+b=1$$
$$\Rightarrow \frac{dx}{dt} = k_1(ab-x)$$
$$\int_{t=0}^{t=t} \frac{dx}{(ab-x)} = k_1 \int_o^t dt$$
$$[-\ln(ab-x)]_{t=0}^{t=t} = k_1 t$$

At $t = 0$, $x = 0$ therefore,

$$-\ln(ab-x) - (-\ln(ab-0)) = k_1 t$$
$$\Rightarrow \ln(ab/(ab-x)) = k_1 t$$
or,
$$\ln(b/(b-r)) = k_1 t \qquad \textbf{Equation 3.7}$$

Where r is the transesterification ratio = x/a. Again in this case a plot of $\ln(b/(b-r))$ against time will give a straight line, the gradient of which will be the rate constant for the forward reaction and this will also be equal to the rate constant for the backward reaction.

It has been shown that transesterification between polyesters and other polyesters or polycarbonates is a reversible second order process.[10] A table of reaction activation energies obtained is given below.

Table 3.8 Literature activation energies for transesterification systems

Blend	Comp. (w/w)	Conditions	E_a/kJ mol^{-1}	Ref
PET/PC	50:50	Blended at 533K for 10 minutes, 10^{-6} mol g^{-1} $Ti(BuO)_4$*, T = 243.5-278.5°C	130	9
POB-PET/PC	50:50	Solution blended, T = 260-280°C	175	10
POB-PET/PC	50:50	"	396	10
PET/PEN	100:0	Solution blended, T = 270-300°C	159±30	1
	75:25	"	158±10	1
	50:50	"	176±2	1
	25:75	"	127±20	1
	0:100	"	93±9	1
PET/LCP	70:30	Blended at 290°C for five minutes, BOZ used as catalyst*, T = 270-290°C	84.4	11
PBT/PC	50:50	Blended at 260°C for ten minutes, 0.15% $Ti(BuO)_4$* T = 224.5-253°C	131	12
	50-50	Blended at 260K for ten minutes, T = 224.5-253°C	249	13

*** See the introduction in chapter 1 for details on $Ti(BuO)_4$ and BOZ**

3.2.6 PBT/PC

The polyester/polycarbonate blend of PBT and PC has been studied and integrated ^{13}C NMR spectra have been published.[7,11] The samples in one study were 50:50 by weight and were held at 253°C for different lengths of time. These data were not plotted in the original paper but are shown here according to Equation 3.7. In this case, *b* is equal to the relative amount of PC at $t = 0$, *a* is equal to the amount of PBT at $t = 0$ and *x* is the concentration of the cross product at time *t*. The data used are in the Appendix I, Table VII.

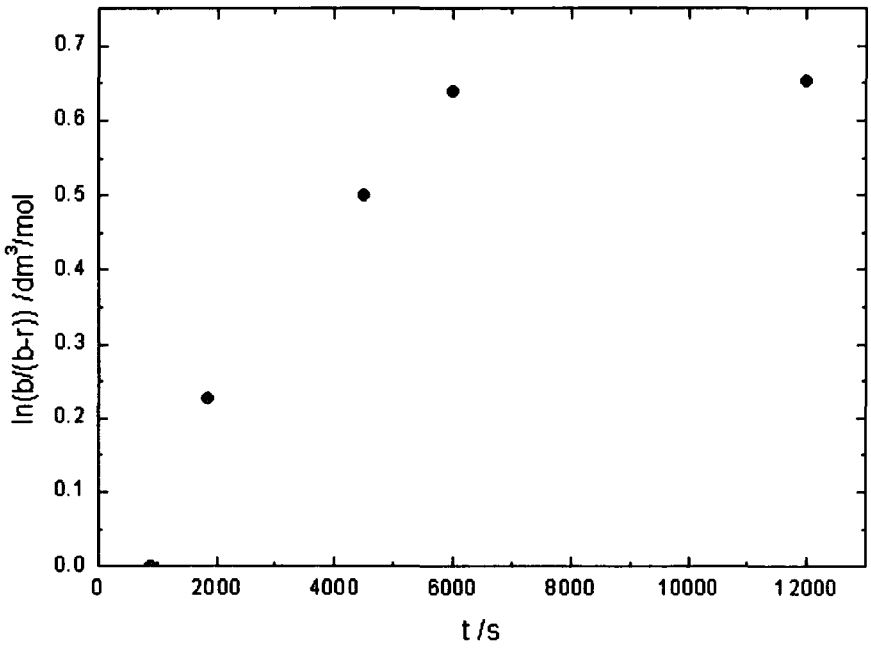

Figure 3.9 Second order plots of literature data obtained from 50:50 blends of PBT/PC at 253°C.[11]

The graph in Figure 3.9 shows analysis of the PBT/PC blend. It is clear there is an induction period of around 15 minutes applicable to this reaction. The data show that no reaction occurs during this time. The reaction appears to be at equilibrium, i.e. a totally

random polymer has been formed after some 6000 seconds and so the reaction co-ordinate remains constant for the next 6000 seconds. The research reports no additional reactions found, no gas evolved and the polymer produced was white.

3.2.7 PET/PEN

The transesterification of PET and poly(ethylene naphthalene-2,6-dicarboxylate) (PEN) has been thoroughly investigated.[12-15] The reaction leads to a change in the chemical environment of the ethylene glycol protons that can be followed by proton NMR.[13,15] The chemical shifts of the three different environments are shown below.

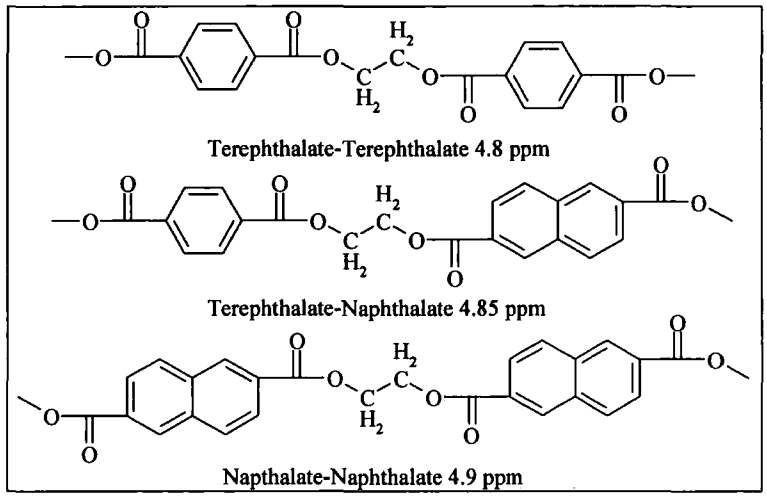

Figure 3.10 Aromatic ^{1}H chemical shifts of PET, PEN and PET/PEN copolymer

Using the relative amounts of PET-PET bonds and PEN-PEN bonds at $t = 0$ as a and b respectively and the relative amount of PEN-PET at time t as x, the following graph can be plotted according to Equation 2.20 which suggests the transesterification of PET/PEN is a second order reversible process.[13]

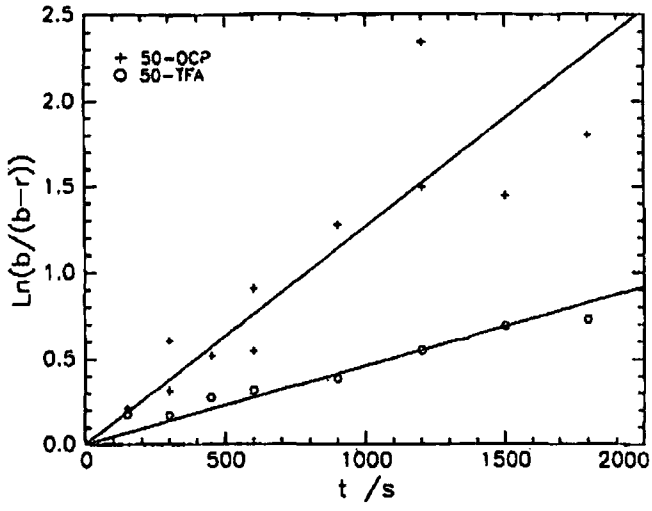

Figure 3.11 Second order plot of NMR data of 50:50 PET/PEN (50-OCP prepared via solution blending 50-TFA produced by solution blending and then end-capped using TFA) and annealed for various times at 300°C under nitrogen[13]

3.3 Experimental

3.3.1 Transesterification

Initial work on 50:50 PET/PC work was carried out as described in 2.3, transesterification being effected by TGA before ^{1}H NMR as laid out below.

Later work, involving more rigorous drying, was carried out on solution blended analogues of the fifteen blends made by extrusion. Preparation of the blends was also in line with 2.3.3.

Transesterification of each blend was carried out simultaneously in an aluminium block (shown in Figure 3.12) of dimensions 100 mm by 200 mm by 15 mm. Holes were drilled in the block (10 mm diameter, 8 mm deep) allowing all fifteen blends to be reacted at once. The PET/PC samples themselves were prepared as described in 2.3.3 but the exact composition varied.

Figure 3.12 Sample block for annealing in vacuum oven

Before reacting, samples were dried at 160°C *in vacuo* for three hours. The whole block was then removed and placed inside a vacuum desiccator whilst the oven was brought up to reaction temperature. Once the oven had equilibrated at the required reaction temperature, the block was removed from the desiccator and placed in the oven which was then evacuated. The duration of the reaction was timed from the when the oven door was closed and the re-pressurisation timed such that the door was opened when the desired reaction time had been reached. The block was then returned to the vacuum desiccator to cool in vacuo and the samples were stored individually once they had cooled to room temperature.

3.3.2 NMR

In order to obtain NMR of the samples, the pans were broken open using clean tweezers and the contents were left to dissolve in a vial containing 1 ml of the 4:1 dDCM/dTFA NMR solvent used. When no sign of the polymer remained in the aluminium pan, the solution was pipetted into an NMR tube which was then analysed by 400 MHz NMR.

3.3.3 End Group Analysis

End group analysis was carried out by the ICI Measurement Science Group, Wilton, Redcar. For this work samples *Base* and *Laser* were supplied in chip form and samples of the same were dissolved in DCM:TFA 4:1 for five days. The solutions were allowed to evaporate after this time and the residual powder collected. The four samples made of *Base* and *Laser* were studied by NMR and the number of hydroxyl end groups determined by integration.

3.4 Results and Discussion

3.4.1 NMR Assignment

Both ^{1}H and ^{13}C NMR spectroscopies have been used to follow the transesterification reaction. Below are the assignments for both the spectra obtained from the unreacted blend.[16]

Table 3.13 Chemical shifts in ^{1}H NMR spectra of unreacted PET/PC blends

Shift /ppm	Atom
1.6	a
4.7	e
5.2	DCM
7.0-7.2	b and c
8.0	d
10.6	TFA

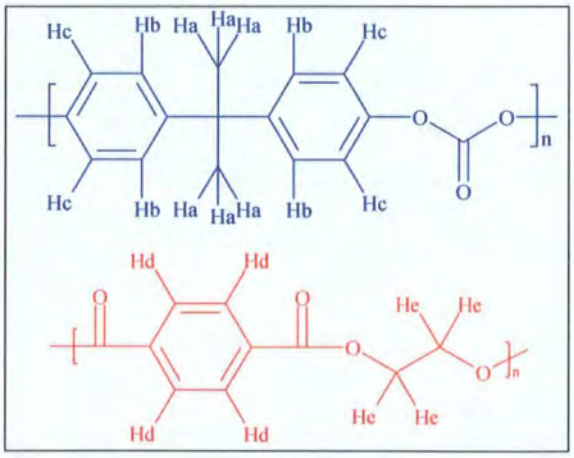

Figure 3.14 Notation for use in Table 3.13

The DCM peak is very small and can be attributed to hydrogenous impurities in the dDCM. The TFA peak is very large indeed and cannot be attributed to impurities. A

likely explanation is that the acid group in the dTFA is capable of proton exchange with the end groups on PET and PC but also with any moisture in the air which dissolves into the NMR solvent. The intensity of this peak indicates that 0.6% of the TFA used as a solvent has been protonated by either the polymer end groups or atmospheric water.

Table 3.15 Chemical shifts in ^{13}C NMR spectra of unreacted PET/PC blends

Shift/ppm	Atom
30.6	a
42.9	b
52.9-53.8	m
64.2	i
111.1-118.0	n
120.6	d or e
128.5	e or d
130.3	k
133.7	j
148.9	f or g
149.5	g or f
156.6	c
160.5-161.1	o
168.1	h

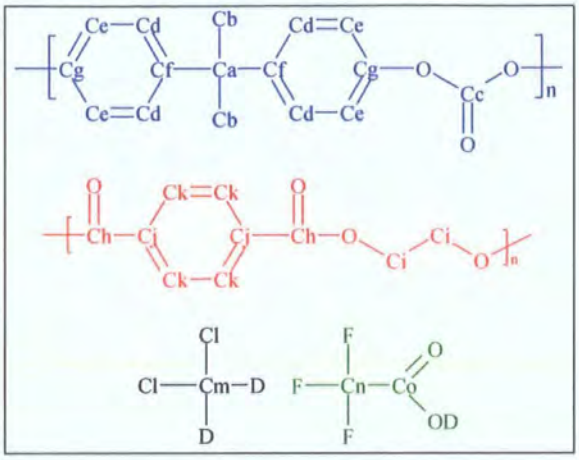

Figure 3.16 Notation for use in table 3.15

PET contains symmetric ethylene glycol (EG) units where adjacent units are both terephthalate. After transesterification, the EG is asymmetric and the protons on it are therefore in a different chemical environment. It is possible to see the effect below.

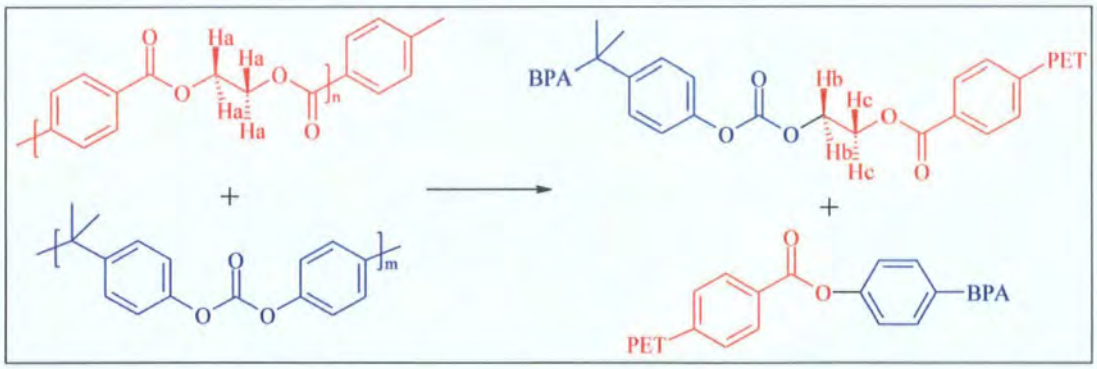

Scheme 3.17 Effect of initial reaction on the aliphatic protons in PET

H_a is the proton environment in raw PET. H_b and H_c are produced in equal measure when an EG unit has a PC unit transesterified onto one end. This unit is still free to react again, either by going back to the initial state or by reacting with another PC unit. The latter case is illustrated below.

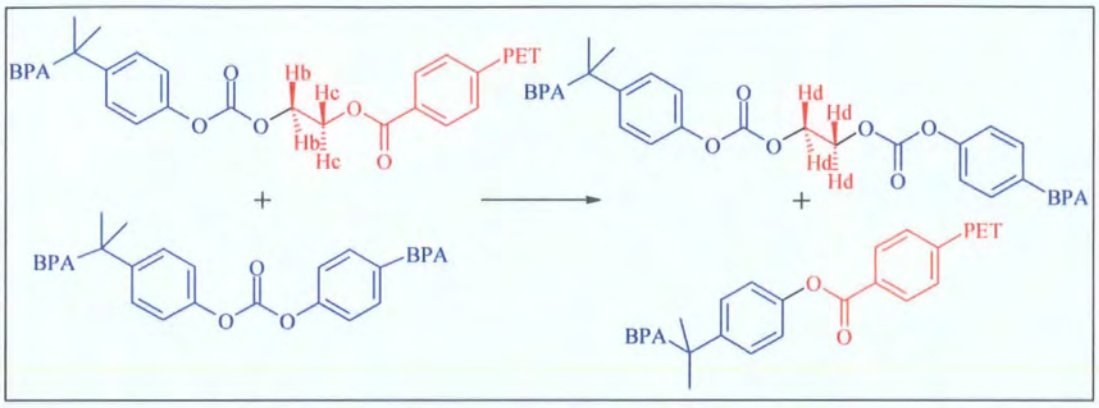

Scheme 3.18 Effect of further reaction on the aliphatic protons of PET

H_d is the environment produced when an EG unit which has PC units transesterified onto both ends. The effect of these reactions on the NMR spectra is shown below.

3.4.2 ^{1}H NMR Analysis

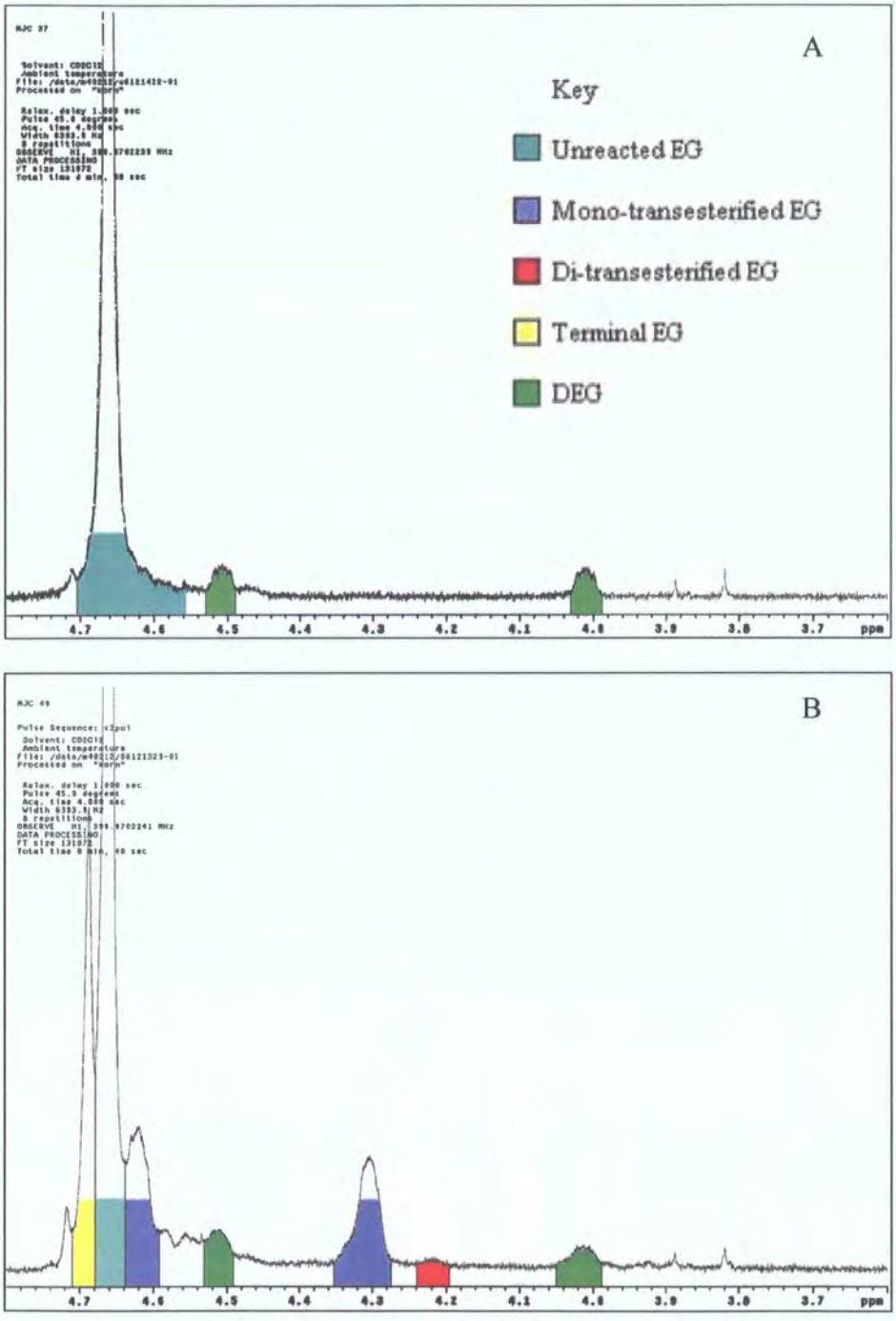

Figure 3.19 ^{1}H NMR spectra of unreacted PET/PC (A) and PET/PC, which have been annealed at 300°C for 1 hour (B)

Figure 3.19 shows two ^{1}H NMR spectra illustrating the change observed after one hour at 300°C. The most obvious difference is the presence of two peaks attributed to the asymmetric EG produced (EG*). There is a new peak visible in spectrum B at 4.33 ppm which corresponds to the EG* proton pairs adjacent to the carbonate group. The pair still bonded to a terephthalate group is visible at 4.62 ppm. This can be compared with the size of the peak corresponding to the unreacted EG, which is the large peak between 4.64 and 4.7 ppm. Care must be taken to avoid including the peak, which grows out of the side of this EG peak on the down field side. This has been attributed to esterification of end groups after the sample has been dissolved in the 1:4 dTFA:dDCM which is used as a solvent.[17] It is clear from the size of this peak with extending reaction times that the transesterification process significantly increases the number of chain ends; i.e. the molecular mass is falling. This is discussed in more detail later in 3.4.5.

There are many variations of the PC-EG-PET, PC-EG-PC and PET-EG-PET motifs that appear in the main reaction. This is because, as stated in the introduction, there are a number of different side reactions which are known to occur and also, as mentioned in the experimental section, the PET used is made up of 2% IPA. This explains why the three peaks corresponding to mono and di-substituted EG are wide and not sharp.

3.4.3 ^{13}C NMR Analysis

It is also possible to see the effect on the EG region by ^{13}C NMR; this is illustrated in Figure 3.20. Spectrum A shows the single peak corresponding to the symmetrical EG carbons in the unreacted polymer. Spectrum B shows PET/PC that has been held at 300°C for two hours. The main peak is still visible but there are also two smaller peaks corresponding to the two asymmetrical EG* carbons. There is the hint of a third peak at around 66.75 ppm which may correspond to the symmetrical di-transesterified EG carbons but this peak is very small in comparison to the baseline so no such assumptions have been made.

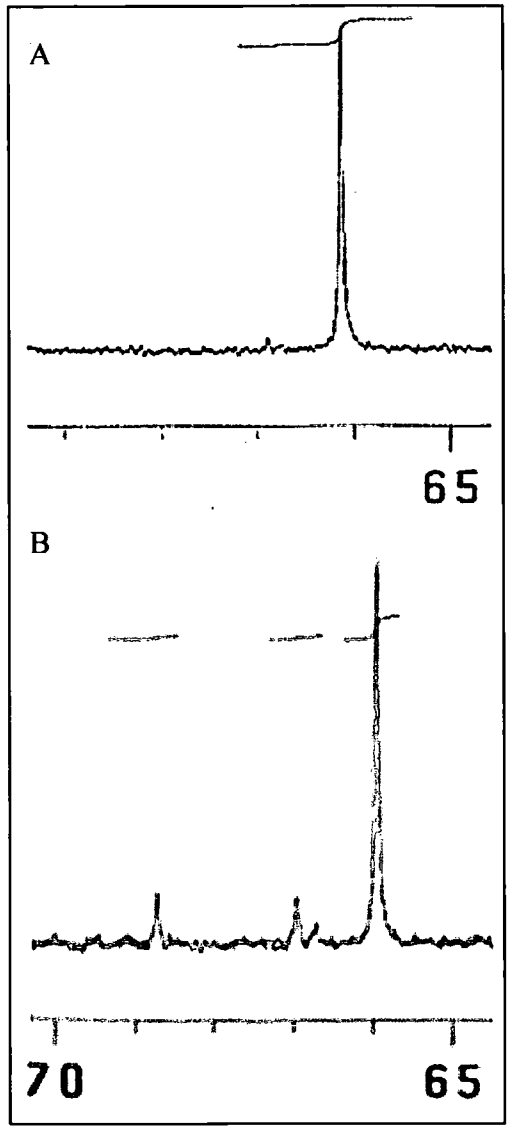

Figure 3.20 ^{13}C NMR spectra of unreacted PET/PC (top) and the same blend annealed for 2 hours at 300°C

Analysis of the data obtained using both ^{1}H and ^{13}C NMR has been performed to confirm that the deductions made are indeed correct. The mole fraction of EG* relative to all the EG present was calculated for both sets of data. The results are presented in Table 3.21.

Table 3.21 Mole fractions of EG* in PET/PC blends held for two hours at 300°C

t /s	Mole fraction EG*	
	^{1}H data	^{13}C data
0	0	0
900	0.0094	0
1800	0.040	0.076
2700	0.077	0.078
3600	0.15	0.15
5400	0.17	0.21
7200	0.23	0.23

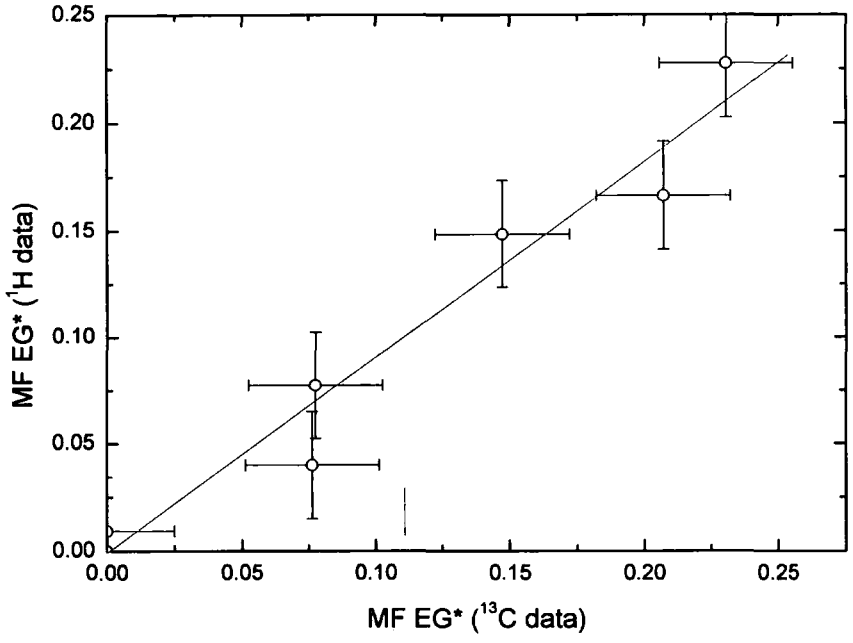

Figure 3.22 A plot of the mole fraction of EG* as obtained from ^{13}C and ^{1}H NMR data

The graph above shows that the data for both the ^{1}H and ^{13}C NMR are consistent with what one would expect to see if both sections of the respective NMR plots corresponded

to the EG region. On the basis of this evidence the kinetic and randomness data are presented below using the 4-5 ppm region of the ^{1}H spectra. ^{13}C data are not used since a ^{13}C NMR spectrum takes around twelve hours to acquire because of the low natural abundance of ^{13}C, whereas ^{1}H NMR spectrum takes 40 sec to acquire. Even after twelve hours the ^{13}C spectra typically exhibit far poorer signal to noise than ^{1}H spectra.

In the analysis of ^{1}H NMR spectra that is detailed below, the area of the new peak at 4.33ppm is taken as proportional to half the total amount of EG* protons and the main peak between 4.64 and 4.7 ppm is proportional to the amount of symmetric EG protons remaining. The former can be related to x (see Scheme 3.3) and the latter can be related to a-x. The amount of b-x is then calculated using the data on how much EG remains and relating that to the stoichiometric amounts of PET and PC that exist in the bulk.

3.4.4 Kinetics

The ^{1}H NMR data taken from the EG region of the spectra are plotted below using Equations 3.4-3.7 and the information in the previous section. The data and calculations used to obtain these plots are contained in the Appendix I in Table VIII A-D.

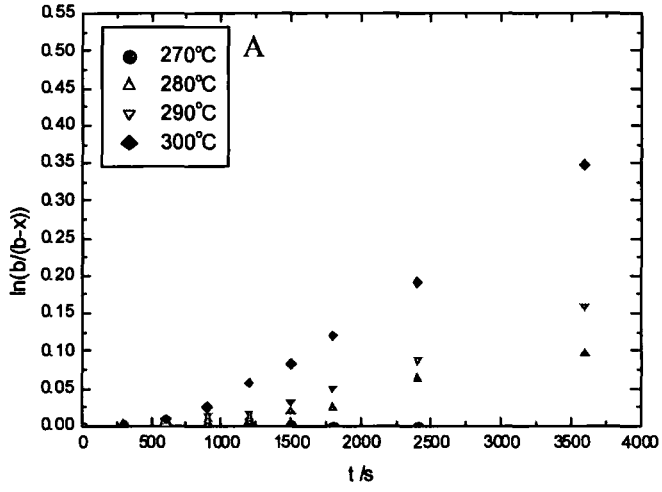

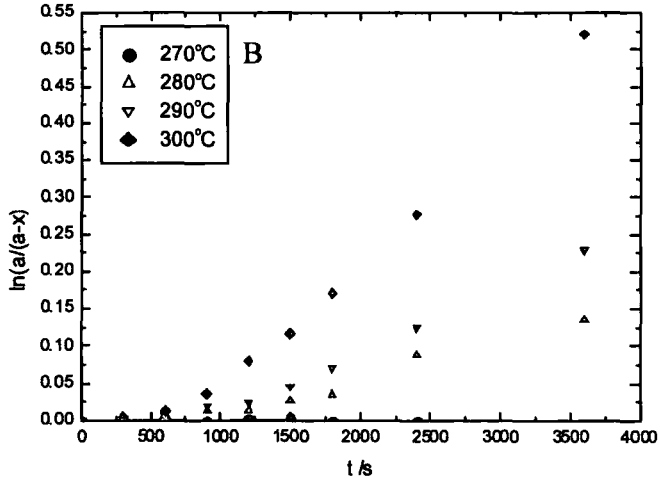

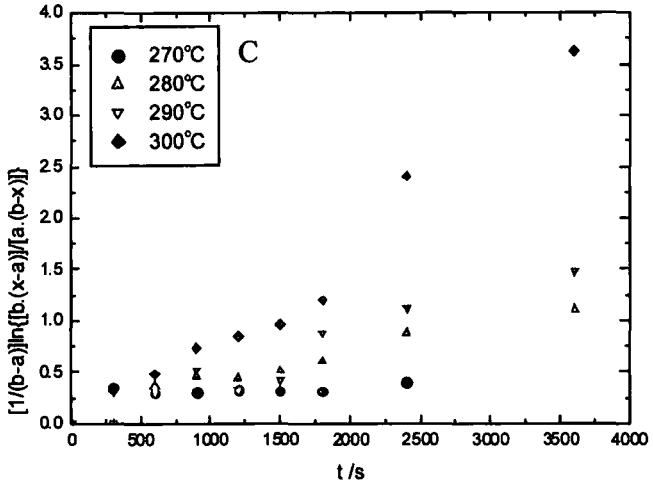

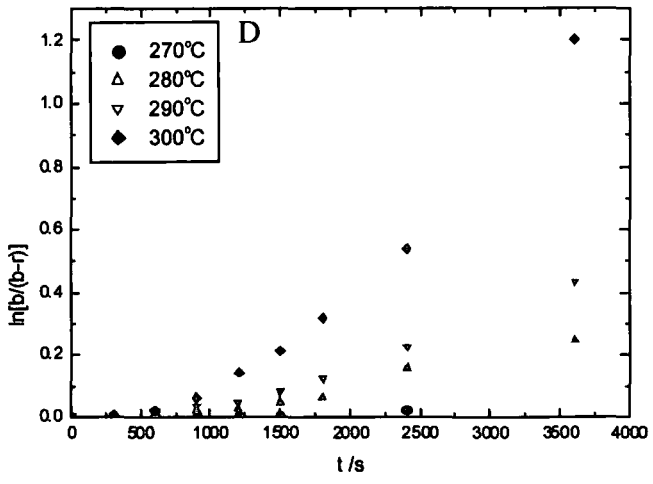

Figure 3.23 Plots of ^{1}H NMR data treating the reaction as first order in PET (A), first order in PC (B), irreversible second order (C) and reversible second order (D)

Plots A, B and D above show a linear section after an induction time of 900s. This suggests there is a reversible second order reaction occurring. It is possible to extract a gradient from the plot from t = 900 s onwards, the gradient being the second order rate constant for the reaction.

Figure 3.24 shows data plotted according to the second order reversible integrated rate law and linear least squares fits for the seven temperatures for the 50:50 blend of PET/PC.

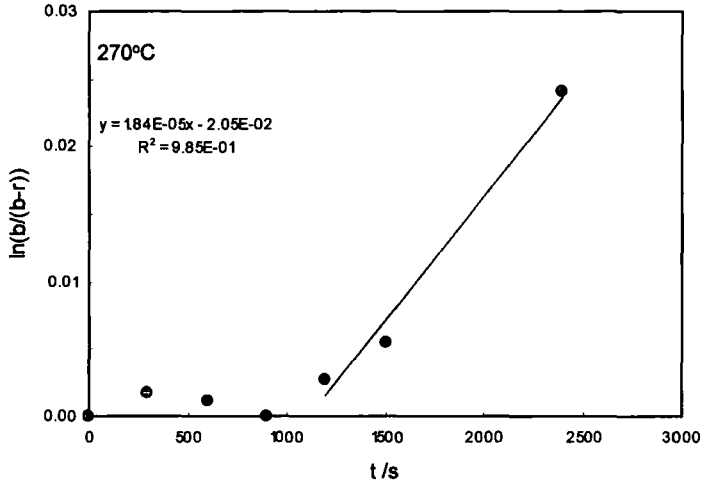

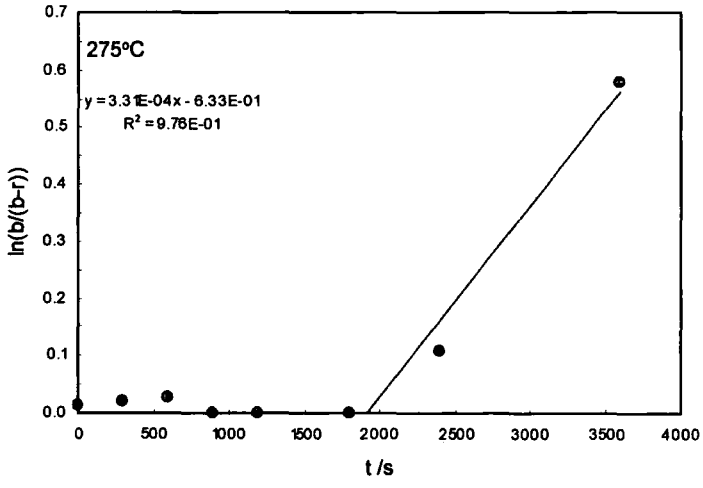

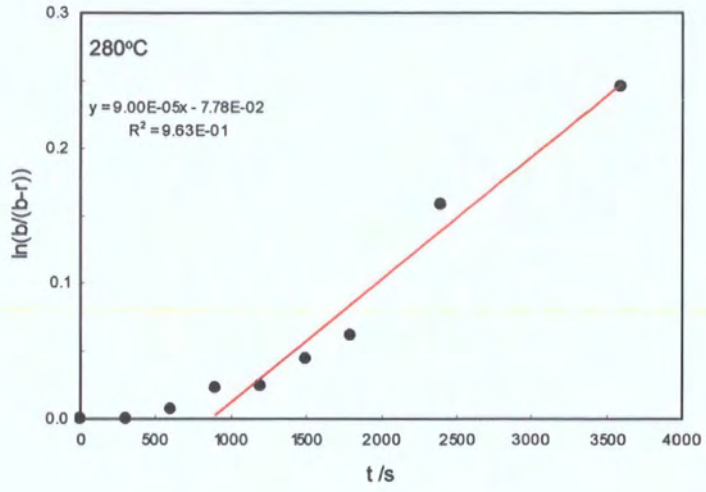
280°C
y = 9.00E-05x - 7.78E-02
R² = 9.63E-01
ln(b/(b-r))
t /s
0.0
0.1
0.2
0.3
0
500
1000
1500
2000
2500
3000
3500
4000

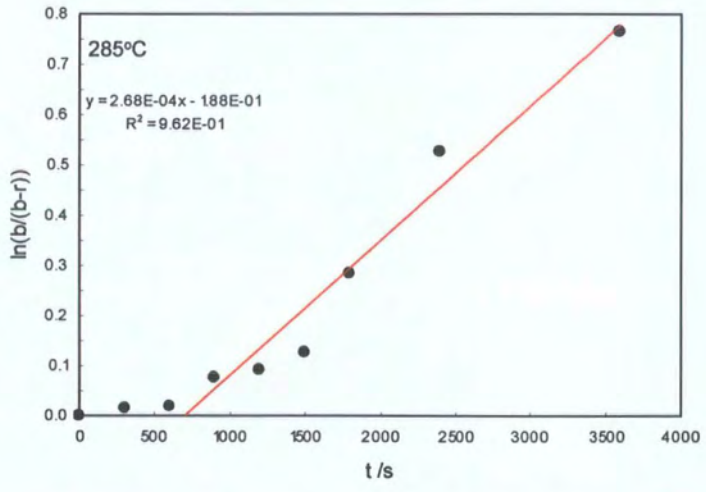
285°C
y = 2.68E-04x - 188E-01
R² = 9.62E-01
ln(b/(b-r))
t /s
0.0
0.1
0.2
0.3
0.4
0.5
0.6
0.7
0.8
0
500
1000
1500
2000
2500
3000
3500
4000

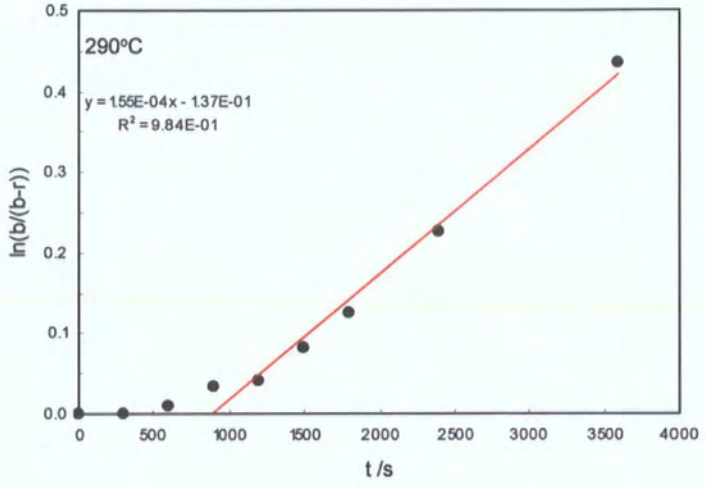
290°C
y = 1.55E-04x - 1.37E-01
R² = 9.84E-01
ln(b/(b-r))
t /s
0.5
0.4
0.3
0.2
0.1
0.0
0
500
1000
1500
2000
2500
3000
3500
4000

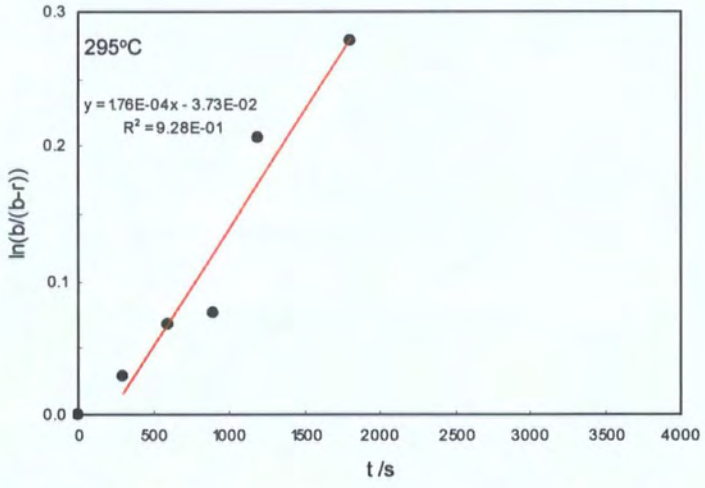
295°C
y = 1.76E-04x - 3.73E-02
R² = 9.28E-01
ln(b/(b-r))
t /s
0.3
0.2
0.1
0.0
0
500
1000
1500
2000
2500
3000
3500
4000

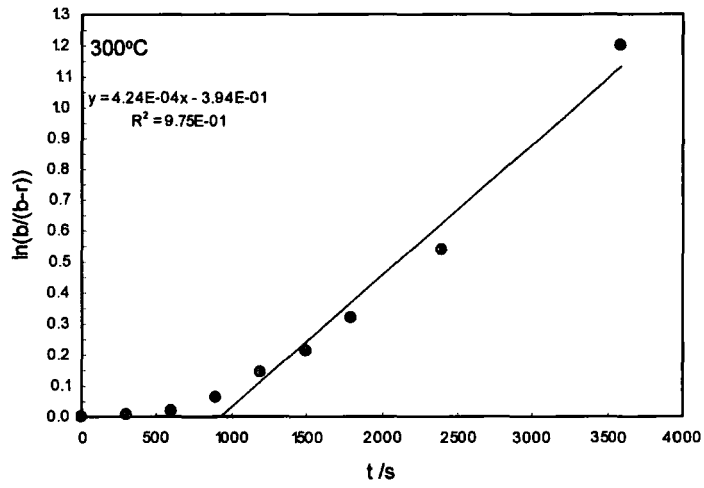

Figure 3.24 Second order reversible plot of ^{1}H NMR data obtained by annealing samples of 50:50 PET/PC samples at 270°C-300°C

Table 3.25 Apparent rate constants from least squares fitting of the plots in Figure 3.24

T /°C	k /s^{-1}
300	4.24×10^{-4}
295	1.76×10^{-4}
290	1.55×10^{-4}
285	2.68×10^{-5}
280	9.00×10^{-5}
275	3.31×10^{-5}
270	1.84×10^{-5}

An Arrhenius plot is shown in Figure 3.26 using the rate constants in Table 3.25 taken from Figure 3.24.

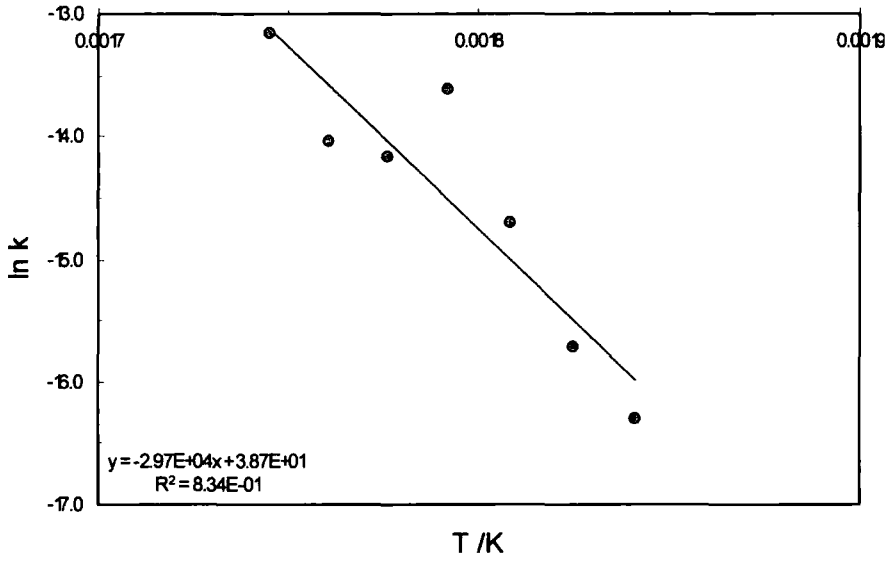

Figure 3.26 An Arrhenius plot of data from Figure 3.24

From the graph above it is possible to conclude that the reaction between PET and PC in the temperature range 270 to 300°C is a reversible second order process and the activation energy associated with the process is 245 kJ mol^{-1}. Table 3.8 lists activation energies for various blends produced and reacted in different ways. Many of the values shown are far lower than 245 kJ mol^{-1} but the work here is quite different from the literature. The earlier research into PET/PC[10] has an activation energy of only 130 kJ mol^{-1}, however this blend is produced by heating for six minutes at 270°C on a two roll mill whilst catalyst was added (TBOT). The polymer was then compression moulded for a further five minutes at 270°C and then granulated. No comment is made as to whether the atmosphere used is inert so one must assume it is not which may lead to decomposition or degradation of the polymer before transesterification has begun. The presence of catalyst and possible degradation products could significantly change the activation energy of the system.

Work on PBT/PC states that the catalysed reaction has an activation energy of 131 kJ mol^{-1} but the uncatalysed reaction has one of 249 kJ mol^{-1} and this is in good agreement with the value obtained in this work.

Further investigations were carried out with more thoroughly dried material as described in 3.3.1. The samples for these reactions were the same as were used in the original reactions, nonetheless it was impossible to obtain kinetic information from the spectra obtained. Whilst in the original reactions, the peak in the EG section of the spectra corresponding to EG* was of a significant intensity, the same peak in the more thoroughly dried material showed such a low level of transesterification that it was impossible to discern the EG* peak from the base line since it coincided with the DEG peaks. In the previous work, the peaks overlapped somewhat but after fifteen minutes of annealing or more for samples reacted at 280°C or more the EG* peaks were clearly visible over and above the peaks for DEG. As is illustrated in Figure 3.27, this is not the case and the two spectra show practically no differences despite the bottom one being the ^1H NMR spectrum for a 50:50 blend of PET and PC annealed at 300°C for an hour. In previous work this would be expected to show a randomness of 0.8 (see Figure 3.32). In reactions using thoroughly dried material held at temperatures of up to 300°C for up to an hour, the process can be thought simply to be a physical blending.

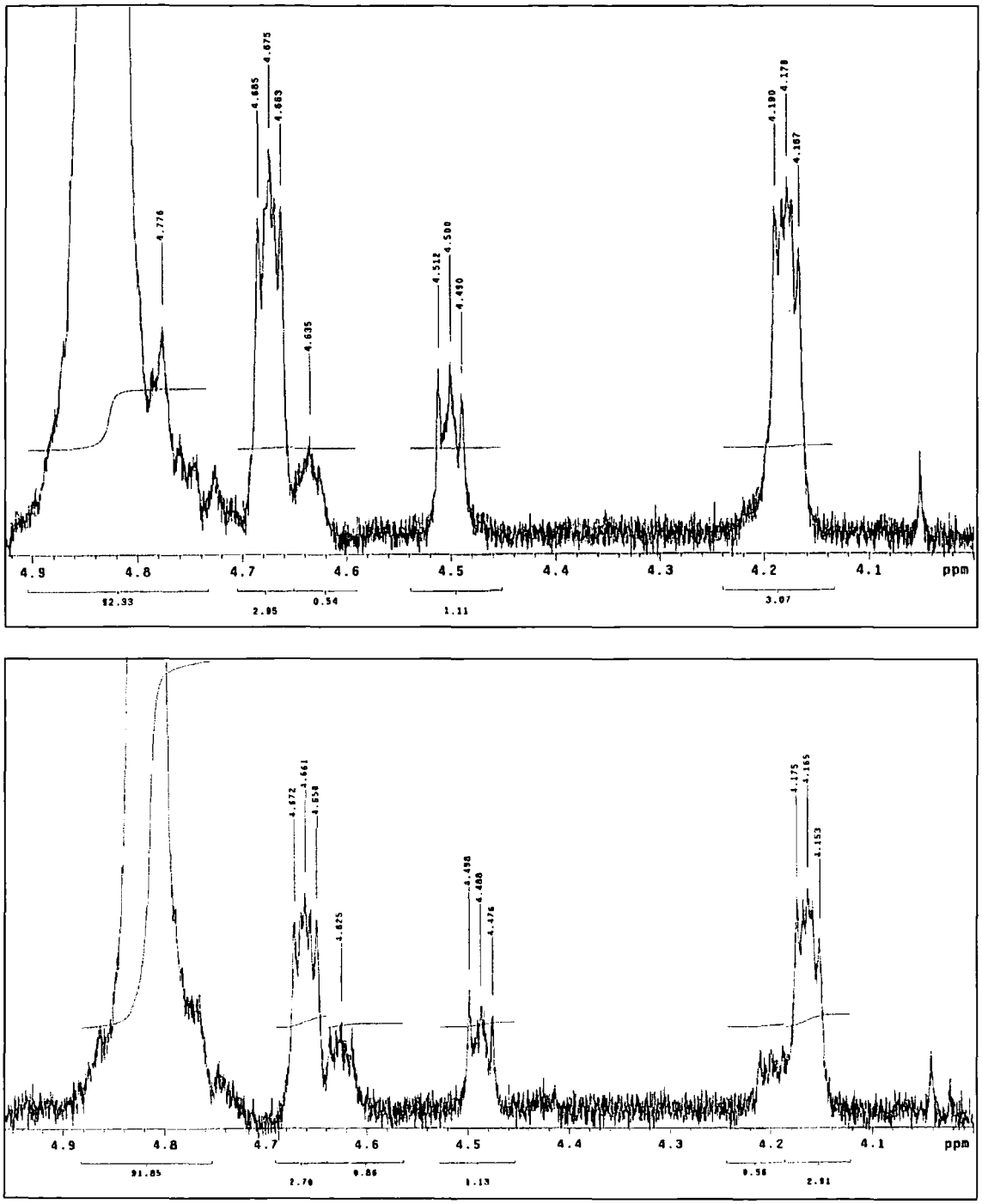

Figure 3.27 ^{1}H NMR (EG region) of Raw PET/PC blend (top) and PET/PC which has been annealed for 1 hour at 300°C (with rigorous drying)

3.4.5 Randomness

Initial transesterification leads to the formation of block copolymers that become increasingly random as the extent of reaction increases. The randomness of the polymer chain can be assessed by ^{1}H NMR using the following formulae:[18,19]

$$P_{PET-BPA} = \frac{(I_{PET-BPA})/2}{(I_{PET-BPA})/2 + I_{PET-PET}} \quad \textbf{Equation 3.28}$$

$$P_{BPA-PET} = \frac{(I_{BPA-PET})/2}{(I_{BPA-PET})/2 + I_{BPA-BPA}} \quad \textbf{Equation 3.29}$$

$$B = P_{PET-BPA} + P_{BPA-PET} \quad \textbf{Equation 3.30}$$

P_{x-y} is the probability that an *x* unit will be adjacent to a *y* unit. I_{x-y} is the intensity of the signal showing that an *x* unit is next to a *y* unit. B is the degree of randomness derived using Bernoulli statistics. When B = 0 the system is made up of a mixture of the two homopolymers with no interchange. When B = 1 the chain is completely random and when B = 2 the chains are made up of strictly alternating units.

The number average length of homopolymer sequence length (L_{x-y}) contained in the polymer can be obtained from P_{x-y} by the following relationship: [18,19]

$L_{x-y} = 1/P_{x-y}$ **Equation 3.31**

In processing the NMR data two assumptions have been made:

1. All ethylene glycol units are adjacent to two units which are either terephthalate or bisphenol units.
2. The proportion of bisphenol groups adjacent to bisphenol groups is equivalent to the stoichiometric proportion at the start less the number of ethylene glycol units that are adjacent to bisphenol units at time t.

The second assumption is necessary because whilst there is a clear peak available for integration for both the terephthalate-ethylene glycol-terephthalate (TET) and terephthalate-ethylene glycol-bisphenol (TEB) units there is no peak available attributable to the amount of bisphenol still adjacent to a bisphenol group (BEB). This introduces a statistical error that results from variations in mixture composition.

On the basis of these assumptions the randomness has been calculated over the first hour of reaction at 270, 280, 290 and 300°C. The results are given in Figure 3.31; tables of these data are in the Appendix I, Tables XI A-D.

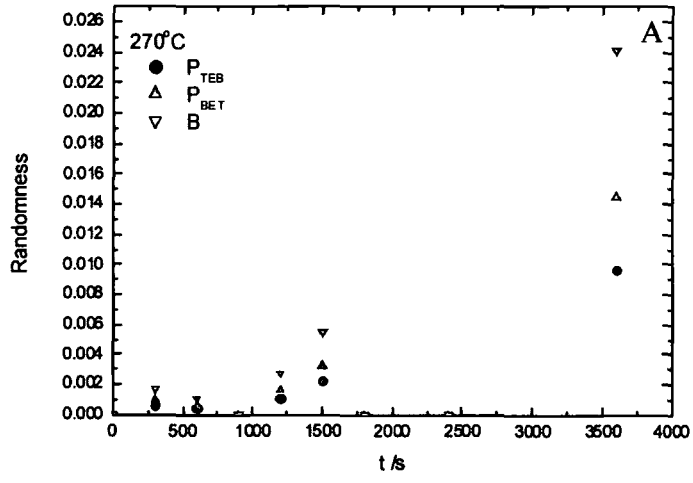

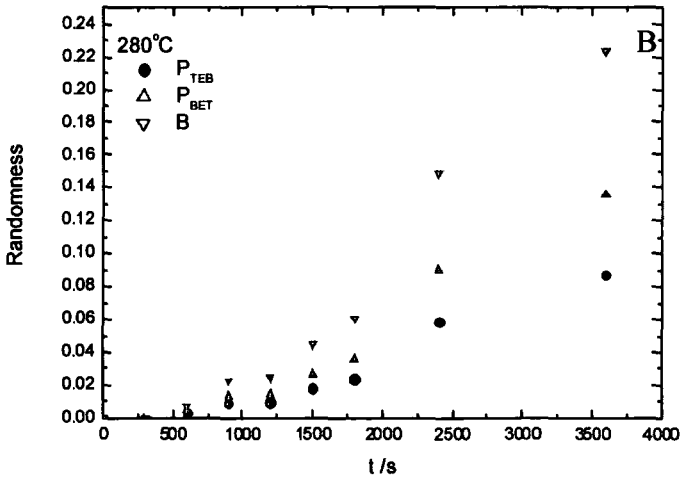
280°C
P_{TEB}
P_{BET}
B
B
Randomness
t /s
0.24
0.22
0.20
0.18
0.16
0.14
0.12
0.10
0.08
0.06
0.04
0.02
0.00
0
500
1000
1500
2000
2500
3000
3500
4000

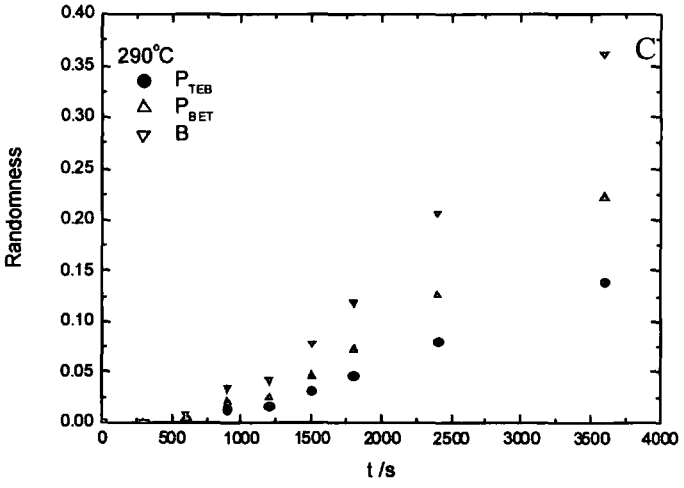
290°C
P_{TEB}
P_{BET}
B
C
Randomness
t /s
0.40
0.35
0.30
0.25
0.20
0.15
0.10
0.05
0.00
0
500
1000
1500
2000
2500
3000
3500
4000

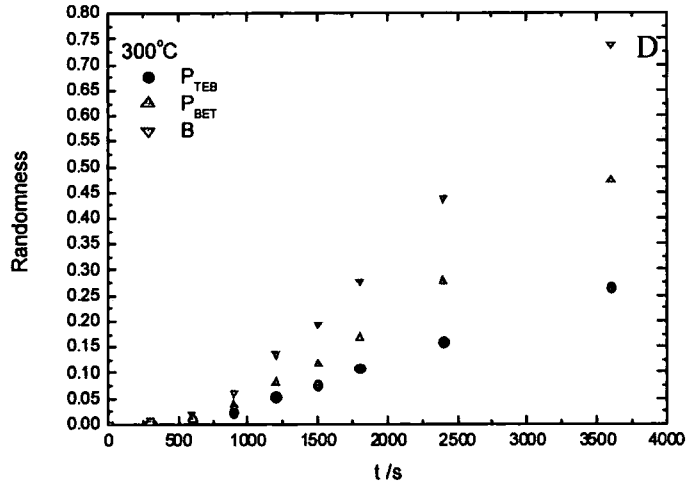

Figure 3.32 Graphs showing the randomness and P_{BET} and P_{TEB} in reactions carried out at 270°C (A), 280°C (B), 290°C (C) and 300°C (D)

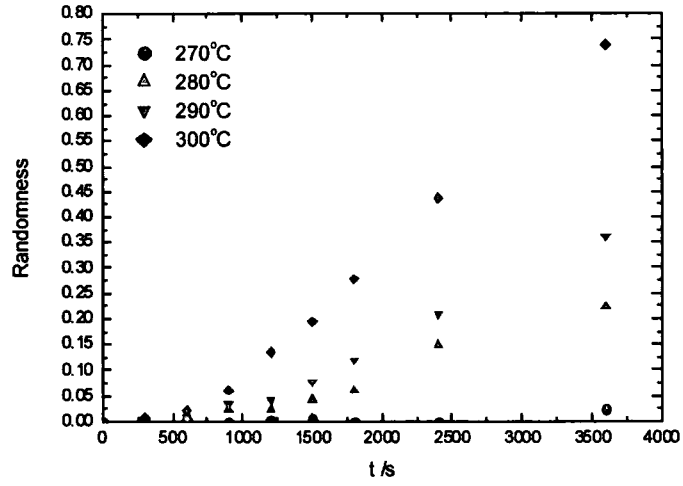

Figure 3.33 B values from Figure 3.31 shown on the same axes

After one hour at 300°C the randomness of the sample is approximately 0.7 which can be thought of as alternating short chains of the two homopolymers. This value is higher than

the value reported for the transesterification of PET and PEN (50:50 blend) of B = 0.61 after 60 min at 280°C.[20] The reaction between PET and PEN would be expected to run faster than that between PET and PC since the two are miscible so it is logical to expect that near equal rates of reaction should be achieved at lower temperatures. The number average length of the homopolymer chains is calculated at 3.8 for PET and 2.1 for PC. The two are not equal since the blend is 50:50 w/w and because of the difference in molecular weight of the two monomers (PC = 254 g mol^{-1}, PET = 192 g mol^{-1}) there are more PET units than PC units (58:42).

Since the ^{1}H NMR spectra of both the solution blended material which was subject to rigorous drying and the melt blended material showed no appreciable sign of transesterification it can only be assumed that the randomness of these samples was 0. If indeed there has been some transesterification in the samples then it is not very widespread and the samples are still very much a physical blend of long chain PET and PC.

3.4.6 Evidence for Side Reactions

The peaks at 4.5 and 4.0 ppm in Figure 3.19 correspond to the di-ethylene glycol (DEG) protons, which occurs as an unavoidable by-product in the production of PET and is also added deliberately to reduce crystallinity and make the final article transparent. It was first thought that the DEG present in the PET may remain constant and that this might be a standard against which the quantity of EG* could be compared. Some preliminary work was carried out comparing the size of one of the two DEG peaks to the whole terephthalate group (around 8 ppm) for samples which had been reacted for different temperatures; the following results were obtained.

Table 3.34 Levels of DEG and EG (relative to terephthalate concentration) in transesterified samples of PET within PET/PC

	^{1}H NMR integration		Composition/[14]		Loss		
Unit	Unreacted	1hour, 573K	Unreacted	1hour, 573K	Loss/mg	Loss/%	Rel. Volatility
DEG	0.012339	0.007325	0.0250	0.0140	0.0110	44.1	418
EG	0.494	0.469	1.00	0.896	0.106	0.105	1.00
Tere	0.493	0.523	1	1	0	0	0

It is clear from the ^{1}H NMR spectra that DEG is lost at a much faster rate than EG during the reaction. This would seem to agree with previous reports that DEG may be lost as a side reaction of transesterification. It is also possible that some of the DEG lost is split at the central oxygen atom and two EG* units are produced. It is impossible to tell whether or not this is the case without analysis of the volatiles produced in the reaction. TG-MS should be carried out to investigate the reported reaction by-products.[21-23]

The number of chain ends increases dramatically throughout the reaction as can be seen by the size of the peak at 4.7 ppm in samples which have been transesterified for long

periods of time. It is likely that this is due to residual water present in the PET and PC, hydrolysing the material at the start of the reaction. The rate at which terminal hydroxyl groups in PET react with TFA present in the NMR solvent used in this work (TFA:DCM 1:4 by volume) has been studied in previous work with stirring.[17] This reaction, shown in Figure 3.34 and known as "end capping" is found to be pseudo first order with a rate constant of 7.8×10^{-6} s^{-1}. It was found that after 50 min there were 8.95×10^{-3} moles of OH end groups per mole of monomer and that after 5 days there were no detectable OH end groups remaining in the sample. The solution examined in the work had 10 g of polymer per 100 ml of solvent. The solution used in the NMR analysed in this project typically contained 10-50 mg of polymer in 0.7 ml of solvent, this makes the latter solution up to 35 times more concentrated but if the reaction is slow when stirred it could be expected that the reaction will be much slower when it is not as is the case with NMR samples.

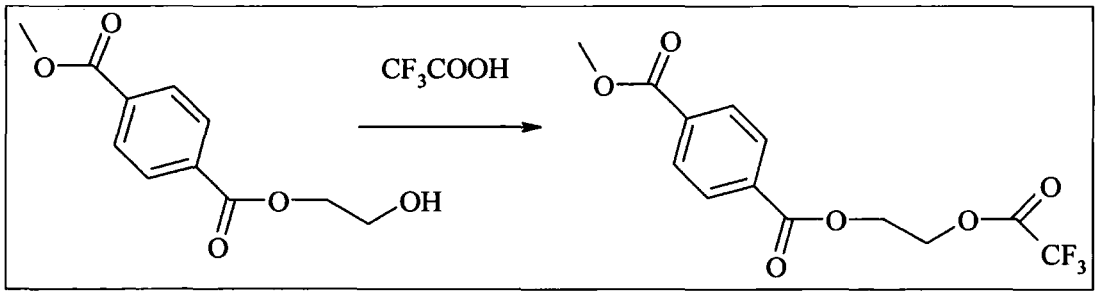

Figure 3.35 End capping of PET polymer chains

A series of NMR spectra was obtained from 5 × 10mg samples of polymer annealed from 15 min to 120 min at 300°C. The order of data collection was ^{1}H NMR, followed by ^{13}C NMR and finally a repeat of ^{1}H NMR. Since the ^{13}C scan takes 12 hours there are two ^{1}H spectra separated by approximately twelve hours for each of the reaction times under investigation. All samples were analysed within an hour of being dissolved in the

solution so if the samples all had equal molecular weights then all of the spectra should show two peaks in roughly the same proportions regardless of temperature. There may be a difference between the first and the second ^{1}H NMR of each run and this would indicate the speed of the end capping reaction. The relevant area of the spectrum is shown below for all of the ^{1}H scans carried out in this series.

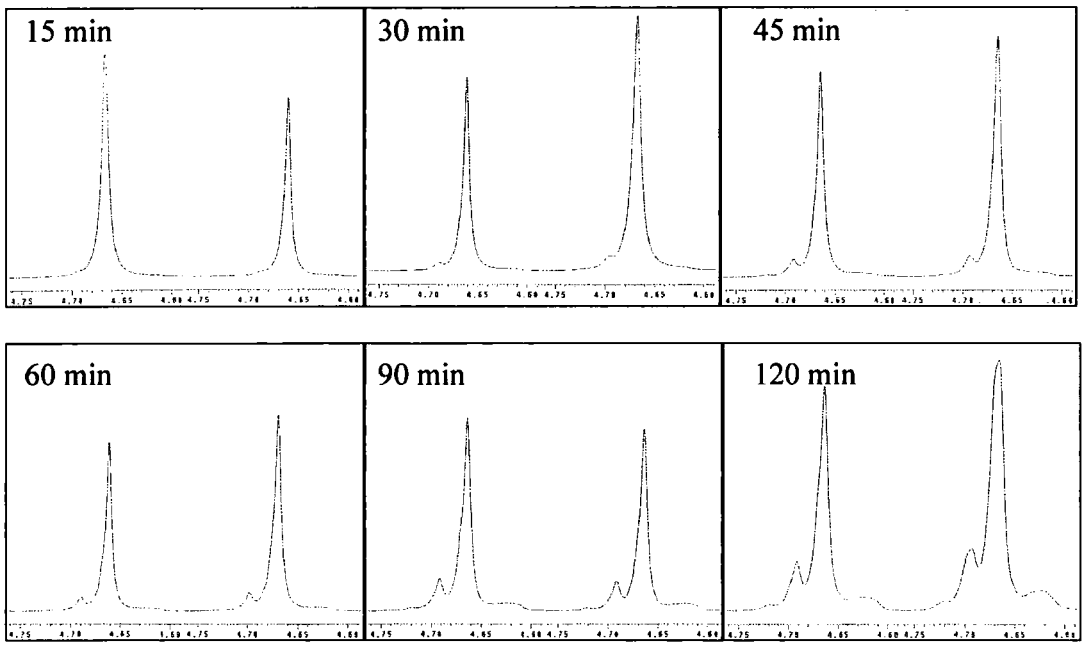

Figure 3.36 ^{1}H NMR spectra of pairs of analysis runs performed on samples of PET/PC (annealed for the time shown) within the first hour of making up the sample (left) and within the thirteen hours of making up the sample (right)

The main peak shown at 4.67 ppm again corresponds to the EG protons. The peak at 4.69 ppm, seen to be growing with extended reaction time, corresponds to the EG adjacent to the TFA ester end cap present on some of the chains. As stated above, all six of the spectra on the left hand side of each pair were acquired within an hour of the polymer being dissolved. The six on the right hand side of each pair were acquired after thirteen hours of the solution being made up. The differences in the pairs are small but

perceptible. They are more obvious in the case of the blends which have been annealed for longer but there is not a particularly large difference which suggests any minor variations in the time taken between preparing the sample and running the ^{1}H NMR will result in a negligible difference in the extent of end capping. There is however a very clear difference between spectra which have been annealed for different times. These two factors suggest that the co-polymer chains are broken up in the transesterification process at 300°C, reducing $\overline{M}_w$ and producing far more chain ends than were present in the original blend. It should also be noted that the peak for the TFA end groups is of the same order of magnitude as the EG* peak which grows out of the upfield side of the EG peak. This means that the reaction is on a scale comparable to the transesterification process itself meaning the reaction cannot be ignored. Detailed kinetics of this process cannot be obtained since no exact timings were taken.

3.4.7 End Group Analysis

By comparing the areas of the peaks associated with the hydroxyl end groups to those associated with the repeat units the number of hydroxyl end groups per repeat units has been calculated. During this analysis it was observed that the number of total end groups increased three fold in the TFA treated material, this was indicated by the appearance of new peaks. Results based on this observation are presented below.

Sample	CH_2OH end groups per 100 repeat units of polymer.	$\overline{M}_n$	DP	End gps/100 units	Hydroxyl end groups
Base	1.22	12,750	66	3.0	41%
Base/TFA	1.1	4,250*	22	9.0	12%
Laser	0.78	22,600	118	1.7	46%
Laser/TFA	0.84	7,533*	39	5.1	16%

Table 3.37 Data on end groups from ^{1}H NMR analysis.

*** Value based on qualitative observations**

The data above show some important points:

- Approximately half of the end groups in raw *Base* and *Laser* are hydroxyl
- The number of hydroxyl end groups is not diminished by exposure to TFA
- Exposure to TFA over a long period causes chain scission

The points above suggest that end capping is not quite simple as has been reported[17] and it is unclear how then TFA treatment has inhibited transesterification (see Figure 3.11). Since TFA can in fact have a detrimental effect on PET questions must be raised as to its use as a solvent, particularly in NMR. A thorough kinetic assessment would clarify whether the reaction is slow enough that short periods of exposure can be tolerated. TFA is a very useful solvent to use in NMR since DCM does not dissolve PET completely. A replacement would be HFIPA which is significantly more expensive. One way of investigating the effects of end-capping PET and PC without using TFA would be to use a different reagent. It is reported that benzophenone derivatives are good end-capping moieties[24] and terminating the synthesis of PET (see 5.1.1) with a bulky derivative could achieve the desired effect.[25] All of this is of course purely of interest to laboratory scale chemistry and has no bearing on large scale PET processing.

Work carried out on extruded blends concerned with analyzing the proportion of carboxyl end groups (CEGs) has suggested that *Laser* may have around 25% CEG whereas *Base* may have up to 50% (data in Table 3.38). Whilst the blends under investigation in this data are not entirely comparable with raw *Laser* or *Base*, it is known that very little reaction takes place during melt blending, so much so that the ^{1}H NMR spectra are largely unchanged.

Table 3.38 – Carboxyl end group data from ^{1}H NMR spectra

Sample	% of end groups which are carboxyls*
Base + 10% 1239	42.9
	44.0
Laser +10% 1239	25.8
Laser +25% 1239	20.9
Laser +50% 1239	12.3
Base +10% 2205	44.3
Base + 25% 2205	35.6
Base +50% 2205	25.3
Laser +10% 2205	27.9
Base +10% 2605	43.1
Base +25% 2605	35.0
Base +40% 2605	26.7
Base +50% 2605	23.4
Base +90% 2605	-
Laser +10% 2605	26.9
Laser +25% 2605	22.0

*** ± 10% of value**

It would be desirable to investigate the end groups of raw *Base* and *Laser* and compare with the three PCs under investigation. Only then could conclusions be drawn as to the mechanisms of any transesterification or indeed the SSP process which converts *Base* into *Laser*.

3.5 Conclusions

When dry, very low levels of transesterification take place between PET and PC. Where the reaction does proceed it is seen as a second order reversible reaction but the cases we have observed this occurring also feature large scale chain scission so any rate constants associated with the process can only be valid for very short chain polymer samples.

DEG can be lost in the transesterification process although it is unclear whether this is volatilized or simply reacts with PET or PC units. Greater understanding of the thermal degradation products of the PET/PC reaction is necessary.

Whilst some understanding of the end groups of PET has been reached, for confirmation of the proposed mechanisms of transesterification characterisation of the end groups and molecular weights of both reactants and the products is necessary.

In order to work with absolutely dry PET/PC it is necessary to heat the sample in its final form at 160°C for three hours *in vacuo* and if it is required to be stored then it should be stored in a vacuum desiccator.

3.6 References

(1) Collins S.; Peace S.K.; Richards R.W.; MacDonald W.A.; Mills P.; King S.M. *Polymer* **2001**, *42*, 7695.

(2) Kotliar A.M. *J. Polym. Sci. Macro. Rev.* **1981**, *16*, 367.

(3) Zheng W.; Wan Z.; Z., Q. *Polym. International* **1994**, *34*, 301.

(4) Godard P.; Dekoninck J.M.; Devlesaver V.; Devaux J. *J. Polym. Sci.: Part A: Polym. Chem.* **1986**, *24*, 3302.

(5) Berti C.; Bonora V.; Pilati F. *Makromol. Chem.* **1992**, *193*, 1679.

(6) Zhang Z.; Xie Y.; Ma D. *Eur Polym. J.* **2001**, *37*, 1961.

(7) Henrichs P.M.; Tribone J.; Massa D.J.; Hewitt J.M. *Macromolecules* **1988**, *21*, 1282.

(8) Ho J.C.; Wei K.H. *Polymer* **1999**, *40*, 717.

(9) Devaux J.; Godard P.; Mercier J.P. *J. Polym. Sci.: Polym. Phys. Ed.* **1982**, *20*, 1901.

(10) Godard P.; Dekoninck J.M.; Devlesaver V.; Devaux J. *J. Polym. Sci.: Part A: Polym. Chem.* **1986**, *24*, 3315.

(11) Devaux J.; Godard P.; Mercier J.P.; Touillaux R.; Dereppe J.M. *J. Polym. Sci: Polym. Phys. Ed.* **1982**, *20*, 1881.

(12) Stewart M.E.; Cox A.J.; Naylor D.M. *Polymer* **1993**, *34*, 4060.

(13) Kenright A.M.; Peace S.K.; Richards R.W.; Bunn A.; MacDonald W.A. *Polymer* **1999**, *40*, 5851.

(14) Alexandrova L.; Cabrera A.; Hernandez M.A.; Cruz M.J.; Abadie M.J.M.; Manero O.; Likhatchev D. *Polymer* **2002**, *43*, 5397.

(15) Yang H.; He J.; Liang B. *J. Polym. Sci.: Part B: Polym. Phys.* **2001**, *39*, 2607.

(16) Devaux J.; Godard P.; Mercier J.P.; Touillaux R.; Dereppe J.M. *J. Polym. Sci.: Polym. Phys. Ed.* **1982**, *20*, 1881.

(17) Kenright A.M.; Peace S.K.; Richards R.W.; Bunn A.; MacDonald W.A. *Polymer* **1999**, *40*, 2035.

(18) Yamadera R.; Murano M. *J. Polym. Sci: Part A: Polym. Chem.* **1967**, *5*, 2259.

(19) Devaux J.; Godard P.; Mercier J.P. *J. Polym. Sci: Polym Phys Ed* **1982**, *20*, 1875.

(20) Yoon K. H.; Lee S. C.; Park I. H.; Lee H. M.; Park O. O.; Son T. W. *Polymer* **1997**, *38*, 6079.

(21) Porter R.S.; Wang L.H. *Polymer* **1992**, *33*, 2019.

(22) Montaudo G.; Puglisi C.; Samperi F. *Polym. Degrad. Stabil.* **1991**, *31*, 291.

(23) Berti C.; Bonora V.; Pilati F. *Makromol. Chem.* **1992**, *193*, 1665.

(24) Okamoto M. *Polymer* **2001**, *42*, 8355.

(25) Oh S. J.; Kim B. C. *J. Polym. Sci: Part B: Polym. Phys. Ed.* **2001**, *39*, 1027.

Chapter 4

Mechanical Properties

4.1 Introduction

To be able to use a blend with better barrier properties than pure PET, it is essential that the new material is as strong as the original. Therefore, the structural properties of PET blends are of significant industrial interest. For an easy switch to be made from bottles made from PET to a PET-based blend it is essential that the materials both injection-mould and blow-mould in a similar manner. If the thickness of the final item needs to be significantly greater than current PET bottles for strength reasons then that will require significant adaptation of the pre-form and will make any change uneconomic. There is significant material in the literature related to mechanical testing of PBT doped with rubber particles[1-8] including cases where PC is used as a compatibilser.[9] PET has also been examined doped with rubber,[10] elastomers,[11-18] PEN[19,20] and Polypropylene[21,22] (PP) but not purely with PC. Much of the interest in PET is related to boosting the properties of recycled PET so a variety of other additives have been investigated.[23] It is possible that PC has not been used since there is a greater environmental and economic pressure to find a method of recycling rubber and PP.

With this in mind, this Chapter presents data and conclusions on the strength, Young's modulus, stress and strain at yield and stress and strain at fracture of two PET/PC blends. The blends investigated were *Laser* + 10% *1239* and *Base* + 10% *2605*, chosen on the basis that the higher molecular weight PET ought to mix best with highest molecular weight PC and the lower molecular weight PET ought to mix best with the lowest molecular weight PC. Below are the desirable properties in a replacement for PET:

Tensile Properties

PET is used in most cases as a film or in other applications where it is blow moulded into a shell. This means that its state in many applications is to be less than 1mm thick and it is undesirable for it to deform elastically, let alone inelastically when being used. Any replacement should have a high resistance to deformation (Young's modulus) and tolerate a high load before fracture. PET/PC blends must therefore have a Young's modulus as high or higher than that of PET.

Impact Strength

As above, PET is often used in thin films and most applications require it to be used below its T_g of 80°C. It would be easy for this to make it brittle but PET has a reasonably high impact strength to make up for this. Any replacement would have to have an impact strength similar to PET, ideally no lower.

4.2 Theory

4.2.1 Tensile Properties Testing

During tensile properties testing, a polymer sample is put under tension and the stress and strain determined. For this it is necessary to have a sample of the material under investigation of uniform cross sectional area and some way to track the length of the section under tension. It is also essential that there is an accurate method of determining the force on the sample throughout.

4.2.2 Stress

When a material experiences a force, stress at any location in the material is defined as force per unit area.

$$\sigma = \frac{F}{A}$$ **Equation 4.1**

Stress is measured in MPa.

4.2.3 Strain

When under tension, any elastic body will stretch. Strain is defined as the ratio of the increase in length to the original length.

$$\varepsilon = \frac{\Delta L}{L_0}$$ **Equation 4.2**

It is unit-less but is reported as a percentage.

4.2.4 Stress-Strain Curves

It is possible to represent the deformation of a sample with a stress-strain graph. A typical stress strain curve for a polymer is shown below.

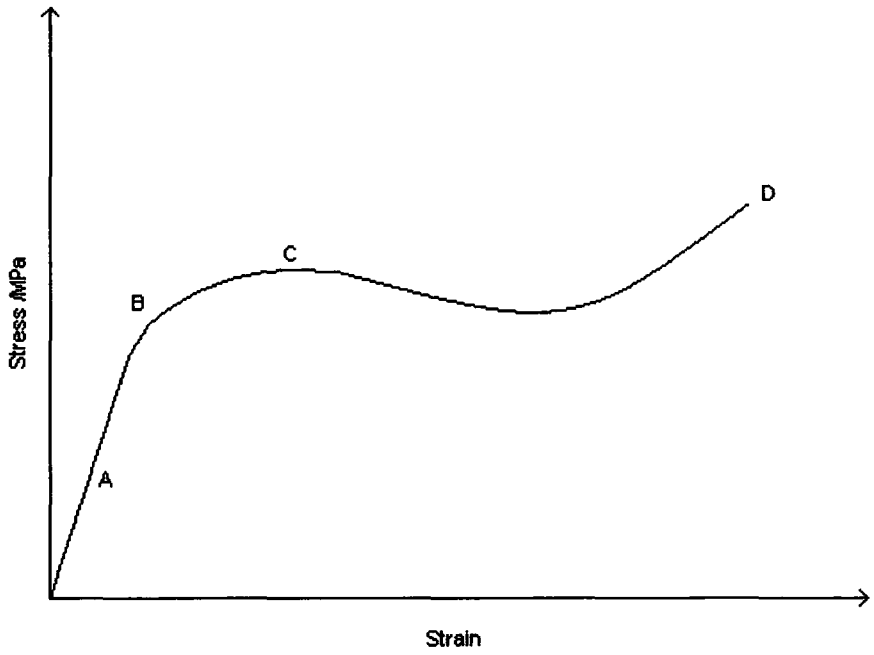

Figure 4.3 A typical stress-strain curve for a ductile material

In Figure 4.3 above, the straight section A corresponds to the elastic regime, strain in the sample is uniform throughout and if the load is removed before B then the material will return to its original dimensions. The slope of this section is equal to the Young's modulus of the material. B marks the elastic limit or yield, at this point some irreversible damage is done to the sample, if the material is ductile, this defective region will spread through the sample. As this happens, the stress experienced falls since the damaged section is initially small and it can expand to encompass the entire sample (C). Once the yield has spread through the whole sample the stress will rise until final fracture (D). If a material is not ductile then it will fracture at the yield or soon after because the strain will be focused at the damaged section much like a weak link in a chain.

There are two important values which are desirable in a material with good structural properties:

1. The material should resist deformation; this means Stress/Strain, known as Young's modulus, must have a high value.
2. The stress and strain at yield and fracture should be high.

It is desirable that the blends resist deformation but when they do deform it is important they do not fracture easily. Materials with high a Young's modulus tend to be rather brittle and fracture early so there is a balance in properties to be found. The strain rate applied is crucial since a fast strain rate will probe a very different property to a slow one. Under sudden loading the polymer gets no chance to deform and will act as if it is glassy. This means a fast strain rate will probe the strength of the sample in the case of a brittle fracture. The response of a polymer to a load will also be dependent on temperature, the response of a sample above or below the T_g will differ both before and after the yield point. Under slow loading ductile polymers would be expected to deform significantly before fracture.

4.2.5 Notched Impact Testing

Notched impact testing is a standard test of the strength of a material, defined as the resistance of the material to break due to flexural shock. A sample of the material is subject to either a vertical impact or impact from a pendulum type hammer. The equipment measures the energy absorbed by the sample which is then equated to the amount of energy to tear a sample per unit width.

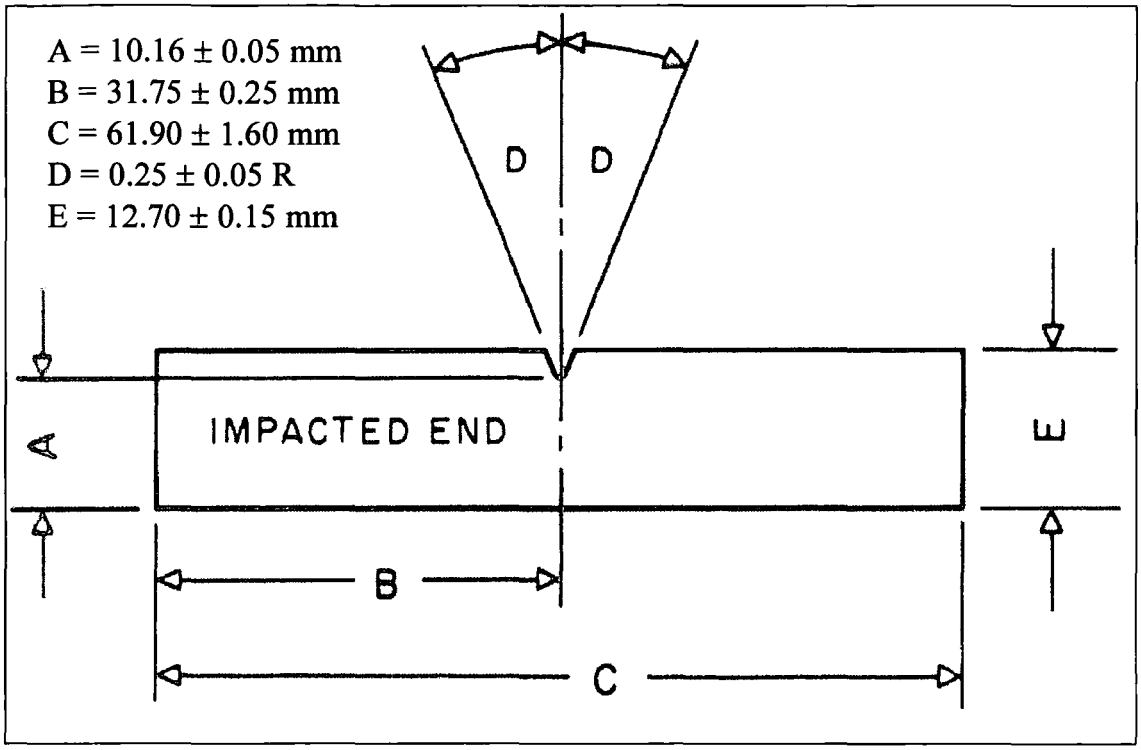

Figure 4.4 Sample shape as dictated by ASTM D256

The profile of the sample, shown in Figure 4.4, is pre-determined in all dimensions apart from width (the dimension not shown in the diagram) which is measured for each individual sample. The equipment gives a force time curve for the impact which can be integrated to give the energy put into the sample during impact. Also obtained is the peak force experienced by the sample, which can be assumed to be the maximum force which the sample can experience before fracture.

It is desirable that the blends have as high a peak force and impact strength as the pure PET samples. Polycarbonate is used in high strength applications and so it could be expected to improve strength. However, since the two polymers are immiscible the strength will be largely dependent on the quality of the mixing at the interface. There is

reason to suspect that the mix will be good since PET and PC are reported to be mechanically compatible.[24]

4.3 Experimental

4.3.1 Sample Preparation

PET/PC chips were produced as described above in 2.3.2. Blends 1 and 10 (*Base* + 10% *2605* and *Laser* + 10% *1239*) were made in larger quantities to enable injection moulding to be carried out. Before moulding, the two blends were dried as described in 2.3.2 and before moulds were taken, the injection line was purged with pure PET (*Base* for blend 1, *Laser* for blend 10) followed by the blend being examined. Moulds were also taken of the pure *Base* and *Laser*. The mould chosen was a disc of diameter 10cm the thickness of which could be varied. Discs of 1.5 and 4 mm thickness were moulded for each of the four polymers, 1.5 mm discs were used for stretch testing whereas the 4mm discs were used for impact testing. Some yellowing occurred in the PET discs as a result of drying for too long.

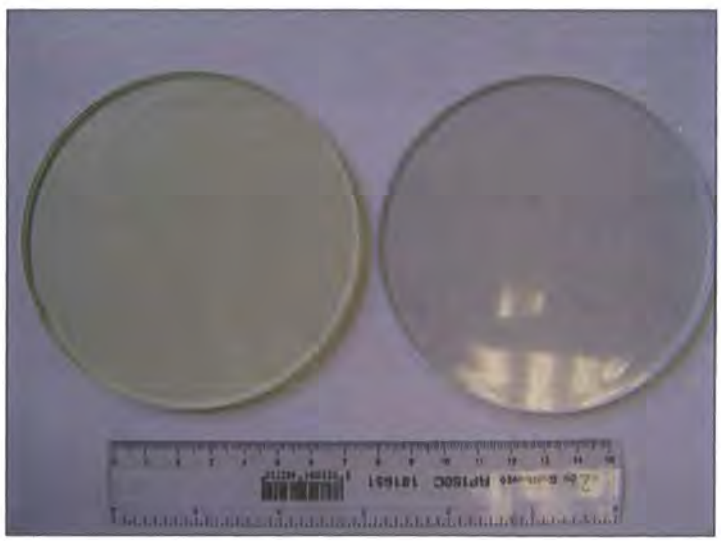

Figure 4.5 Yellowed *Laser* with 10% *1239* and pure *Laser* in 4 mm x 10 mm discs

Some surface crazing was observed on one side of the 1.5 mm discs made with *Laser* + 10% *1239* only, the cause of this is unknown.

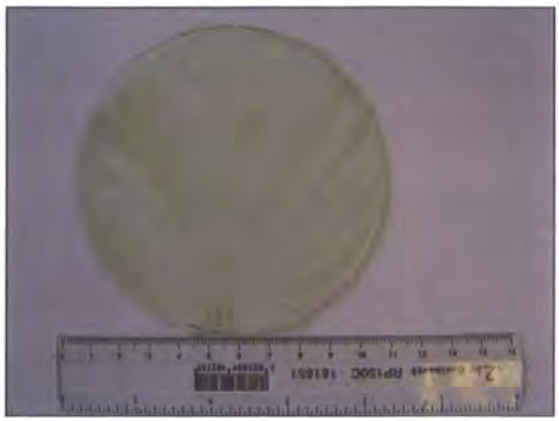

Figure 4.6 Surface anomalies in 1.5mm x 100mm *Laser* + 10% *1239* disc

From the discs moulded samples were cut for impact testing and stretch testing. Samples were cut such that the sample lay as much in the direction of flow as possible (see Figure 4.7). The aim was to make the sample as homogenous as possible in the longitudinal dimension.

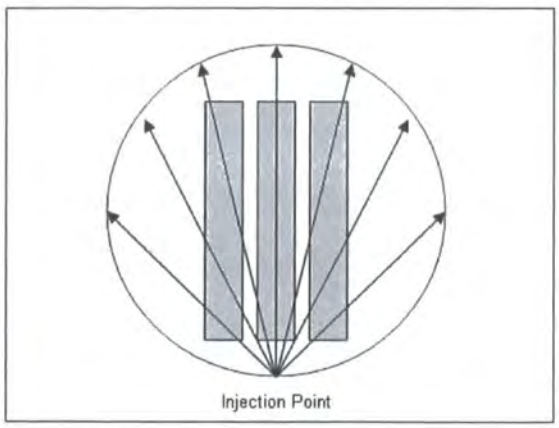

Figure 4.7 Example of how mechanical testing samples were cut from the extruded discs

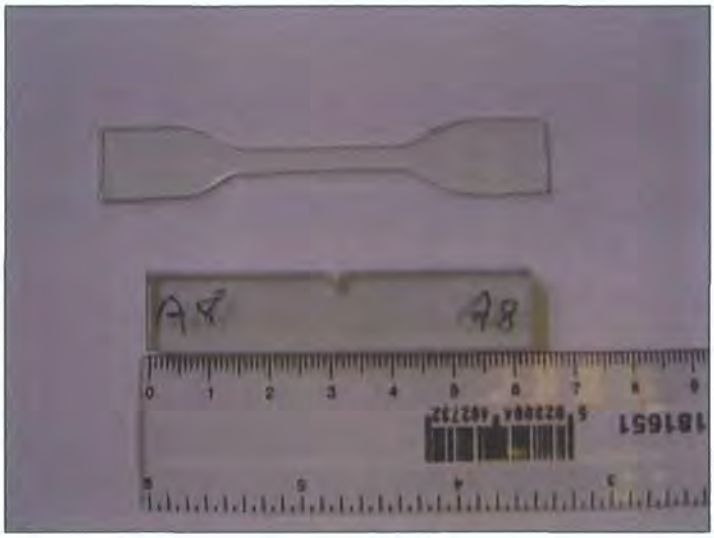

Figure 4.8 Top: 1.5 mm thick stretch test sample. Bottom: 4mm thick impact test sample

4.3.2 Tensile Properties Testing

The samples and tests used for this study conform to the American National Standard ASTM D638 type IV. The sample was held such that only the straight section of the sample was visible between the grips (see Figure 4.11 A) and the strain rate used was 0.5 mm s^{-1}. For Young's modulus investigations, the sample was painted with a permanent marker pen on both sides and two white bands were painted so they were both roughly perpendicular to the sample (see Figure 4.9). The lines were painted roughly 14 mm apart on the straight section of the sample. When mounted vertically between two clamps as shown in Figure 4.10, software was used to track the two white bands, a black background was used to improve contrast.

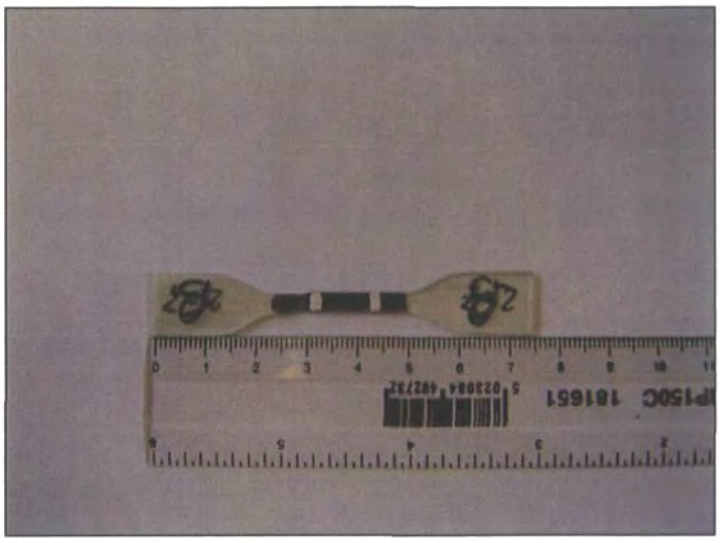

Figure 4.9 Sample after analysis, the yield can be seen to the left of the left hand stripe

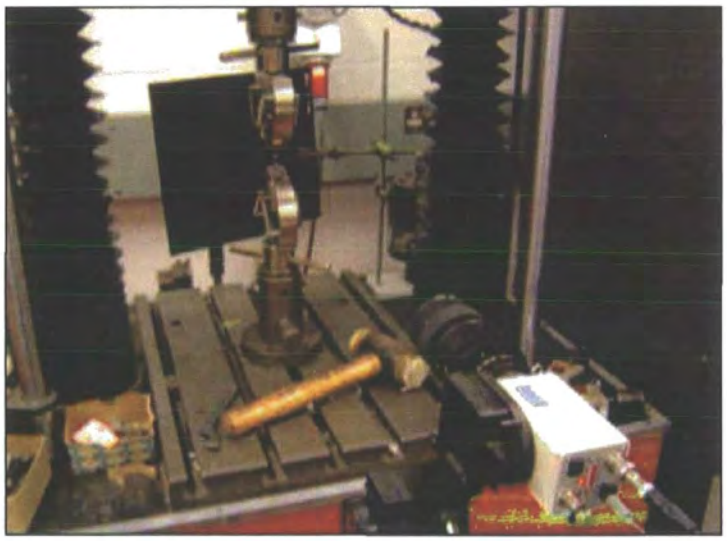

Figure 4.10 Setup for automatic tracking of white bands on samples

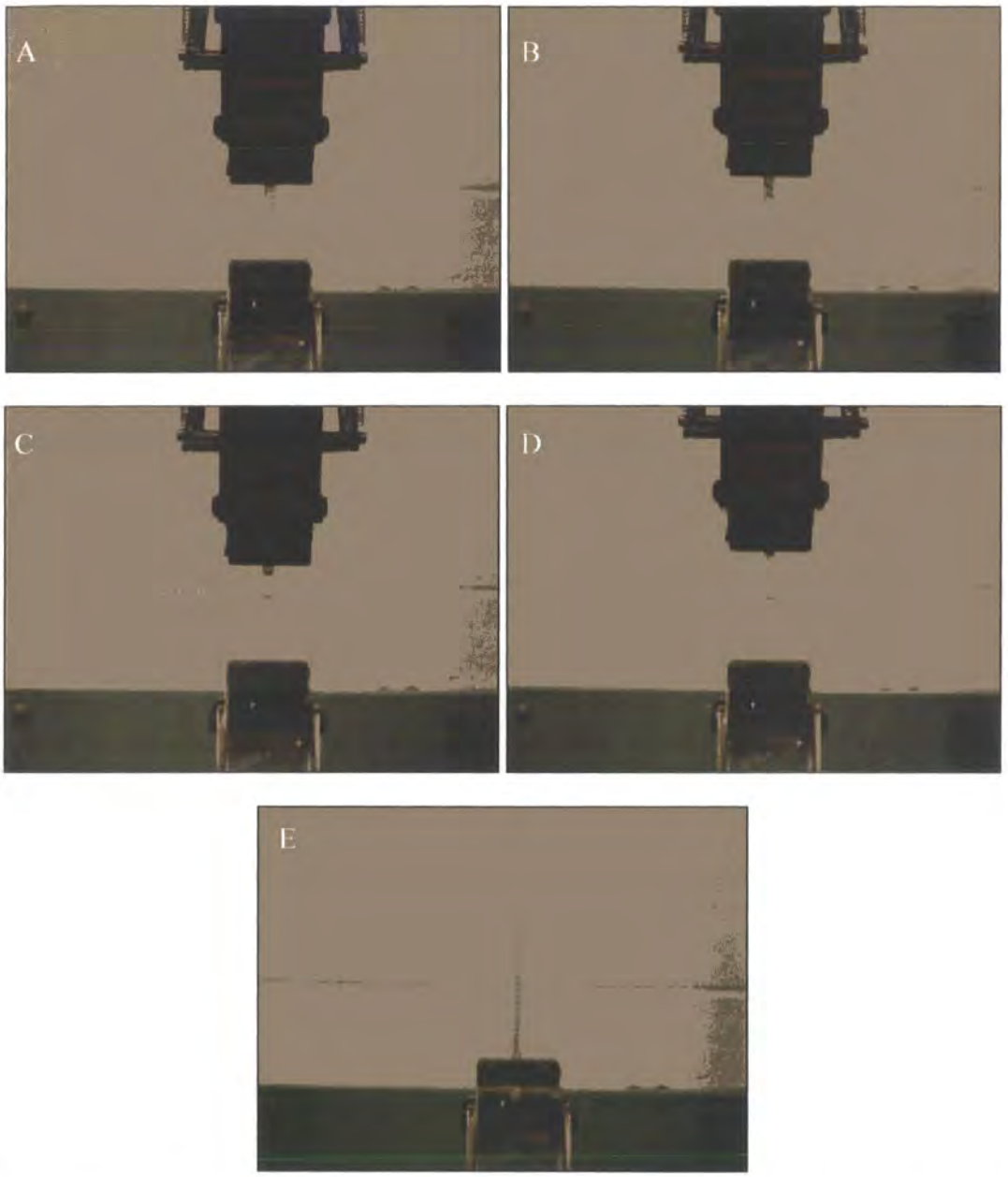

Figure 4.11 A. Unstretched sample. B. Sample immediately after yield. C. Sample as yield spreads upwards. D. Yield spread to top grip. E. Yield spread to bottom grip

Preliminary investigations revealed that the final fracture point was frequently around one or other of the white lines. It was decided that to remove the possibility of solvent damage leading to premature failure that the painted samples would only be used for accurate determination of the Young's modulus. This was the most practical option in

any case since if the yield occurred outside of the bands the resulting deformation would distort the nearest band and the computer software would lose its lock.

All other results were obtained using unpainted samples with the information on the tensile force experienced being charted on square plotting paper. The curves obtained were up to 20cm long and the value for the curves was read off manually every mm in the x direction. The scale on the x axis was determined by the chart speed of 20.02 mm min^{-1} and the strain rate of 30mm min^{-1}. The scale on the y axis was calibrated by applying a 10 kg load to the sensor and plotting the output.

Samples were measured using a micrometer and averaged along the sample length before testing. In the case of samples which were tested to failure, the final dimensions were also measured in order to determine the change in cross sectional area.

4.3.3 Notched Impact Testing

Samples of pure *Base*, pure *Laser*, *Laser* + 10% *1239* and *Base* + 10% *2605* were prepared as dictated by American National Standard D256. The testing was carried out using a Rosand Type 5 Falling weight impact tester shown in Figure 4.13 and five samples of each material were used. Each sample was placed in the sample holder as shown in Figure 4.12. The sample was then mounted such that it would be hit by the load at the desired point. At the point of impact the hammer, weighing 6 kg, was traveling at 3.5 m s^{-1}. It was found that when the hammer weighed 25 kg and was traveling at 3.5 m s^{-1} or 1 m s^{-1} the sample was made to oscilate and so did not give a clean break. Data from the instrument were recorded on a computer as a force time curve. The peak force was read off the plot and the software calculated the area under the curve during impact.

The bounds for this were set manually to before the sample experienced a force to when the force curve returned to 0 N once again. After this point, some noise was visible, which was ruled out as vibrational interference.

Samples were measured using a micrometer and averaged along the sample length before testing.

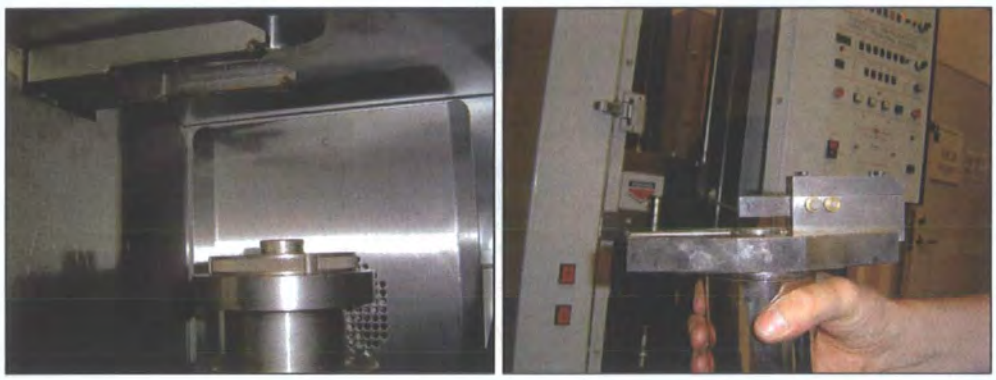

Figure 4.12 Sample holder and mount

Figure 4.13 Rosand Type 5 Falling weight impact tester

4.4 Results and Discussion

4.4.1 Tensile Properties

Eight samples of each material were subject to tensile tests; five of the samples were painted so that stress-strain curves could be produced. From these, the Young's modulus was extracted from the linear section. The data in Table 4.14 show the information extracted before yield, for *Base*, *Laser* the blends thereof. The data for all are averaged across all five samples.

Table 4.14 Stress, strain and Young's modulus data obtained for all four blends before yield

	E /GPa	Y_{stress} /MPa	Y_{strain}
Laser	2.2 ± 0.3	58 ± 1	3.6% ± 0.3%
Laser blend	2.5 ± 0.3	60.0 ± 1	3.5% ± 0.4%
Base	2.6 ± 0.4	59 ± 1	3.5% ± 0.2%
Base blend	2.8 ± 0.3	61 ± 4	3.3% ± 0.3%

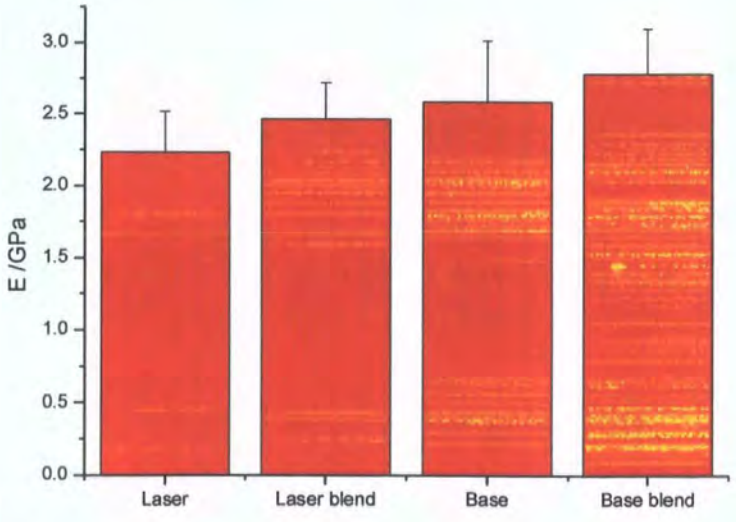

Figure 4.15 Young's moduli of *Laser* and *Base* and the blends thereof

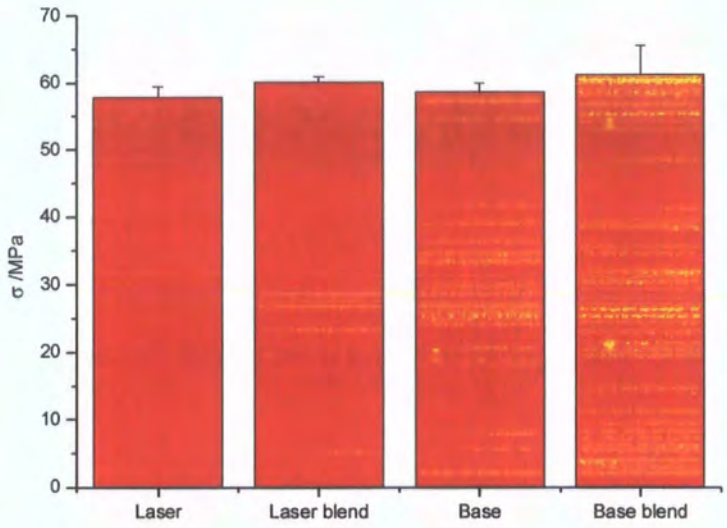

Figure 4.16 Stress at yield of *Laser* and *Base* and the blends thereof

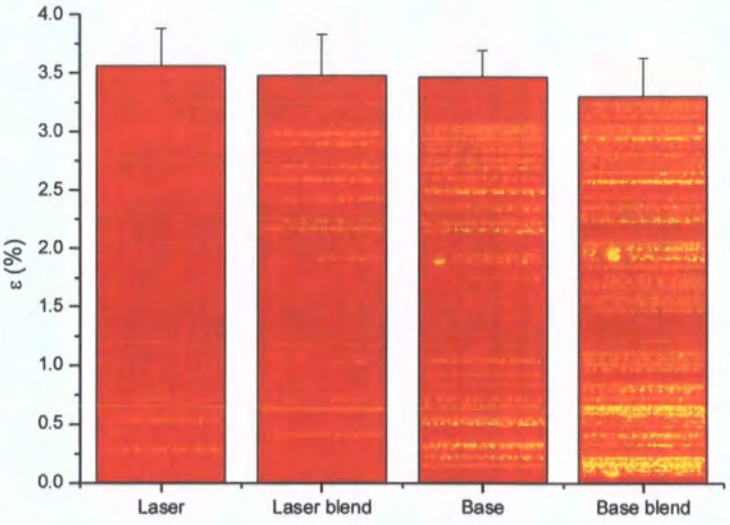

Figures 4.17 Strain at yield of *Laser* and *Base* and the blends thereof

The data in Figure 4.15 show both blends have superior Young's modulus to their homopolymer analogues. The blends are also able to withstand higher stress before yield

but show lower strain. This means that both blends are more resistant to deformation than the pure PETs. The deviation of each sample from the average observed characteristics for that blend was calculated using Equation 4.18. The four samples with values most similar to the average values are plotted in Figure 4.19 as the most representative data. All of them show very similar behaviour.

$$Deviation = \frac{1}{3}\left(\frac{|E - E_{av}|}{E_{av}} + \frac{|\sigma - \sigma_{av}|}{\sigma_{av}} + \frac{|\varepsilon - \varepsilon_{av}|}{\varepsilon_{av}}\right) \quad \textbf{Equation 4.18}$$

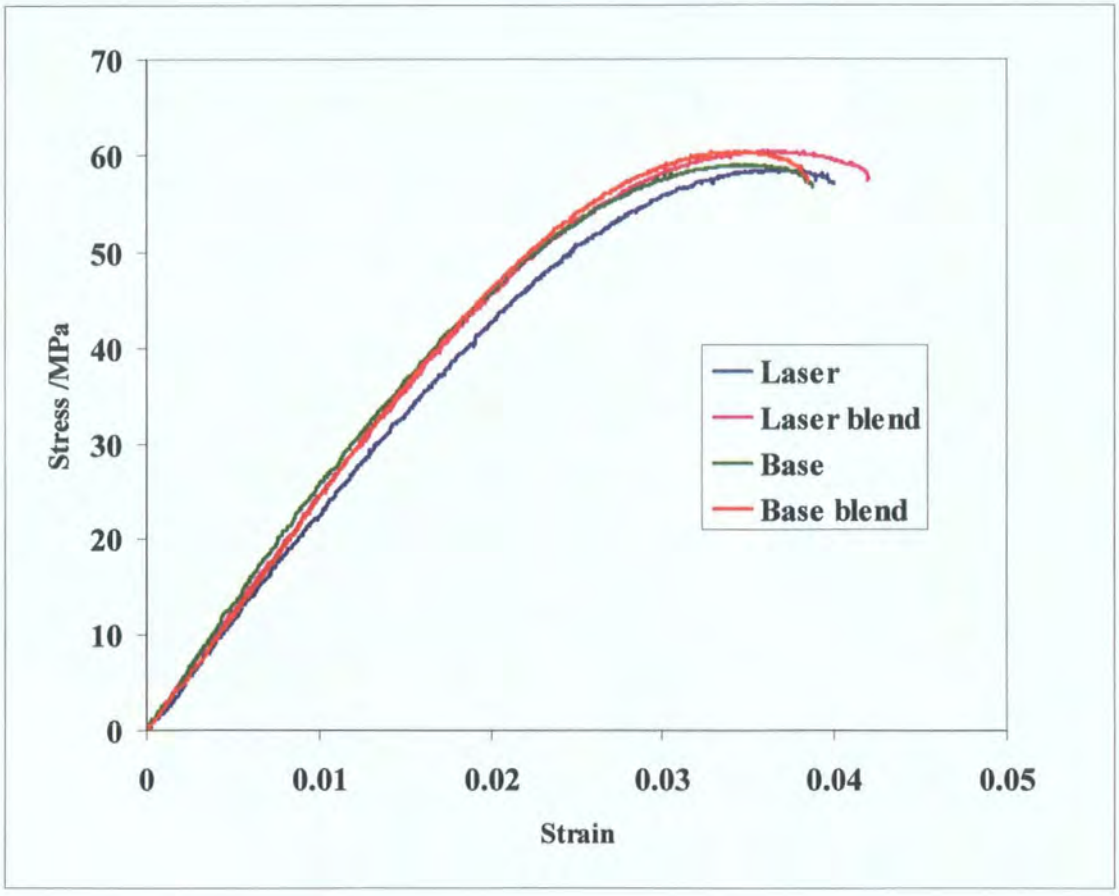

Figure 4.19 Stress-strain curves of all four materials to yield

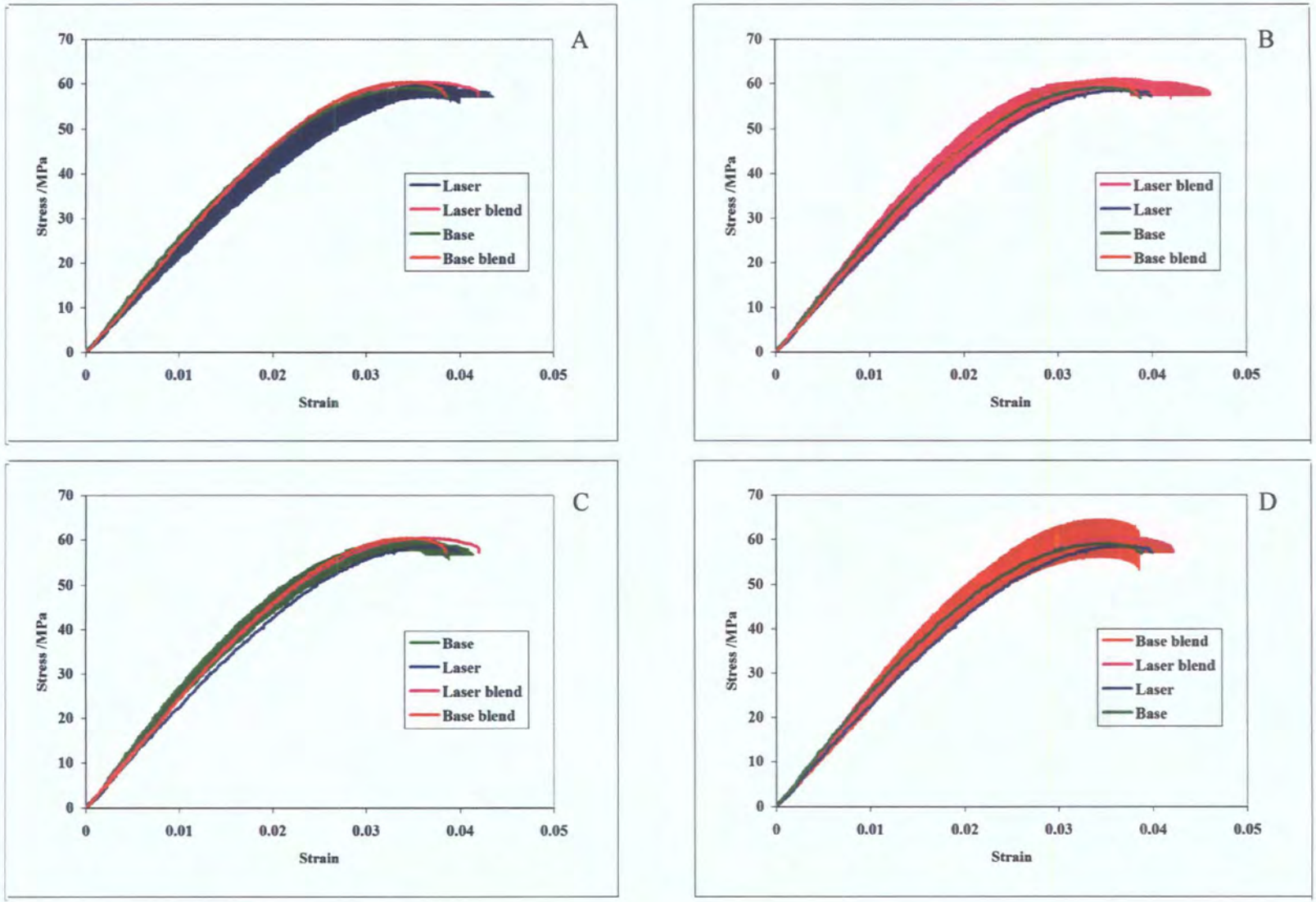

Figure 4.20 Properties of all four materials to yield with error bars

Figure 4.20 A-D illustrates this by showing each plot in turn with the error bars calculated from the standard deviation of the results collected. No plot is significantly different to another when errors are taken into account. It can be concluded that PET, *Laser* and the blends thereof have very similar properties up to the yield point.

4.4.2 Strength to Failure

Three samples of each material were tested to failure; the curves obtained are shown in Figures 4.21-4.22. It is not possible to convert the force-extension plots into stress-strain plots since the samples are not uniform in cross-sectional area along their length during most of the test. Data extracted from the curves and from measurements of the samples before and after testing are in Appendix I, Table X.

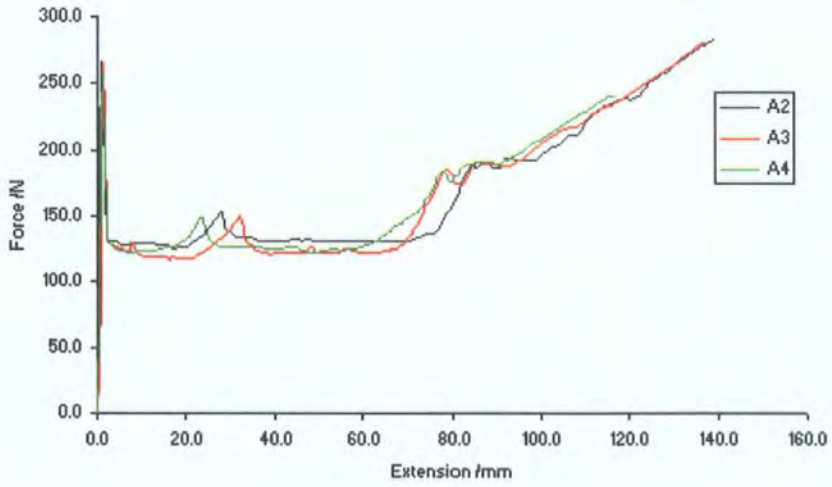

Figure 4.21 Force extension curves of *Laser* samples to failure

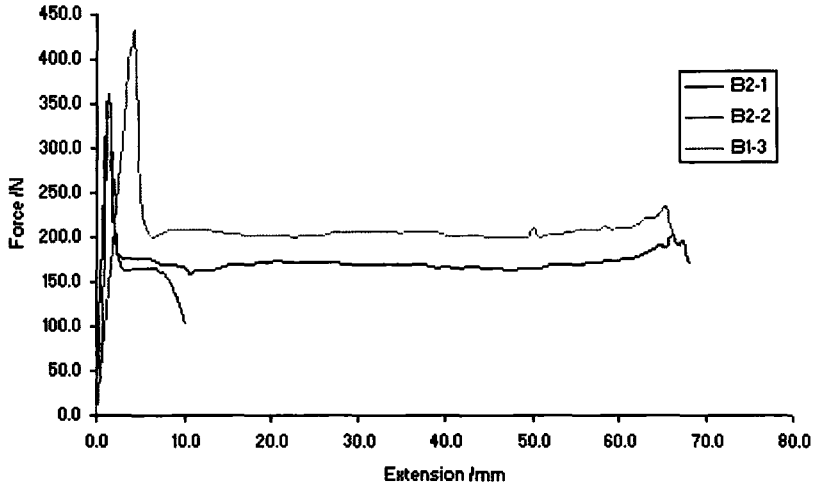

Figure 4.22 Force extension curves of *Laser* blends samples to failure

All three curves shown in Figure 4.21 show a number of features which can be related to macroscopic events. The first peak corresponds to the linear section before the first yield. After yielding, the stress on the sample is reduced very rapidly and the yield starts to draw in more of the sample. The rise shown around 20mm extension corresponds to the point when this yield reaches the end of the sample. The stress rises temporarily before the yield starts to draw in material in the opposite direction. The next feature is the rise at around 80mm which is the point at which the yield has reached the other end of the sample and the sample then thins uniformly along its entire length. The break finally comes after some 120-140 mm of extension for *Laser*. The *Laser* blend breaks far sooner indicating that it is less ductile than pure *Laser*. Some of this may also indicate flaws in the moulding process, certainly one of the samples of the blend fractured soon after the yield. It may be that moulding the *Laser* blend would require conditions different to those used in PET moulding. The blend takes far more force in order to yield but this is related to a difference in the cross-sectional area of the initial samples. Figure 4.25

illustrates that the behaviour at the yield is very similar for all 4 materials tested; in agreement with the data in Figure 4.16.

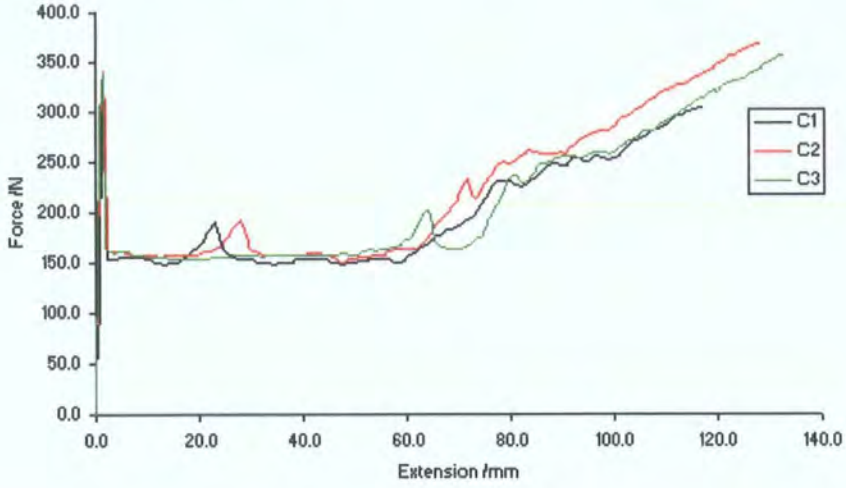

Figure 4.23 Force extension curves of *Base* samples to failure

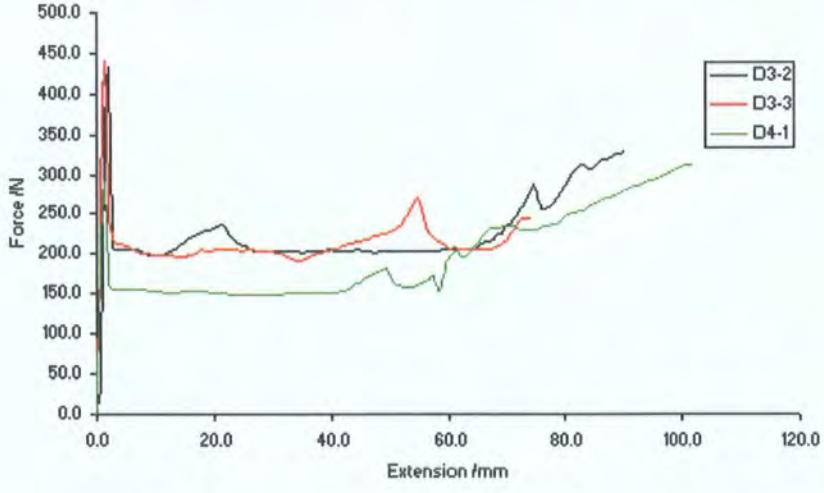

Figure 4.24 Force extension curves of *Base* blends samples to failure

The *Base* material shows similar behaviour to that exhibited by *Laser*. The peak force is a little higher, again a result of a difference in cross-sectional area. After this, the same hump, plateau and final slope are visible, again corresponding to the expansion of the yield. The *Base* blend is similar to pure *Base* in that all three of the samples of the blend show that the yield does extend through the whole sample before fracture. The fracture

occurs sooner in the blend than in pure *Base*, this again can be put down to the material being more brittle but the final breaking point is also more variable so this may relate to weaknesses in the structure.

The dimensions of the sample were measured before and after the test so it is possible to give the strain required to yield and fracture the samples. The *Laser* blend that fractured soon after yield (B2-2) was taken into account for the Stress at yield but not at fracture since the sample was not of a consistent cross-section at the point of fracture.

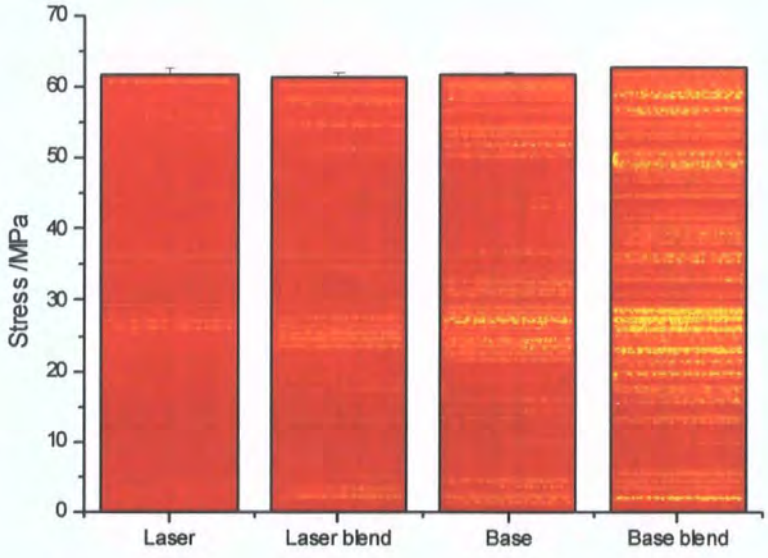

Figure 4.25 Stress at yield of *Laser* and *Base* and the blends thereof

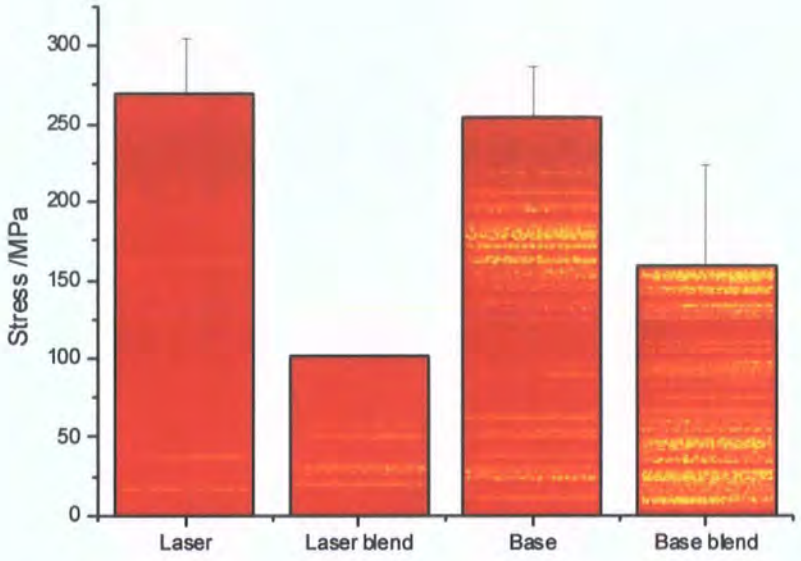

Figure 4.26 Stress at failure of *Laser* and *Base* and the blends thereof

It is possible to see that whilst all four materials have very similar properties in the elastic regime, both blends are far weaker at fracture than either *Base* or *Laser*. This could be due to their phase separated nature providing a weaker structure than pure PET. It was observed that when the blends were drawn out they appeared cloudy, indicative of micro-voiding. It is known that micro-voiding occurs in polymer blends between incompatible polymers[25,26] and that the higher the interfacial energy between the polymers the lower the stress required to cause separation at the interfaces.[27] It is known that in PET/PC the interfacial energy is high enough to cause phase separation because it is observed. It is also believed that water can form voids and it is known that crystalline PET rejects water, leading to super-saturation in amorphous areas.[28] The act of drawing a polymer also orders the polymer chains, potentially accentuating the voiding process, particularly since both blends contain large amorphous areas in the form of PC. Since these voids appear during drawing the effective cross-sectional area of the blends falls during the drawing

process faster than would be expected purely by the thinning related to extension. This would explain why the blends appear to be of the same strength at yield but much weaker at fracture.

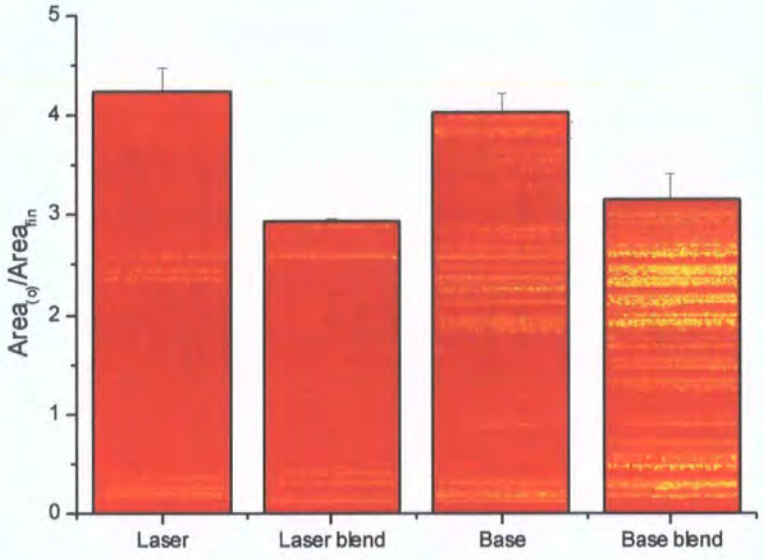

Figure 4.27 Ratio of original cross-sectional area to cross-sectional area at failure of *Laser* and *Base* and the blends thereof

Figure 4.27 shows the ratio of the starting cross-sectional area to that at fracture. The result is a plot similar to Figure 4.26. Again, the *Base* and *Laser* PETs are able to withstand a higher load before fracture, it would be interesting to know what proportion of the area of the blends at fracture is voided. This would give an indication of how much of the weakness after yielding is caused by voiding and how much can be attributed to a loss of ductility with the incorporation of PC.

Table 4.28 below allows comparison of the data acquired in this study with literature values.

Table 4.28 Comparison of tensile properties with literature values

Sample	Ultimate Stress /MPa	Strain /%	Strain Rate /mm s^{-1}	Source
Laser	270 ± 40	4.3 ± 0.2	0.5	This work
Laser blend	101.3 ± 0.5	2.94 ±0.03	0.5	This work
Base	250 ± 30	4.0 ± 0.2	0.5	This work
Base blend	160 ± 70	3.1 ± 0.3	0.5	This work
PET	66 ± 2	18 ± 7	1.67	[29]*
PET	262	-	-	[30]
PET	63	2.8	Fast (¥)	[31]

* Compression moulded film

¥ Data derived from impact measurements

The data above are within the limits set by the literature. The two values of 66 and 63 MPa can be understood by the fast strain rates and, in the case of the former, the method of film moulding. We can only presume that this use of compression moulding is responsible for the 18% strain although it should be noted that in a series of values attributed to PET blends the same techniques account for strain of 100% in a 50:50 blend.

4.4.3 Impact Strength

Impact testing involves a very sudden impact to the material being tested and thus the ductility of the material is not under inspection. The information gained is purely a measure of how strong is the material. Figure 4.29, below, shows the data collected for the maximum force divided through by the width of the sample.

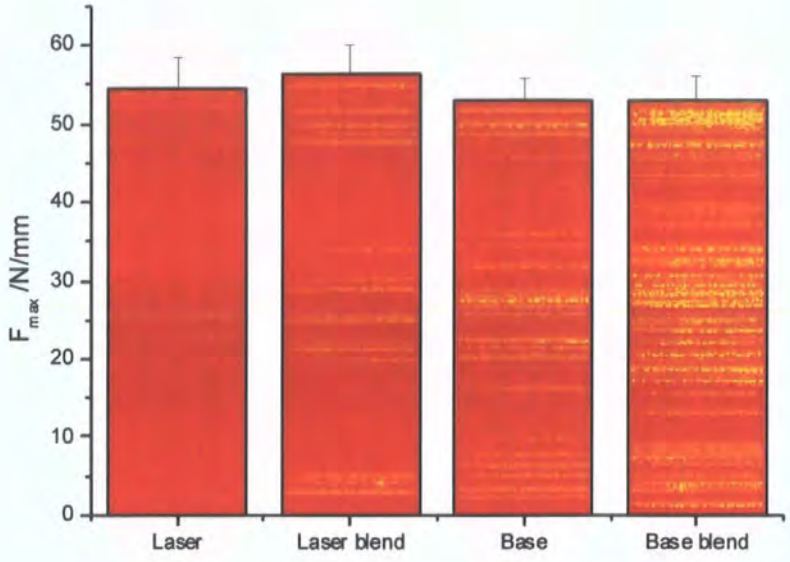

Figure 4.29 Maximum tolerable force per mm thickness for *Laser* and *Base* and blends thereof

All four samples exhibit the same maximum force per mm within experimental errors. This suggests that the two interfaces present in the blends are mechanically stable under such a shock.

Figure 4.30 shows the energy required to break the sample of each material per m of thickness (data in Appendix, Table X). There is very little difference between any of the materials but blending appears to lend strength to *Base* but to weaken *Laser*. Since *Base* is significantly lower in molecular weight than *Laser*, it is perhaps unsurprising that it should benefit most from blending with a high strength polymer such as PC. It is certainly fair to say that blending does not affect either *Base* or *Laser* significantly.

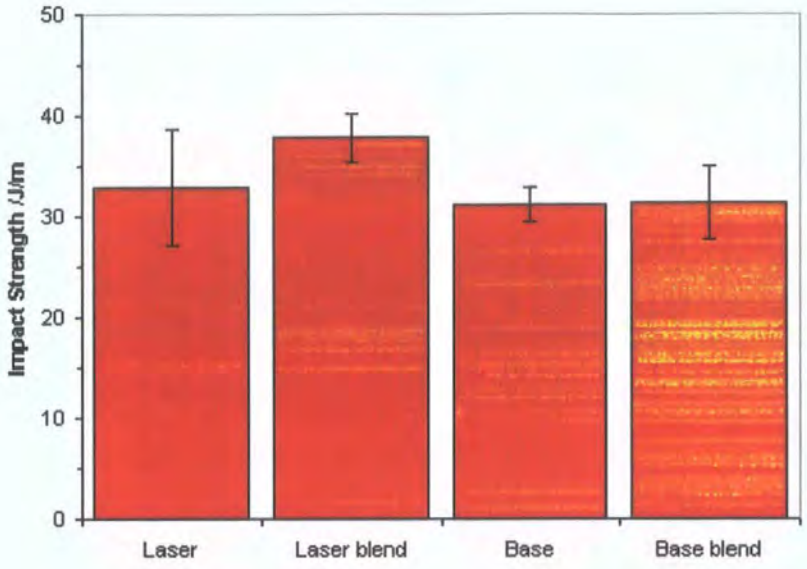

Figure 4.30 Notched impact strength of *Laser* and *Base* and blends thereof

Table 4.31 Comparison with literature notched impact strength data

Sample	Impact Strength /J/m	Source
PET	16	[31]
Base	31	This work
PBT	45	[9]
PBT + 10% PC	45	[9]
PBT + 20% EXL	40	[9]
PBT + 20% EXL + 10% PC	925	[9]

Table 4.31 above shows a selection of notched impact strength data which has been collected using a similar method to the method used in this work. The literature value of PET is lower than the one we present (for *Base*), there may be some difference in grades or preparation which has lead to this difference. There is far more work on PBT on which to draw and it is interesting to note that whilst the addition of 10% PC or of EXL (EXL 3607), a core-shell additive made of a rubber core with a butadiene shell, results in very little change to the impact properties however a combination of the two leads to a

huge rise in impact strength. Should an increase in impact strength be desirable this is one additive which may be of use.

4.5 Conclusions

PET blends containing 10% PC are not significantly stronger or weaker than the pure PET. PET/PC blends perform very similarly to PET before the yield point however they are less ductile and fail sooner than their homopolymer analogues, possibly as a result of voiding. Further studies quantifying the extent to which voiding affects the strength at fracture are necessary in order to determine its relative importance in weakening PET blends. Surface crazing is an issue with moulded PET/PC blends and it would be favourable to investigate this further and vary moulding conditions to see if this can be eliminated. PET/PC has similar characteristics under impact to PET.

4.5 References

(1) Modic M. J.; Pottick L. A. *Plast. Eng.* **1991**, *July*, 37.

(2) Hobbs S. Y.; Bopp R.C.; Watkins V. H. *Polym. Eng. Sci.* **1983**, *23*, 380.

(3) Wu S. *Polymer* **1985**, *26*, 1855.

(4) Borggreve R. J. M.; Gaymans R. J.; Schuijer J.; Ingen Housz J. F. *Polymer* **1987**, *28*, 1489.

(5) Lawson D. F.; Hergenrother W. L.; Matlock M. G. *J. Appl. Polym. Sci.* **1990**, *39*, 2331.

(6) Oshinski A. J.; Keskkula H.; Paul D. R. *Polymer* **1992**, *33*, 268.

(7) Oshinski A. J.; Keskkula H.; Paul D. R. *Polymer* **1992**, *33*, 284.

(8) Gilmore D. W.; Modic M. J. *Plast. Eng.* **1989**, *April*, 29.

(9) Brady A. J.; Keskkula H.; Paul D. R. *Polymer* **1994**, *35*, 3665.

(10) Loyens W.; Groeninckx G. *Polymer* **2002**, *43*, 5679.

(11) Kanai H.; Sullivan V.; Auerbach A. *J. Appl. Polym. Sci.* **1994**, *53*, 527.

(12) Sanchez-Solis A.; Estrada M. R.; Cruz J.; Manero O. *Polym. Eng. Sci.* **2000**, *40*, 1216.

(13) Cecere A.; Greco R.; Ragosta G.; Scarzini G.; Tagliatela A. *Polymer* **1990**, *31*, 1239.

(14) Akkapeddi M. K.; Van Buskirk B.; Mason C. D.; Chung S. S.; Swamikannu X. *Polym. Eng. Sci.* **1995**, *35*, 72.

(15) Penco M.; Pastorino M.A.; Ochiello E.; Garbassi F.; Braglia R.; Giannotta G. *J. Appl. Polym. Sci.* **1995**, *57*, 329.

(16) Mouzakis D. E.; Papke N.; Wu J. S., K.-K. J. *J. Appl. Polym. Sci.* **2001**, *79*, 842.

(17) Tanrattanakul V.; Hiltner A.; Baer E.; Perkins W.G.; Massey F.L.; Moet A. *Polymer* **1997**, *38*, 2191.

(18) Hert M. *Angew. Macromol. Chem.* **1992**, *196*, 89.

(19) Kyotami M.; Pudjiastuti W.; Saeed A.J. *Macromol. Sci Phys* **1999**, *B38*, 197.

(20) Bedia E. L.; Murakami S.; Kitade T.; Kohjiya S. *Polymer* **2001**, *42*, 7299.

(21) Pang Y. X.; Jia D. M.; Hu H. J.; Hourston D. J. *Polymer* **2000**, *41*, 357.

(22) Santos P.; Henrique Pezzin S. *J. Mater. Process. Tech.* **2003**.

(23) Girija B.G.; Sailaja R.R.N.; Madras G. *Polym. Degrad. Stabil.* **2005**, *90*, 147.

(24) Kim, W. N.; Burns, C. M. *J. Appl. Polym. Sci.* **1990**, *41*, 1575.

(25) Loyens W.; Groeninckx G. *Polymer* **2003**, *44*, 4929.

(26) Ramsteiner F.; Heckmann W.; McKee G.E.; Breulmann M. *Polymer* **2002**, *43*, 5995.

(27) Ito K.; Yamashita K.; Nonomura C.; Suzuki T.; Ishihara H.; Nakai A.; Yamada T. *Plastics, Rubber and Composites* **2002**, *31*, 151.

(28) Launay A.; Thominette F.; Verdu J. *J. Appl. Polym. Sci.* **1999**, *73*, 1131.

(29) Papadopoulou C. P.; Kalfoglou N. K. *Polymer* **1997**, *38*, 631.

(30) Du X. H.; Wang Y. Z.; Chen X. T.; Tang X. D. *Polym. Degrad. Stabil.* **2004**, *88*, 52.

(31) Abu-Isa I. A.; Jaynes C. B.; O'Gara J. F. *J. Appl. Polym. Sci.* **1996**, *59*, 1957.

Chapter 5

Conclusions and Future Work

5.1 Physical Properties

5.1.1 Conclusions

PET/PC blends are immisible and the degree of crystallinity observed in PET regions is heavily influenced by the concentration of PC in the blend and this can fluctuate widely on the microscale. Crystallinity is inhibited when the blend contains 10% PC and is prevented when the PC concentration reaches 30%. The degree of crystallinity achievable for blends containing up to 25% PC, ranges from 5 to 35% and is likely to be influenced by the length of time and the temperature at which the blend is heated in the extruder. These factors are in turn influenced by the molecular weight and composition of the blend. Thermal degradation occurs when the blend is not rigorously dry. No anecdotal observations have been recorded of yellowing or bubbling of dry material during heating including holds of up to an hour at 300°C.

5.1.2 Future Work

- Study the volatiles released during heating of dry PET/PC by TGA-MS
- Vary the screw speed and temperature to optimise the melt extrusion of PET/PC to give the desired degree of crystallinity

5.2 Chemical Properties

5.2.1 Conclusions

PET/PC blends are very slow indeed to react when the blend is dried thoroughly. When reaction occurs it does so at the PET/PC interface and proceeds via a second order reversible process. DEG is lost in the heating process for PET/PC blends, it is not known

how much of this is subject to scission by reaction (DEG cut into two EG units with a PC unit between) and how much is due to volatilization. The reaction of PET/PC can be followed by comparing the integrals of the EG, EG*, Terephthalate and Bisphenol-A unit protons (4.7 ppm, 4.5 ppm (and 4.0 ppm), 8.0 ppm, 7.0-7.2 ppm respectively). End-capping is not observed at an appreciable rate for either carboxyl or hydroxyl end groups exposed to TFA.

5.2.2 Future Work

- Produce high molecular mass of known end groups and study the reaction between these end groups and TFA
- Produce high molecular mass PC of known end groups and compare the reaction rates resulting between different end groups

5.3 Mechanical Properties

5.3.1 Conclusions

Melt blending produces high molecular weight material which has similar impact strength and elastic behaviour to *Base* and *Laser* PET. Melt blended PET/PC is less ductile than PET and as a result it fractures much sooner after the yield point. It is suspected voiding may play a part in this. Surface crazing is observed in thin mouldings which have been injection moulded under the same conditions as would be used for PET.

5.3.1 Future Work

- Experiment with plasticizers to improve inelastic behaviour
- Vary injection temperature and speed to optimise injection moulding process

Appendix I

5.1 Other Techniques

5.1.1 SANS

Small angle neutron scattering (SANS) of unreacted and transesterified PET/PC blends was carried out on LOQ at ISIS in the Rutherford-Appleton Laboratories in Didcot, Oxfordshire. In order to get contrast between the two polymers deuterium labeling was necessary, dPET was synthesized due to the relative complexity of synthesizing PC. The synthesis used is set out below.

5.1.2 Esterification of d-Terephthalic Acid

The synthesis used involved the esterification of d-terephthalic acid followed by a transesterification step as proposed by Hallas.[1] d4 Terephthalic acid (shown in figure x) purchased from CK Gas Products in 98% purity was dried at room temperature *in vacuo* for twentyfour hours prior to reaction. Drying was carried out at room temperature to prevent the terephthalic acid subliming.

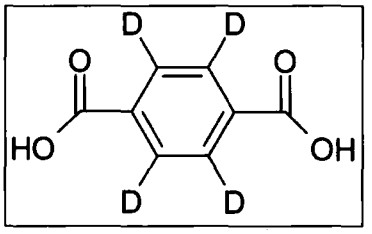

Figure 5.1 Terephthalic acid used in dPET synthesis

All glassware was dried over night before use, the methanol which was used was dried over anhydrous $MgSO_4$ and stored over 4 Å molecular sieves.

A two neck 500 ml round bottom flask was placed in a stirring isomantle and fitted with a stirrer bar and condenser and purged with nitrogen. Once the apparatus had been

thoroughly purged the nitrogen flow was reduced to a low level and a bubbler attached. The dry d-terephthalic acid was placed in the flask and a rubber stopper added to keep out moisture. It was known from prior work that the solubility of dimethyl terephthalate was 5.7 g in 100 ml of methanol. With this in mind, sufficient methanol was used to dissolve the d-dimethyl terephthalate expected to be produced by the reaction; assuming a quantitative yield. Methanol was injected through the rubber stopper using a dry syringe. Two equivalents (relative to the d-terephthalic acid) of BF_3-methanol complex were added likewise. The BF_3-methanol complex used was purchased from Aldrich and was in the form of a 50% solution in methanol. The mixture was refluxed under nitrogen until a clear, colourless solution had formed. The reaction was then let down to room temperature and pressure.

The d-dimethyl terephthalic acid (d-DMT) produced was isolated by neutralising the solution and filtering off the resultant solution. The neutralisation was carried out with $NaHCO_3$, purchased from Aldrich in 99.9% purity which used as supplied. A solution containing six equivalents (relative to the BF3-methanol complex) was prepared in a beaker larger than twice the total liquid volume of the methanol and base solutions to allow for evolution of CO_2. The methanol solution was then added very slowly with stirring. Once fully added the foam formed on the surface was allowed to dry down and the residue on the sides was washed off into the solution below with more distilled water. During the neutralisation the d-DMT precipitated as a white crystalline solid and was recovered by filtration. Once isolated, the d-DMT was filtered hot in methanol by means of solvent extracting apparatus. The solution obtained was then left to cool to room

temperature and white needle-like crystals collected and dried. The eluent from this filtration was then left and more d-DMT then precipitated and was filtered.

The purity of the d-DMT was checked by proton NMR and by melting point. Pure d-DMT gave a melting point of 140-142°C in agreement with literature.[1] A melting point apparatus was used to avoid complications in the DSC related to the d-DMT subliming.

5.1.3 Transesterification of dDMT

The transesterification step was carried out as described by Gumther and Zachman[2]. The reaction was catalysed with 0.112 mol % $Mn(OAc)_2$ (98% pure, used as purchased from Sigma-Aldrich), 0.0288 mol % Sb_2O_3 (99.999% purity, used as purchased from Sigma-Aldrich) and 0.03 mol % triphenyl phosphate (99+% purity, used as purchased from Sigma-Aldrich). The catalysts and d-DMT were added to the hot finger, then 2.5 equivalents (relative to d-DMT) of d_4-ethylene glycol were added (structure shown in Figure 5.3). The vessel used, shown in Figure 5.2, incorporates a hot finger and glass stirring rod with air tight seal. The glass rod was connected to a motor via a rubber tube to prevent the rod shearing at the head of the motor. All glassware was dried overnight before use. The reagents were all placed in the hot finger (at room temperature) then the apparatus was purged with N_2 (via the right hand socket in Figure 5.2), a cold finger

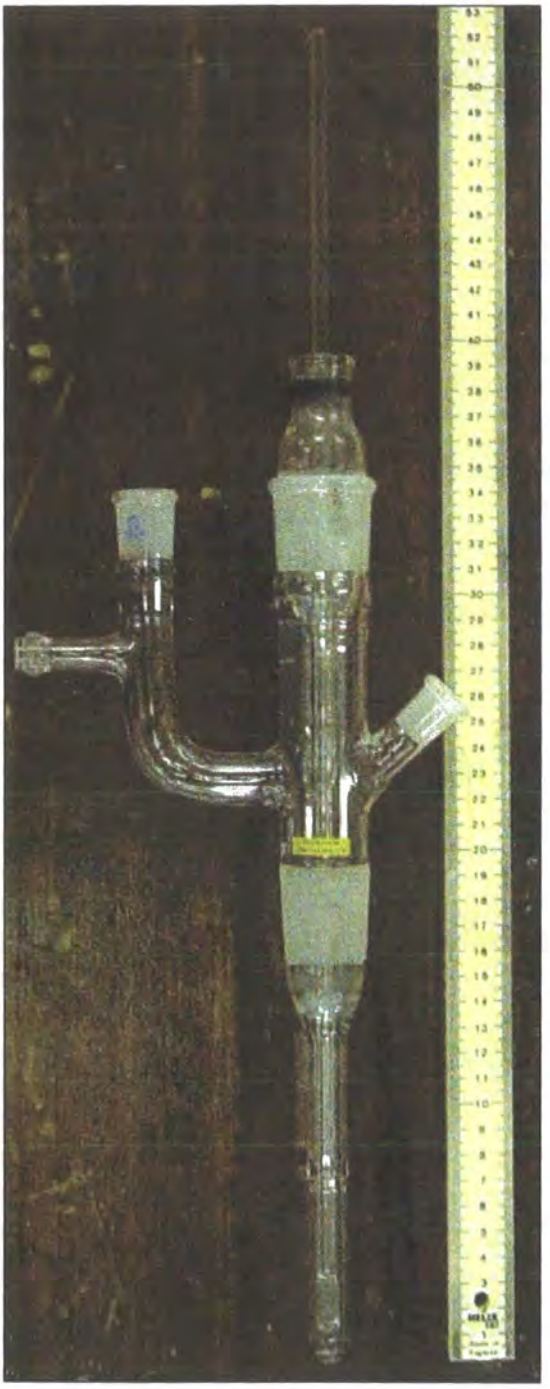

Figure 5.2 Reaction vessel for production of dPET

inserted (in the left top neck) and a condenser was attached. The condenser initially lead out to a bubbler while the device was being purged with N_2. The cold finger was initially set to 69°C to allow methanol to leave via the condenser but not ethylene glycol. The hot finger was then immersed in a round bottom flask of high temperature oil bath making use of the quickfit neck to keep a better seal and improve heating. During heating the stirrer was set to 300 rpm, the oil bath was heated using the profile shown in Figure 5.4.

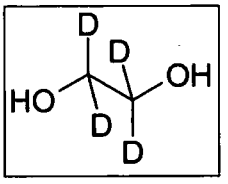

Figure 5.3 d_4 Ethylene Glycol

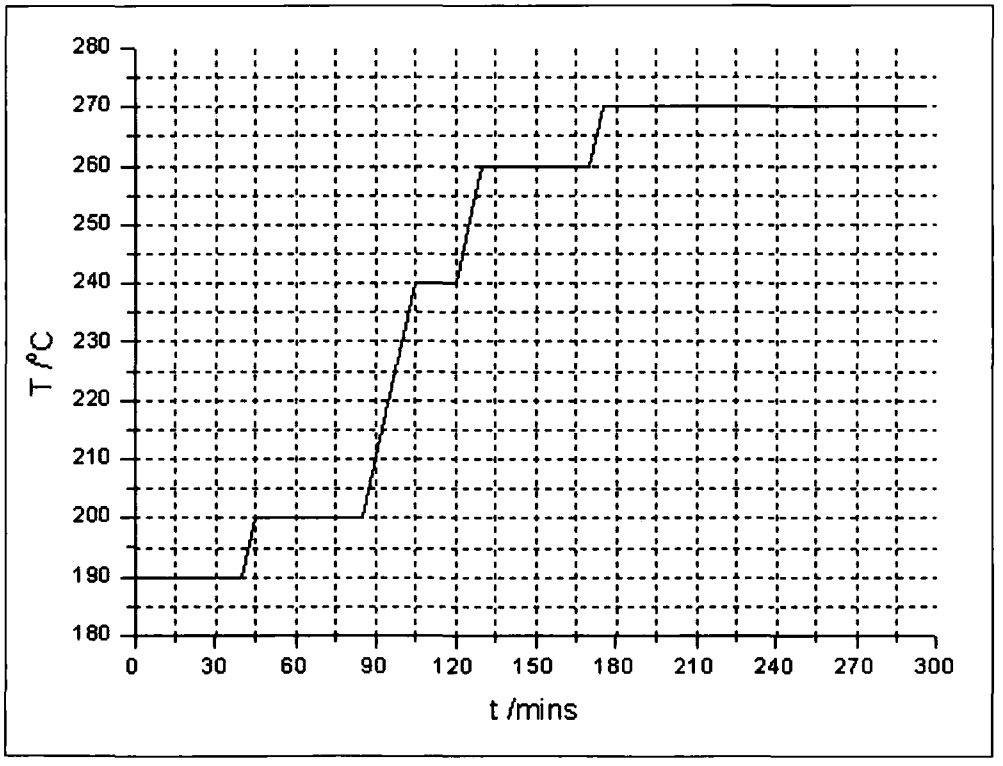

Figure 5.4 Heating profile for dPET reaction

Once the reaction had reached 270°C the cold finger was replaced with a stopper and the gas inlet was also stoppered. The stirrer was reduced to 100 rpm and the pressure was

then slowly reduced slowly to 0.05 Torr over the course of 90 min. During this period the vessel was lagged with Al foil to assist the removal of EG. After an additional 30 min the reaction was let down to N_2 and allowed to cool overnight. The stirrer was raised out of the hot finger at this point.

The product was removed by cutting the hot finger off of the vessel and dissolving the contents in boiling OCP. Once cooled, the product was isolated by precipitation into excess methanol followed by filtration and solvent extraction as described into methanol. The material was characterised by SEC and ^{1}H and ^{13}C NMR.

Samples of 50% hPC and 50% PET were made up by dissolution in OCP and subsequent isolation as for PET. The blend was then pressed into disks 16mm in diameter and 1mm thick using 5 Tons of pressure. Once made the disks were placed inside a steel ring some 5 mm deep which was sealed top and bottom with aluminium plates covered with polyimide film. The samples were then placed between two pre-heated hot plates which were put under 0.5 Tons of pressure. The samples then heated for between 1 and 15 min at temperatures between 270 and 300°C. When the reaction was complete the pressure was removed and the sample was rapidly cooled in ice water. The polymer material was then removed from the steel ring and pressed back into a disc because bubbling during the reaction had lead to distortion.

5.1.4 Neutron Scattering

Small angle neutron scattering was carried out on the ISIS LOQ beamline at the Rutherford Appleton Laboratories. LOQ is used to investigate the shape and size of large molecules and structures with dimensions in the range 1 - 100 nm. The SANS samples received 85-130 mAmp hours beamtime and the TRANS samples just 15 mAmp hours.

5.1.5 Results

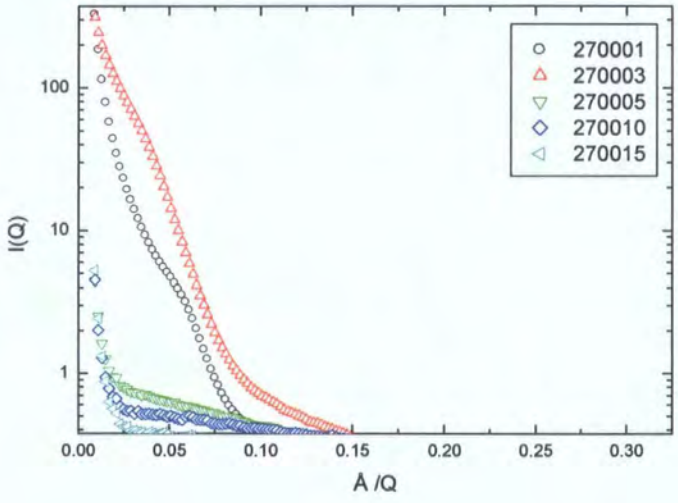

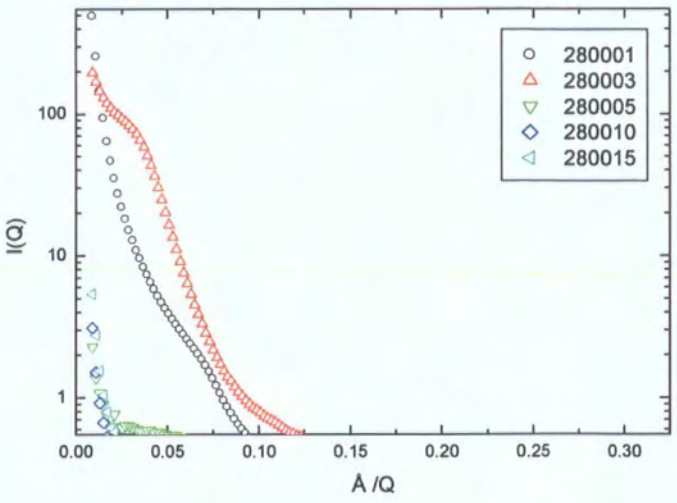
280001
280003
280005
280010
280015
100
10
1
I(Q)
0.00
0.05
0.10
0.15
0.20
0.25
0.30
Å /Q

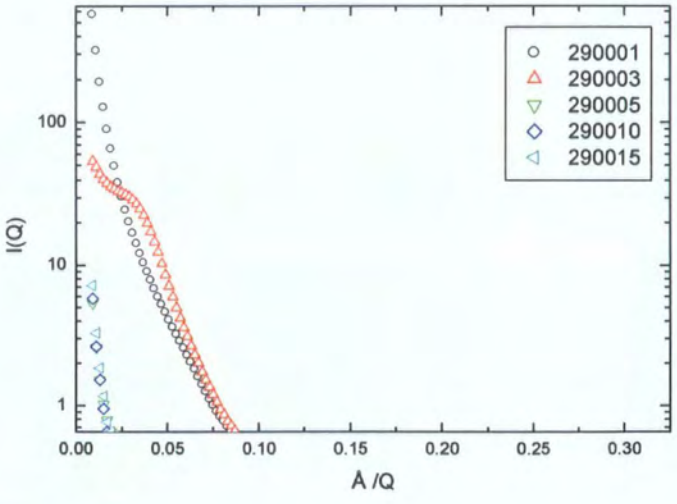
290001
290003
290005
290010
290015
100
10
1
I(Q)
0.00
0.05
0.10
0.15
0.20
0.25
0.30
Å /Q

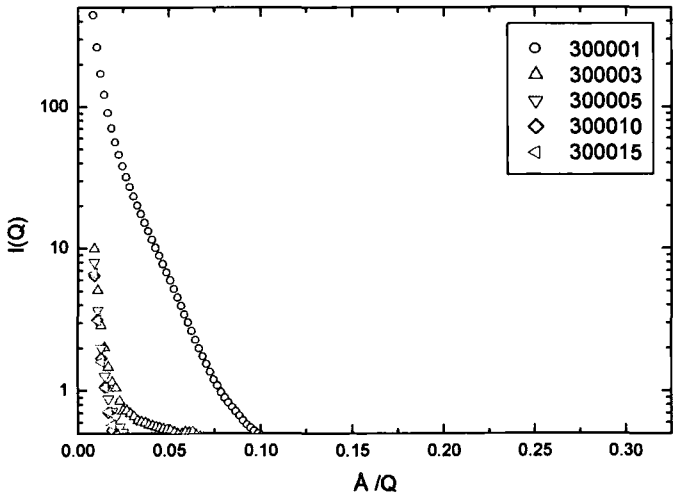

Figure 5.5 Zimm plot of Q data obtained from SANS

Zimm plots of the scattering data are presented in Figure 5.5, the first three digits of the sample codes refer to the reaction temperature (°C) and the next three to the number of minutes reaction that sample received.

The Zimm plot should show some detail at lower Q ($\frac{1}{Q} > 0.15$ Å) the positions of which would refer to structural repeat units such as lattice dimensions or particle sizes. All of this area is however dominated by a very large feature thought to be caused by the macroscopic dispersion of PC within the PET. This inhomogeniety means that useful data cannot be extracted if indeed it does underlie the curves.

5.1.6 Conclusions

SANS is not a suitable probe for PET/PC systems due to inhomogeneity in the sample.

5.1.7 ESEM/EDX

Conventional Scanning Electron Microscopy (SEM) uses a beam of electrons which interact with the atoms in a sample and give out secondary electrons. These are detected and the surface of the object mapped out as a function of the intensity of the electron scattered. In Enviromental SEM (ESEM) the need for a high vacuum is removed and the atmosphere is instead around 10 Torr of an imaging gas, commonly water. In this case as secondary electrons are ejected from the material they cause a cascade of further electrons in the atmosphere and this is then detected. ESEM is a far simpler technique and no preparation time is necessary in most cases but resolution is lower than in conventional SEM.

In Energy Dispersive X-ray (EDX) analysis an electron beam is used to strike the surface of a sample. The energy of the beam is typically in the 10-20 keV range and causes the region of the sample being probed to emit X-rays. The energy of the X-rays emitted depends on the elemental content of the material and it can sometimes be possible to obtain quantitative information about the sample. Since the technique has a narrow beam it can also be possible to obtain information along a series of points on the same sample. The intention was to use EDX to look at the morphology of PET/PC blends and to scan across the interface to obtain information about inter-diffusion in the sample under annealing.

5.1.8 Experimental

ESEM was carried out using a Philips XL30 ESEM with combined MCTRL 6.0 microscope at Durham University. Water was used as the imaging gas.

EDX was carried out using a Jeol Scanning Microscope at Newcastle University.

5.1.9 Results

Figures 5.6 and 5.7 show the level of contrast which was observed in PET/PC systems. The light grey colour is indicative of PET, as shown in Figure 5.7 where spherulites are visible. Some pockets of PET are present in the PC shown in Figure 5.6 but for the most part the material is made up of large continuous regions of homopolymer.

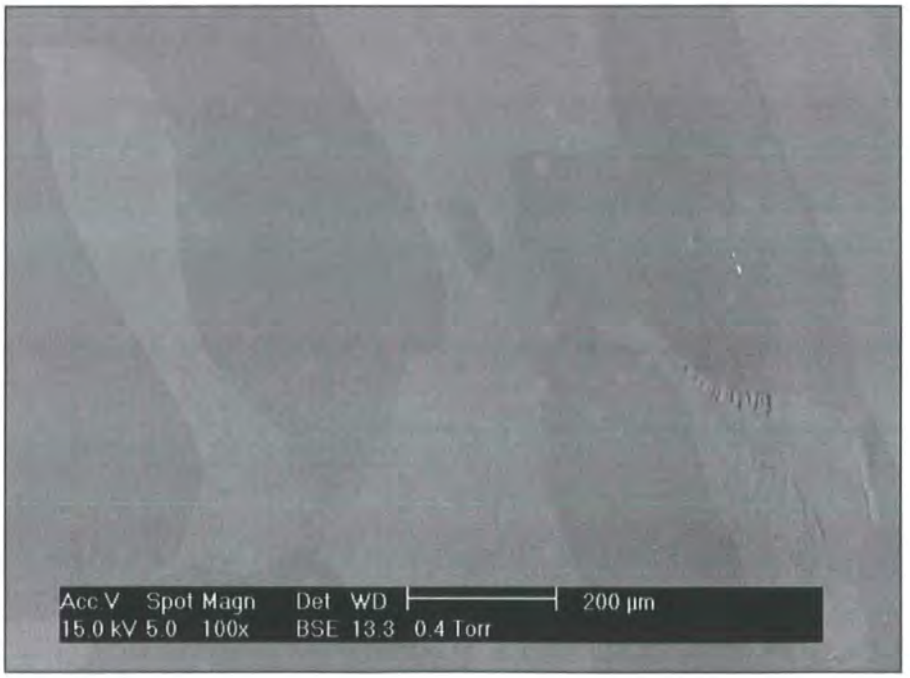

Figure 5.6 PET/PC imaged using ESEM

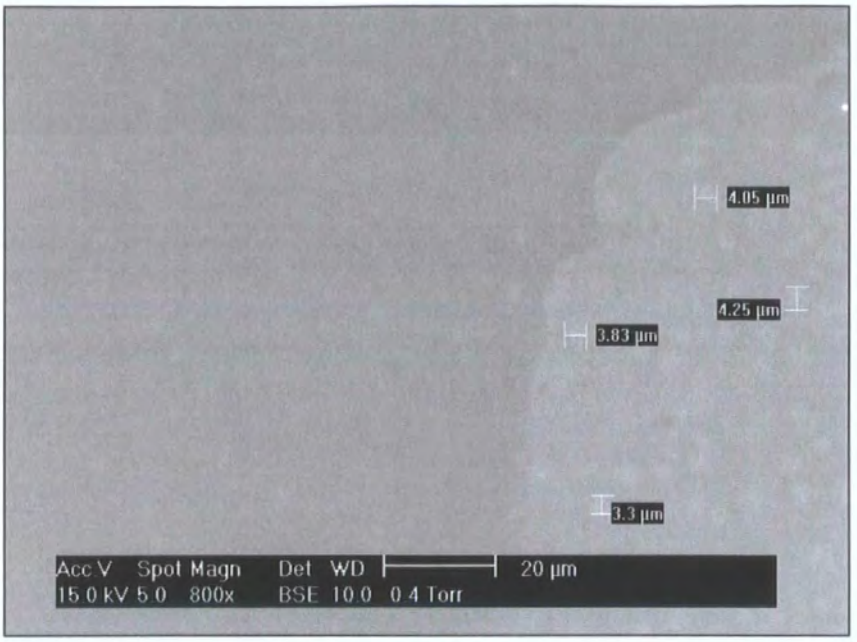

Figure 5.7 ESEM of spherulite in PET component of PET/PC

EDX was used to probe this boundary but the two polymers were not sufficiently different to allow quantitative analysis of inter-diffusion.

5.1.10 Conclusions

The contrast between PET and PC is not great enough to allow quantitative EDX.

5.2 Tables

Table I – DSC data (glass transitions, melting point and endotherm) of PET/PC 50:50 blends transesterified for time t_{rxn}.

T /°C	t_{rxn} /min	T_g 1 /°C	T_g 2 /°C	T_m /°C	ΔH /J/g
270	0	80	143	255	24
270	5	76	146	248	20
270	10	84	133	250	20
270	15			250	22
270	20	75	129	251	22
270	25	80	132	252	22
270	30	80	143	252	22
270	40	84	140	257	19
270	60	93	145	255	23
270	90	92	104	256	24
270	120		103		
280	0	80	143	255	24
280	5				
280	10			256	9
280	15	80	139		
280	20	81	146	258	12
280	25	80	141	258	8
280	30			260	6
280	40	84	139	213	5
280	60	82	138	209	3
280	90	87	123	181	7
280	120	82	109	194	6
290	0	80	143	255	24
290	5	83		241	
290	10	83		225	12
290	15	81		220	12
290	20	81		223	
290	25	93	138	218	8
290	30	83		212	9
290	40	99			
290	60	99	115		
290	90	101			
290	120	97	110		
300	0	80	143	255	24
300	5	80		233	10
300	10	83	136	219	11
300	15	87	134	220	6
300	20	106	126		
300	25	103			
300	30				
300	40		107		

T /°C	t_{rxn} /min	T_g 1 /°C	T_g 2 /°C	T_m /°C	ΔH /J/g
300	60		113		
300	90				
300	120	92	101		

Table II – DSC data from melt blended PET/PC (variable composition). The data given are the size and onset of the crystallization and melting endotherms.

	% PET		% PC			Data					
Blend	Laser	Base	2605	1239	2205	$Area_{250}$ /mJ	ΔH /J g^{-1}	$Area_{150}$ /mJ	ΔH /J g^{-1}	$Onset_{250}$°C	$Onset_{150}$°C
1		90	10			314	33	-256	-27	232	142
2		75	25			222	24	-187	-20	239	142
3		60	40			325	32			237	
4		50	50			212	19	-138	-13	232	139
5		10	90			40	4			238	
6		90		10		313	32	-266	-28	249	141
7		90			10	334	32	-295	-28	233	143
8		75			25	295	27	-228	-21	240	140
9		50			50	188	18	-118	-11	241	140
10	90			10		317	29	-273	-25	229	142
11	75			25		291	26	-220	-20	240	142
12	50			50		161	15	-120	-11	229	136
13	90				10	304	30	-283	-28	235	144
14	90		10			292	29	-241	-16	230	163
15	75		25			257	25	-195	-19	231	143

Tables III – Data from solution IV of solid state polymerized material.

Hours SSP	$\overline{M}_n$	$\overline{M}_w$	PDI
0	38100	61900	1.62
0	39200	64400	1.64
1	42100	68000	1.62
1	40800	67400	1.65
2	45200	74500	1.65
2	45400	74400	1.64
3	44600	74800	1.68
3	44700	75500	1.69
4	44200	76500	1.73
4	43700	76500	1.75
5	43800	74800	1.71
5	44100	73400	1.66
6	43700	74700	1.71
6	45400	75400	1.66
7	44000	72900	1.66
7	45900	75900	1.65
10	43200	74500	1.72
10	42900	74100	1.73

Table IV – Optical Microscopy data showing the temperature the sample was reacted at, for how long, the temperature at which it was crystallized at, the interval between the two images being acquired and the diameter of each spherulite in the first and second image.

T_{rxn} /°C	t /s	T_c /°C	t_c /s	D_1 /nm	D_2 /nm	G /nm/s
270	180	150	130	4000	7000	23.08
270	180	150	130	3500	6250	21.15
270	180	150	130	3000	4500	11.54
270	180	150	130	4000	6000	15.38
270	180	150	130	4250	7000	21.15
270	180	150	120	7000	9750	22.92
270	300	150	540	2000	4250	4.17
270	300	150	540	2000	5000	5.56
270	480	150	720	3000	4250	1.74
270	480	150	720	3000	4000	1.39
270	480	150	720	3000	4000	1.39
270	600	150	830	5000	6750	2.11
270	600	150	830	4750	6000	1.51
270	600	150	830	4000	5000	1.20
270	600	150	830	4000	5000	1.20
270	1200	150	600	6000	7750	2.92
270	1200	150	600	4250	6000	2.92
270	1200	150	600	5000	7000	3.33
270	1200	150	600	4500	5000	0.83
270	1200	150	665	6000	7250	1.88
270	1200	150	665	5000	6000	1.50
270	1200	150	665	3750	4500	1.13
270	1200	150	625	4500	5000	0.80
270	1200	150	625	7000	8500	2.40
270	1200	150	3840	7000	12025	1.31
280	180	150	360	3250	4500	3.47
280	180	150	360	3750	5750	5.56
280	180	150	360	4000	6000	5.56
280	180	150	600	4500	6500	3.33
280	180	150	600	2750	5000	3.75
280	180	150	750	6500	9500	4.00
280	300	150	530	5500	7000	2.83
280	300	150	530	6000	7250	2.36
280	300	150	530	5000	6000	1.89
280	300	150	530	6000	7000	1.89
280	300	150	530	7500	8500	1.89
280	300	150	530	8000	8750	1.42
280	300	150	530	7750	9000	2.36
280	300	150	530	5000	6500	2.83
280	300	150	530	7250	9000	3.30
280	300	150	530	6250	7000	1.42

T_{rxn} /°C	t /s	T_c /°C	t_c /s	D_1 /nm	D_2 /nm	G /nm/s
280	300	150	530	6500	7000	0.94
280	480	150	1200	3500	5000	1.25
280	480	150	1200	2500	3250	0.63
280	480	150	2595	3250	4500	0.48
280	480	150	2595	5000	6250	0.48
280	600	150	615	7000	8000	1.63
280	600	150	615	6000	7000	1.63
280	600	150	615	5500	6000	0.81
280	600	150	840	7250	8000	0.89
280	600	150	840	4500	5000	0.60
280	600	150	840	5500	6000	0.60
280	600	150	840	7000	8000	1.19
280	600	150	840	8000	8500	0.60
280	600	150	840	7000	7250	0.30
280	600	150	840	6000	6250	0.30
280	1200	150	185	3500	4000	2.70
280	1200	150	185	3750	4750	5.41
280	1200	150	185	3500	3500	0.00
280	1200	150	185	3500	3750	1.35
280	1200	150	300	8000	8500	1.67
280	1200	150	300	6750	7000	0.83
280	1200	150	300	7000	7250	0.83
280	1200	150	300	8500	9000	1.67
280	1200	150	300	7000	7000	0.00
280	1200	150	300	7250	7250	0.00
280	1200	150	300	9000	9500	1.67
280	1200	150	300	7000	7250	0.83
280	1200	150	305	9500	9500	0.00
280	1200	150	305	7250	7500	0.82
280	1200	150	325	9500	10000	1.54
280	1200	150	325	7250	7750	1.54
280	1200	150	285	7750	8000	0.88
280	1200	150	305	8000	8250	0.82
280	1200	150	280	8250	8500	0.89
290	180	150	300	4000	5000	3.33
290	180	150	300	3500	5500	6.67
290	180	150	300	3750	5000	4.17
290	180	150	300	5000	6250	4.17
290	180	150	300	6000	6500	1.67
290	180	150	300	3750	4000	0.83
290	180	150	300	3250	4000	2.50
290	180	150	300	4250	5250	3.33
290	180	150	300	4000	4500	1.67
290	180	150	300	4000	5000	3.33
290	180	150	300	5250	6000	2.50
290	300	150	1440	6000	9000	2.08
290	300	150	1440	6000	8500	1.74

T_{rxn} /°C	t /s	T_c /°C	t_c /s	D_1 /nm	D_2 /nm	G /nm/s
290	300	150	1440	4750	6250	1.04
290	300	150	725	6250	7250	1.38
290	300	150	725	4500	6000	2.07
290	480	150	420	7000	7500	1.19
290	480	150	420	5750	6250	1.19
290	600	150	2645	4500	7250	1.04
290	600	150	2645	5000	7250	0.85
290	600	150	2645	5500	7000	0.57
290	600	150	2645	4500	5500	0.38
290	600	150	2645	3500	6000	0.95
290	1200	150	1950	3000	3750	0.38
290	1200	150	1950	3250	3750	0.26
290	1200	150	1950	3000	4500	0.77
290	1200	150	1950	3000	3750	0.38
300	180	150	960	8000	8500	0.52
300	180	150	960	4000	5000	1.04
300	180	150	960	5300	6300	1.04
300	180	150	960	4000	5000	1.04
300	180	150	960	4300	5000	0.73
300	300	150	570	8600	9600	1.75
300	480	150	1820	3500	4750	0.69
300	480	150	1820	4500	5000	0.27
300	480	150	1820	7500	8750	0.69
300	480	150	1860	4750	5000	0.13
300	480	150	1860	5000	5250	0.13
300	480	150	1860	8750	9250	0.27
300	480	150	1860	5750	7000	0.67
300	600	150	2100	4300	5000	0.33
300	600	150	2100	4600	6500	0.90
300	600	150	2100	6300	8000	0.81
300	600	150	2100	3600	4500	0.43

Table V – Rates of spherulitic growth for PET and PC at specified crystallization temperatures.

Polymer	T_{cryst}	G/(nm/s)	References
PET	120	3.28	[3]
PET	130	8.50	[3]
PET	140	19.9	[3]
PET	150	36.8	[3]
PET	160	56.2	[3]
PET	180	72.1	[3]
PET	190	63.6	[3]
PET	200	43.9	[3]
PET	210	20.2	[3]
PC	180	0.0833	[4]
PC	185	0.042	[4]

Table VI – Raman data for each sampling point on the samples used. I_{855} and I_{735} refer to the area of the peaks at $855cm^{-1}$ and 735^{-1}.

Sample 270005		
Sampling Point	I_{855}	I_{735}
1	1	3865
2	1616	2062
3	3687	5396
4	14021	28394
5	6042	31968
6	6324	38957
7	9278	38908
8	20291	35186
sample 270010		
Sampling Point	I_{855}	I_{735}
1	10365	1138
2	26611	8850
3	9636	12428
4	32374	46071
5	32202	48324
6	12070	57185
7	63670	42314
8	167463	4289
9	185695	5852
10	191354	7893

Sample 2700030		
Sampling Point	I_{855}	I_{735}
1	1	412
2	1	1
3	1	66
4	27212	14632
5	14769	22465
6	12845	20119
7	21360	21304
8	88516	9762
9	97458	11930
10	86373	10900
Sample 300005		
Sampling Point	I_{855}	I_{735}
1	414	446
2	3285	1692
3	6325	1741
4	16317	25045
5	21954	30408
6	7231	37893
7	22761	24493
8	31657	23142
9	63586	9367
10	71189	5817
sample 300010		
Sampling Point	I_{855}	I_{735}
1	630	4894
2	1	4683
3	200	3280
4	2488	13753
5	20272	19563
6	13759	22032
7	9930	24544
8	59664	4000
9	58029	6482
10	30622	14044
sample 300030		
Sampling Point	I_{855}	I_{735}
1	7255	8425
2	3597	9263
3	3014	7435
4	2974	5940
5	878	5220
6	375	1677
7	1	1328
8	1	1
9	1	1

Table VII – Literature data on the rate of reaction of PBT and PC by ^{13}C NMR (chemical shifts relative to TMS).[5]

Reaction Time /s	Old/New PC peak		[PC] (b-x)	[PC*] (x)	[PBT] (a-x)	Ln(b/(b-x))
	119.1ppm	119.6ppm				
900	75	0	1	0	1.2	0.000
1860	59	19	0.756	0.244	0.9	0.227
4500	46	41	0.529	0.471	0.7	0.499
6000	36	47	0.434	0.566	0.6	0.638
12000	34	46	0.425	0.575	0.6	0.652

Table VIII – ^{1}H NMR data of 50:50 PET/BPA samples analysed as first order in PET, PC, second order irreversible and first order reversible.

I(EG) – Intensity of the peak at 4.65ppm attributed to the EG protons between two terephthalate units

I(EG*) – Intensity of the peak at 4.30ppm attributed to the EG* protons between one terephthalate and one carbonate unit

I(BCB) – Intensity of Bisphenol-A units adjacent to another Bisphenol-A unit relative to the amount of EG and based on I(EG*)

$I(EG^*)_{tot}$ – I(EG*) × 2 to account for the two protons not covered by the peak at 4.30

Mole fractions – conversion of peak intensity to mole fractions

A – 270°C

	4.30ppm	4.65ppm	4.30ppm		Mole Fractions			Kinetic Plots			
t /s	I_{EG^*}	I_{EG}	I_{EG^*} (Tot)	I_{BCB}	EG	EG*	PC	Ln(b/(b-x))	Ln(a/(a-x))	Irrev 2nd	Rev 2nd
0	0.00	100.00	0.00	72.35	0.58	0.00	0.42	0.000000	0.000000	0.000000	0.000000
300	0.03	87.19	0.06	59.54	0.59	0.00	0.41	0.000704	0.000974	0.360205	0.001679
600	0.02	88.96	0.04	61.31	0.59	0.00	0.41	0.000459	0.000634	0.302874	0.001093
900	0.00	88.79	0.00	61.14	0.59	0.00	0.41	0.000000	0.000000	0.308258	0.000000
1200	0.05	88.30	0.10	60.65	0.59	0.00	0.41	0.001156	0.001598	0.323921	0.002757
1500	0.10	88.58	0.20	60.93	0.59	0.00	0.41	0.002302	0.003183	0.314945	0.005493
1800	0.00	88.46	0.00	60.81	0.59	0.00	0.41	0.000000	0.000000	0.318783	0.000000
2400	0.00	85.97	0.00	58.32	0.60	0.00	0.40	0.000000	0.000000	0.401420	0.000000
3600	8.40	59.94	16.80	32.29	0.48	0.13	0.26	0.261509	0.382813	1.838435	0.794451

B – 275°C

	4.30ppm	4.65ppm	4.30ppm		Mole Fractions			Kinetic Plots			
t /s	I_{EG^*}	I_{EG}	I_{EG^*} (Tot)	I_{BCB}	EG	EG*	PC	Ln(b/(b-x))	Ln(a/(a-x))	Irrev 2nd	Rev 2nd
0	0.00	100.00	0.00	72.35	0.58	0.00	0.42	0.000000	0.000000	0.000000	0.000000
300	0.00	96.53	0.46	68.88	0.57	0.00	0.43	0.004948	0.006845	-	0.011827
600	0.23	90.83	0.76	63.18	0.58	0.00	0.41	0.008503	0.011772	0.188047	0.020377
900	0.38	90.00	1.02	62.35	0.59	0.01	0.40	0.011339	0.015707	0.375542	0.027226
1200	0.51	91.53	0.00	63.88	0.00	0.00	1.00	0.000000	0.000000	-	0.000000
2400	1.84	83.21	3.68	55.56	0.57	0.03	0.38	0.044373	0.061867	0.500223	0.109140
3600	7.22	66.85	14.44	39.20	0.50	0.11	0.29	0.203889	0.294293	1.309761	0.578728

C – 280°C

	4.30ppm	4.65ppm	4.30ppm		Mole Fractions			Kinetic Plots			
t /s	I_{EG^*}	I_{EG}	I_{EG^*} (Tot)	I_{BCB}	EG	EG*	PC	Ln(b/(b-x))	Ln(a/(a-x))	Irrev 2nd	Rev 2nd
0	0.00	100.00	0.00	72.35	0.58	0.00	0.42	0.000000	0.000000	0.000000	0.000000
300	0.00	100.00	0.00	72.35	0.58	0.00	0.42	0.000000	0.000000	0.000000	0.000000
600	0.14	86.76	0.28	59.11	0.59	0.00	0.40	0.003301	0.004566	0.374568	0.007882
900	0.40	84.18	0.80	56.53	0.59	0.01	0.40	0.009736	0.013482	0.464580	0.023351
1200	0.43	84.75	0.86	57.10	0.59	0.01	0.40	0.010378	0.014373	0.444108	0.024901
1500	0.76	82.90	1.52	55.25	0.59	0.01	0.39	0.018729	0.025981	0.511834	0.045207
1800	1.00	80.53	2.00	52.88	0.59	0.01	0.38	0.025406	0.035289	0.604325	0.061619
2400	2.32	74.31	4.64	46.66	0.57	0.04	0.36	0.063364	0.088683	0.883293	0.158131
3600	3.34	70.06	6.68	42.41	0.56	0.05	0.34	0.095957	0.135209	1.111496	0.245853

D – 285°C

	4.30ppm	4.65ppm	4.30ppm		Mole Fractions			Kinetic Plots			
t /s	I_{EG^*}	I_{EG}	I_{EG^*} (Tot)	I_{BCB}	EG	EG*	PC	Ln(b/(b-x))	Ln(a/(a-x))	Irrev 2nd	Rev 2nd
0	0.00	100.00	0.00	72.35	0.58	0.00	0.42	0.000000	0.000000	0.000000	0.000000
300	0.32	90.00	0.64	62.35	0.59	0.00	0.41	0.007206	0.009974	0.270473	0.017252
600	0.38	90.61	0.76	62.96	0.58	0.00	0.41	0.008482	0.011742	0.251892	0.020325
900	1.39	86.83	2.78	59.18	0.57	0.02	0.39	0.032122	0.044677	0.372218	0.078291
1200	1.59	84.72	3.18	57.07	0.57	0.02	0.39	0.037696	0.052487	0.445177	0.092256
1500	2.05	81.23	4.10	53.58	0.57	0.03	0.37	0.050674	0.070741	0.576300	0.125233
1800	4.23	75.66	8.46	48.01	0.54	0.06	0.34	0.109493	0.154726	0.817730	0.283773
2400	6.63	66.98	13.26	39.33	0.50	0.10	0.30	0.188805	0.271560	1.301233	0.527399
3600	8.49	61.93	16.98	34.28	0.48	0.13	0.26	0.254663	0.372150	1.669234	0.766947

E – 290°C

	4.30ppm	4.65ppm	4.30ppm		Mole Fractions			Kinetic Plots			
t /s	I_{EG^*}	I_{EG}	I_{EG^*} (Tot)	I_{BCB}	EG	EG*	PC	Ln(b/(b-x))	Ln(a/(a-x))	Irrev 2nd	Rev 2nd
0	0.00	100.00	0.00	72.35	0.58	0.00	0.42	0.00000	0.00000	0.00000	0.00000
300	0.00	100.00	0.00	72.35	0.58	0.00	0.42	0.00000	0.00000	0.00000	0.00000
600	0.16	88.22	0.32	60.57	0.59	0.00	0.41	0.00370	0.00511	0.32650	0.00883
900	0.58	82.71	1.16	55.06	0.59	0.01	0.39	0.01437	0.01992	0.51900	0.03459
1200	0.76	88.10	1.52	60.45	0.58	0.01	0.40	0.01743	0.02418	0.33038	0.04204
1500	1.41	85.44	2.82	57.79	0.57	0.02	0.39	0.03319	0.04618	0.41978	0.08096
1800	1.83	74.33	3.66	46.68	0.58	0.03	0.36	0.05040	0.07036	0.88230	0.12454
2400	3.07	69.94	6.14	42.29	0.56	0.05	0.34	0.08882	0.12497	1.11847	0.22623
3600	5.24	64.42	10.48	36.77	0.53	0.09	0.30	0.16002	0.22864	1.47786	0.43426

F – 295°C

	4.30ppm	4.65ppm	4.30ppm		Mole Fractions			Kinetic Plots			
t /s	I_{EG^*}	I_{EG}	I_{EG^*} (Tot)	I_{BCB}	EG	EG*	PC	Ln(b/(b-x))	Ln(a/(a-x))	Irrev 2nd	Rev 2nd
0	0.00	100.00	0.00	72.35	0.58	0.00	0.42	0.000000	0.000000	0.000000	0.000000
300	0.54	89.75	1.08	62.10	0.58	0.01	0.40	0.012160	0.016847	0.278178	0.029214
600	1.23	87.72	2.46	60.07	0.57	0.02	0.39	0.028157	0.039131	0.342739	0.068428
900	1.33	85.31	2.66	57.66	0.58	0.02	0.39	0.031404	0.043672	0.424325	0.076501
1200	3.20	78.14	6.40	50.49	0.55	0.05	0.36	0.081201	0.114066	0.704821	0.205540
1500	8.30	64.61	16.60	36.96	0.48	0.12	0.27	0.238624	0.347327	1.464092	0.704642
1800	4.22	76.82	8.44	49.17	0.54	0.06	0.34	0.107380	0.151671	0.763755	0.277791
2400	16.47	40.98	32.94	13.33	0.34	0.27	0.11	0.639331	1.058108	4.983216	-
3600	17.03	41.67	34.06	14.02	0.34	0.28	0.11	0.642710	1.065221	4.772694	-

G – 300°C

	4.30ppm	4.65ppm	4.30ppm		Mole Fractions			Kinetic Plots			
t /s	I_{EG^*}	I_{EG}	I_{EG^*} tot	I_{BCB}	EG	EG*	PC	Ln(b/(b-x))	Ln(a/(a-x))	Irrev 2nd	Rev 2nd
0	0.00	100.00	0.00	72.35	0.58	0.00	0.42	0.000000	0.000000	0.000000	0.000000
300	0.13	88.75	0.26	61.10	0.59	0.00	0.41	0.002985	0.004128	0.309529	0.007124
600	0.36	83.75	0.72	56.10	0.59	0.01	0.40	0.008822	0.012214	0.480254	0.021144
900	0.96	77.52	1.92	49.87	0.59	0.01	0.38	0.025540	0.035476	0.732183	0.061950
1200	2.13	75.11	4.26	47.46	0.57	0.03	0.36	0.057638	0.080575	0.844073	0.143204
1500	3.01	72.78	6.02	45.13	0.56	0.05	0.35	0.083210	0.116936	0.961433	0.210968
1800	4.17	68.58	8.34	40.93	0.54	0.07	0.32	0.120934	0.171314	1.199823	0.316563
2400	5.17	54.42	10.34	26.77	0.53	0.10	0.26	0.192299	0.276810	2.404836	0.539124
3600	8.43	46.43	16.86	18.78	0.47	0.17	0.19	0.347753	0.520857	3.624781	1.203026

Table IX – Randomness data from ^{1}H NMR results

A – 270°C

t /s	4.30ppm $I_{EG'}$	4.65ppm I_{EG}	4.30ppm $I_{EG'}$ tot	I_{BCB}	Mole Fractions EG	EG	EG	P_{TEB}	P_{BET}	B
0	0.00	100.00	0.00	72.35	0.58	0.00	0.42	0.0000	0.0000	0.0000
300	0.03	87.19	0.06	59.54	0.59	0.00	0.41	0.0007	0.0010	0.0017
600	0.02	88.96	0.04	61.31	0.59	0.00	0.41	0.0004	0.0007	0.0011
900	0.00	88.79	0.00	61.14	0.59	0.00	0.41	0.0000	0.0000	0.0000
1200	0.05	88.30	0.10	60.65	0.59	0.00	0.41	0.0011	0.0016	0.0028
1500	0.10	88.58	0.20	60.93	0.59	0.00	0.41	0.0023	0.0033	0.0055
1800	0.00	88.46	0.00	60.81	0.59	0.00	0.41	0.0000	0.0000	0.0000
2400	0.00	85.97	0.00	58.32	0.60	0.00	0.40	0.0000	0.0000	0.0000
3600	0.40	82.18	0.80	54.53	0.59	0.01	0.39	0.0096	0.0145	0.0241

B – 280°C

t /s	4.30ppm $I_{EG'}$	4.65ppm I_{EG}	4.30ppm $I_{EG'}$ (Tot)	I_{BCB}	Mole Fractions EG	EG*	PC	P_{TEB}	P_{BET}	B
0	0.00	100.00	0.00	72.35	0.58	0.00	0.42	0.0000	0.0000	0.0000
300	0.03	87.19	0.06	59.54	0.59	0.00	0.41	0.0007	0.0010	0.0017
600	0.02	88.96	0.04	61.31	0.59	0.00	0.41	0.0004	0.0007	0.0011
900	0.00	88.79	0.00	61.14	0.59	0.00	0.41	0.0000	0.0000	0.0000
1200	0.05	88.30	0.10	60.65	0.59	0.00	0.41	0.0011	0.0016	0.0028
1500	0.10	88.58	0.20	60.93	0.59	0.00	0.41	0.0023	0.0033	0.0055
1800	0.00	88.46	0.00	60.81	0.59	0.00	0.41	0.0000	0.0000	0.0000
2400	0.00	85.97	0.00	58.32	0.60	0.00	0.40	0.0000	0.0000	0.0000
3600	0.40	82.18	0.80	54.53	0.59	0.01	0.39	0.0096	0.0145	0.0241

C – 290°C

t /s	4.30ppm I_{EG^*}	4.65ppm I_{EG}	4.30ppm I_{EG^*} (Tot)	I_{BCB}	Mole Fractions EG	EG*	PC	P_{TEB}	P_{BET}	B
0	0	100.0	0.0	72.3	0.58	0.00	0.42	0.00000	0.00000	0.00000
300	0	100.0	0.0	72.3	0.58	0.00	0.42	0.00000	0.00000	0.00000
600	0.16	88.2	0.3	60.6	0.59	0.00	0.41	0.00361	0.00526	0.00887
900	0.58	82.7	1.2	55.1	0.59	0.02	0.39	0.01383	0.02063	0.03446
1200	0.76	88.1	1.5	60.4	0.58	0.02	0.40	0.01696	0.02453	0.04149
1500	1.41	85.4	2.8	57.8	0.57	0.04	0.39	0.03195	0.04653	0.07848
1800	1.83	74.3	3.7	46.7	0.58	0.06	0.36	0.04693	0.07271	0.11964
2400	3.07	69.9	6.1	42.3	0.56	0.10	0.34	0.08070	0.12678	0.20749
3600	5.24	64.4	10.5	36.8	0.53	0.17	0.30	0.13992	0.22181	0.36173

D – 300°C

t /s	4.30ppm I_{EG^*}	4.65ppm I_{EG}	4.30ppm I_{EG^*} (Tot)	I_{BCB}	Mole Fractions EG	EG*	PC	P_{TEB}	P_{BET}	B
0	0.00	100.0	0.0	72.3	0.58	0.00	0.42	0.0000	0.0000	0.0000
300	0.13	88.8	0.3	61.1	0.59	0.00	0.41	0.0029	0.0042	0.0072
600	0.36	83.8	0.7	56.1	0.59	0.01	0.40	0.0085	0.0127	0.0212
900	0.96	77.5	1.9	49.9	0.59	0.03	0.38	0.0242	0.0371	0.0612
1200	2.13	75.1	4.3	47.5	0.57	0.06	0.36	0.0537	0.0824	0.1360
1500	3.01	72.8	6.0	45.1	0.56	0.09	0.35	0.0764	0.1177	0.1941
1800	4.17	68.6	8.3	40.9	0.54	0.13	0.32	0.1084	0.1693	0.2777
2400	5.17	54.4	10.3	26.8	0.53	0.20	0.26	0.1597	0.2786	0.4383
3600	8.43	46.4	16.9	18.8	0.47	0.34	0.19	0.2664	0.4731	0.7395

Table X – Data from force extension curves of PET samples tested to failure

In the tables below the thickness, width and cross sectional area of the samples before and after testing are given as are the stress and the errors calculated on the standard deviation of results. The starting stress refers to the stress at the yield point.

A - *Laser*

A2	t /mm	w /mm	A /mm^2	Stress /MPa
t = 0s	1.103	3.837	4.232211	62.11842
Error	0.028	0.002	0.107437	1.576912
t = end	0.498	1.905	0.94869	297.6443
Error	0.003	0.015	0.005774	1.811492
A3	t /mm	w /mm	A /mm^2	Stress /MPa
t = 0s	1.107	3.839	4.249773	62.43451
Error	0.011	0.006	0.042239	0.62055
t = end	0.506	1.96	0.99176	281.282
Error	0.001	0.055	0.002741	0.777384
A4	t /mm	w /mm	A /mm^2	Stress /MPa
t = 0s	1.096	3.847	4.216312	60.62064
Error	0.018	0.003	0.069249	0.995631
t = end	0.504	2.085	1.05084	229.3309
Error	0.004	0.022	0.008457	1.845619

B – *Laser* blend

B2-1	t /mm	w /mm	A /mm^2	Stress /MPa
t = 0s	1.518	3.805	5.77599	62.5841
Error	0.044	0.011	0.167468	1.814555
t = end	0.757	2.576	1.950032	104.2338
Error	0.014	0.029	0.036311	1.940917
B2-2	t /mm	w /mm	A /mm^2	Stress /MPa
t = 0s	1.51	3.821	5.76971	60.54271
Error	0.052	0.006	0.198706	2.085064
t = end	-	-	-	-
Error	-	-	-	-
B1-3	t /mm	w /mm	A /mm^2	Stress /MPa
t = 0s	1.826	3.82	6.97532	61.24589
Error	0.077	0.05	0.295335	2.593151
t = end	0.951	2.512	2.388912	98.33115
Error	0.012	0.016	0.030241	1.244761

C – *Base*

C1	t /mm	w /mm	A /mm^2	Stress /MPa
t = 0s	1.425	3.818	5.44065	61.29623
Error	0.013	0.009	0.049664	0.559534
t = end	0.675	2.093	1.412775	215.3778
Error	0.003	0.037	0.006721	1.024543
C2	t /mm	w /mm	A /mm^2	Stress /MPa
t = 0s	1.433	3.804	5.451132	62.07147
Error	0.026	0.014	0.098978	1.12705
t = end	0.672	2.014	1.353408	271.589
Error	0.012	0.096	0.027243	5.466875
C3	t /mm	w /mm	A /mm^2	Stress /MPa
t = 0s	1.432	3.841	5.500312	61.29519
Error	0.036	0.01	0.138313	1.541356
t = end	0.667	1.953	1.302651	272.8279
Error	0.01	0.035	0.019948	4.177996

D – *Base* blend

D3-2	t /mm	w /mm	A /mm^2	Stress /MPa
t = 0s	1.814	3.785	6.86599	62.75294
Error	0.078	0.026	0.295554	2.701268
t = end	0.917	2.44	2.23748	146.8719
Error	0.04	0.089	0.100577	6.60203
D3-3	t /mm	w /mm	A /mm^2	Stress /MPa
t = 0s	1.847	3.802	7.022294	62.74275
Error	0.077	0.01	0.292803	2.616131
t = end	0.967	2.486	2.403962	100.247
Error	0.006	0.056	0.016136	0.672877
D4-1	t /mm	w /mm	A /mm^2	Stress /MPa
t = 0s	1.213	3.839	4.656707	62.7287
Error	0.014	0.01	0.053778	0.724417
t = end	0.609	2.234	1.360506	229.02
Error	0.008	0.057	0.018758	3.157566

Table XI – Data on notched impact strength

A - *Laser*

	t /mm	SD	Fmax /N	Fmax/mm /N/mm	E /J	File	Is /J/m
A1	3.951	0.004	Test				
A2	3.957	0.002	Test				
A3	3.953	0.005	202	51.1	0.122	6	30.9
A4	3.954	0.005	132	*	0.0565	7	*
A5	3.954	0.001	227	57.4	0.13475	8	34.1
A6	3.95	0.002	199.4	50.5	0.1043	9	26.4
A7	3.956	0.013	231.7	58.6	0.159	10	40.2
			Av	54.4		Av	32.9
			SD	4.2		SD	5.8

* Data rejected

B – *Laser* blend

	t /mm	SD	Fmax /N	Fmax/mm /N/mm	E /J	File	Is /J/m
B1	4.157	0.001	Test				
B2	4.162	0.006	Test				
B3	4.18	0.01	241	57.7	0.148	1	35.4
B4	4.13	0.001	252	61.0	0.161	2	39.0
B5	4.159	0.004	225	54.1	0.156	3	37.5
B6	4.158	0.017	239	57.5	0.172	4	41.4
B7	4.171	0.007	215	51.5	0.15	5	36.0
			Av	56.4		Av	37.8
			SD	3.6		SD	2.4

C - *Base*

	t/mm	SD	Fmax /N	Fmax/mm /N/mm	E /J	File	Is /J/m
C1	4.124	0.01	230	55.8	0.137	11	33.2
C2	4.116	0.001	225	54.7	0.1322	12	32.1
C3	4.116	0.011	198	48.1	0.12	13	29.2
C4	4.172	0.001	218.4	52.3	0.1227	14	29.4
C5	4.172	0.012	222.8	53.4	0.132	15	31.6
			Av	52.9		Av	31.1
			SD	3.0		SD	1.8

D – *Base* blend

	t /mm	SD	Fmax /N	Fmax/mm /N/mm	E /J	File	Is /J/m
D1	3.954	0.043	208.9	52.8	0.1145	16	29.0
D2	3.97	0.012	204.6	51.5	0.1324	17	33.4
D3	3.983	0.007	213.9	53.7	0.1143	18	28.7
D4	3.956	0.003	193.3	48.9	0.1135	19	28.7
D5	3.974	0.01	229.1	57.6	0.1459	20	36.7
			Av	52.9		Av	31.3
			SD	3.2		SD	3.6

5.3 References

(1) Hallas, G. *J. Chem. Soc.* **1965**, *OCT*, 5770.

(2) Gumther B.; H.G., Z. *Polymer* **1983**, *24*, 1008.

(3) Antwerpen F. van **1971**.

(4) Falkai B.V.; Rellensmann W. *Makromol. Chem.* **1964**, *75*, 112.

(5) Devaux J.; Godard P.; Mercier J.P.; Touillaux R.; Dereppe J.M. *J. Polym. Sci.: Polym. Phys. Ed.* **1982**, *20*, 1881.

Appendix II

6.1 Optical Micrographs

Below are the optical micrographs obtained of PET/PC. Each Reaction condition has one low magnification image and 15 of the 20 have higher magnification images of spherulites, the remaining 5 having no spherulites to magnify.

Reaction temperature 270°C
Reaction time 5 minutes

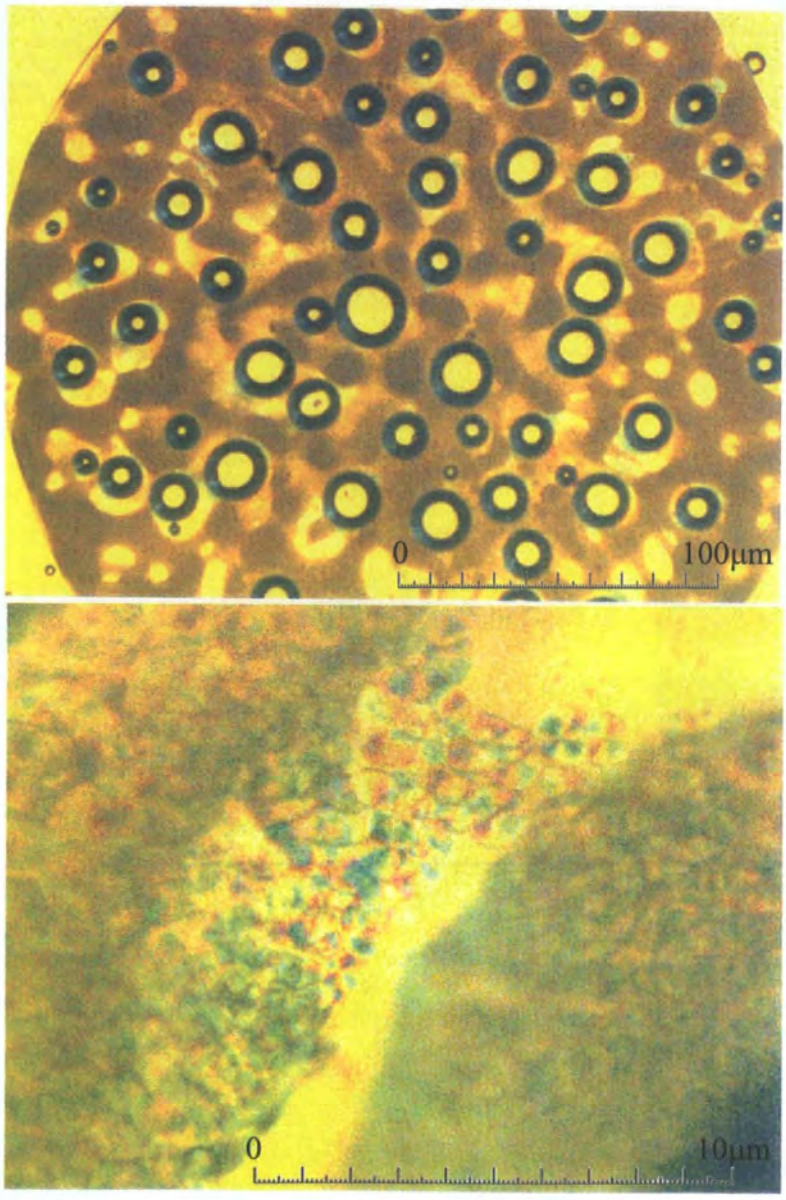

Reaction temperature 270°C
Reaction time 10 minutes

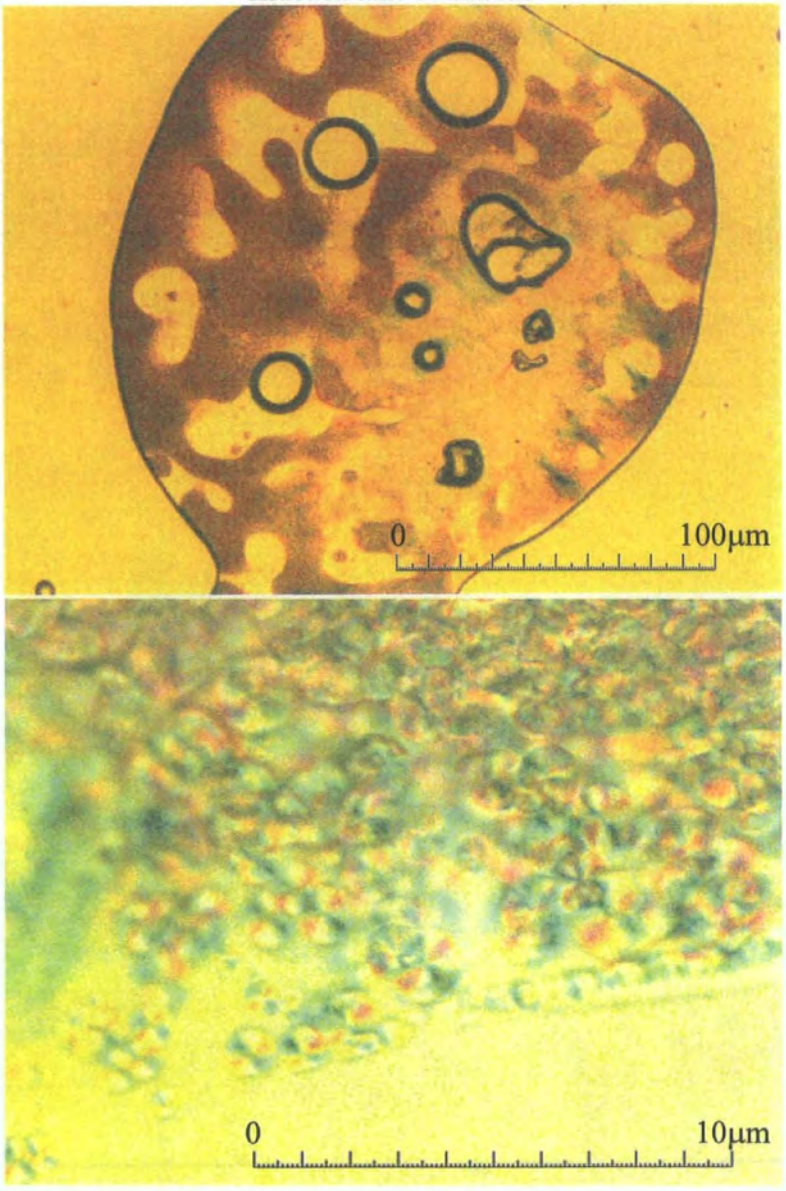

Reaction temperature 270°C
Reaction time 15 minutes

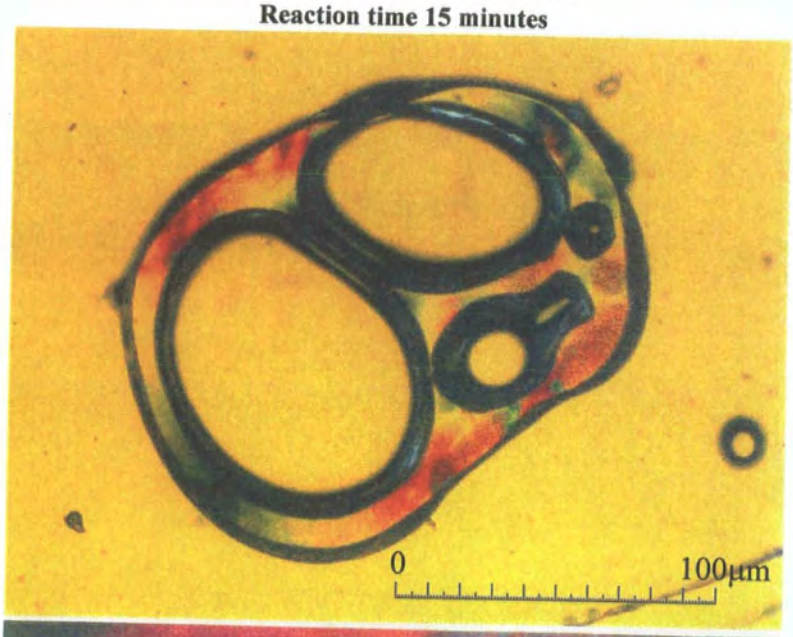

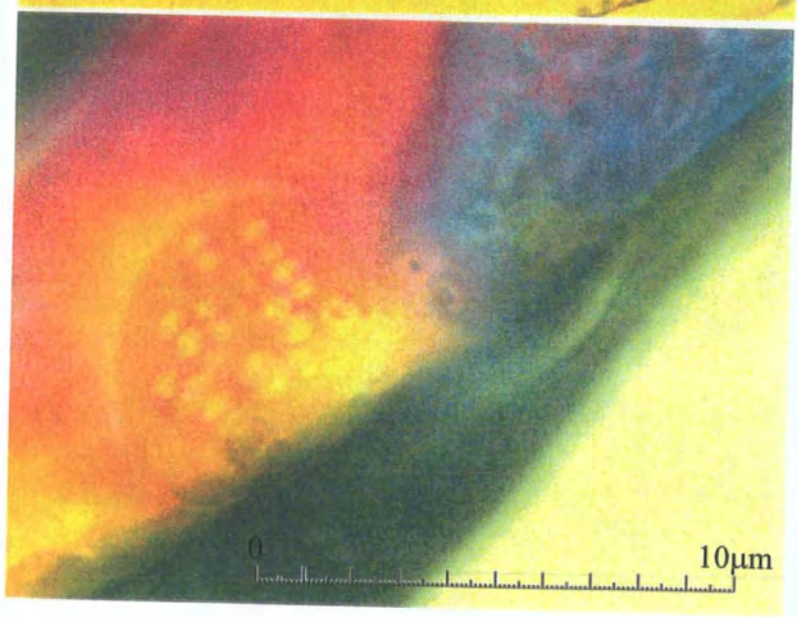

Reaction temperature 270°C
Reaction time 30 minutes

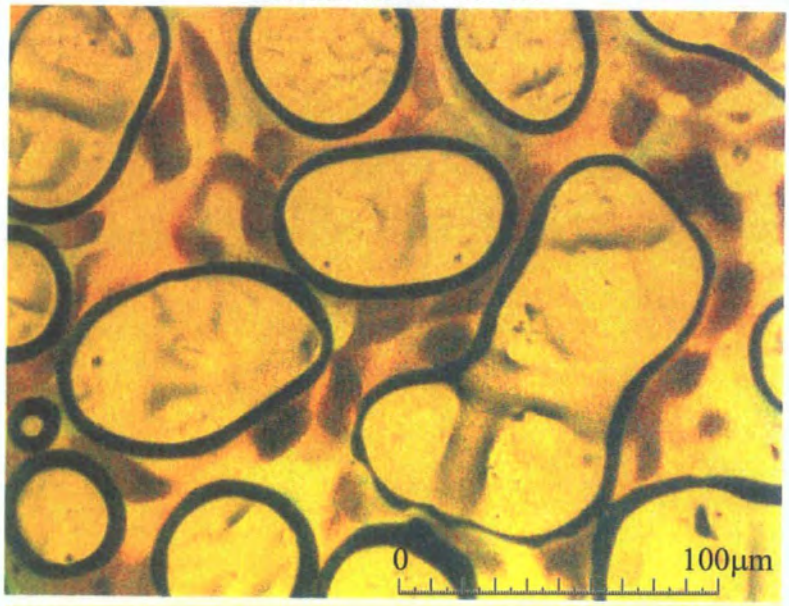

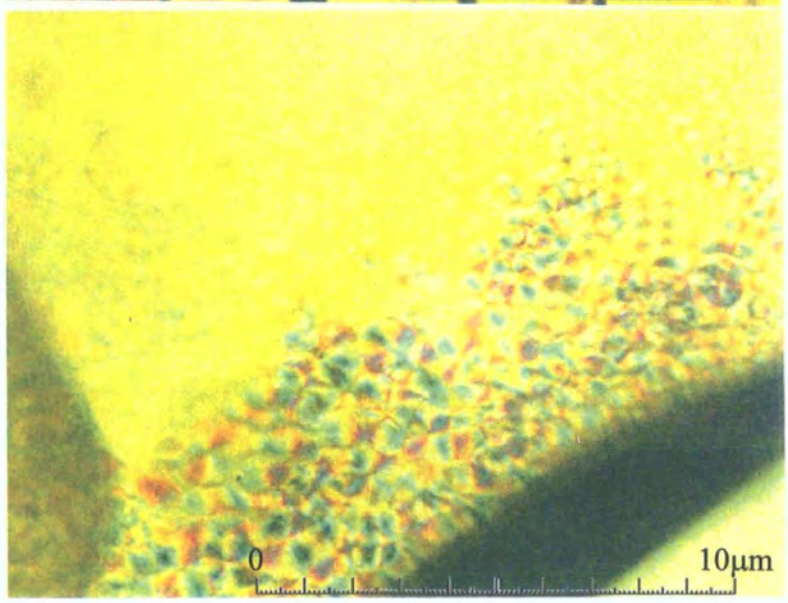

Reaction temperature 270°C
Reaction time 60 minutes

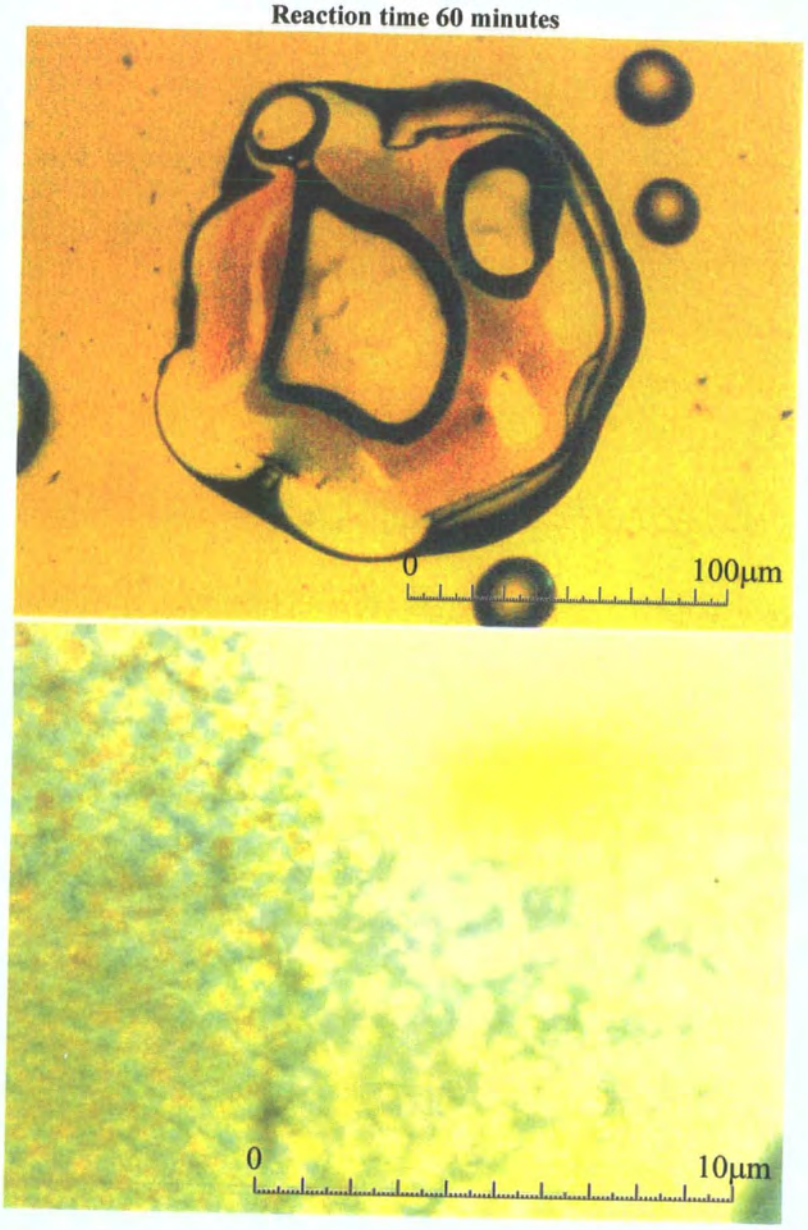

Reaction temperature 280°C
Reaction time 5 minutes

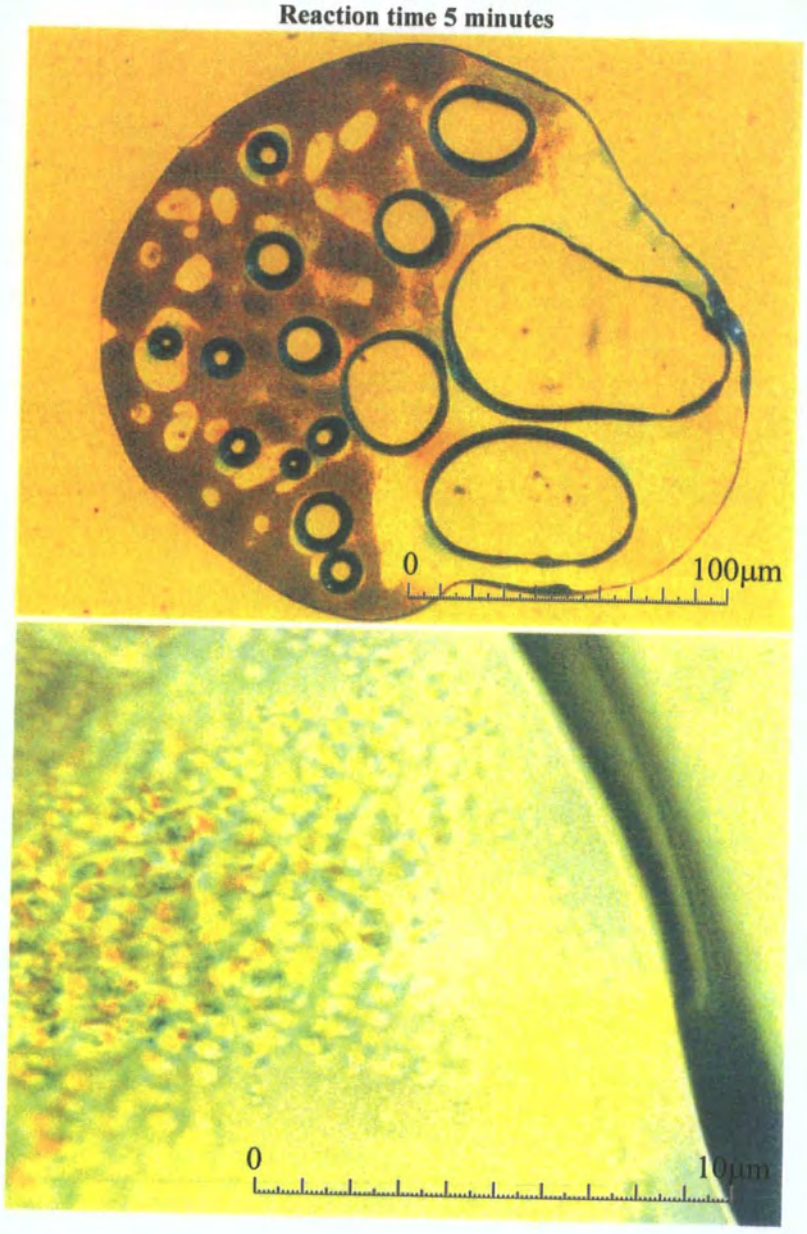

Reaction temperature 280°C
Reaction time 10 minutes

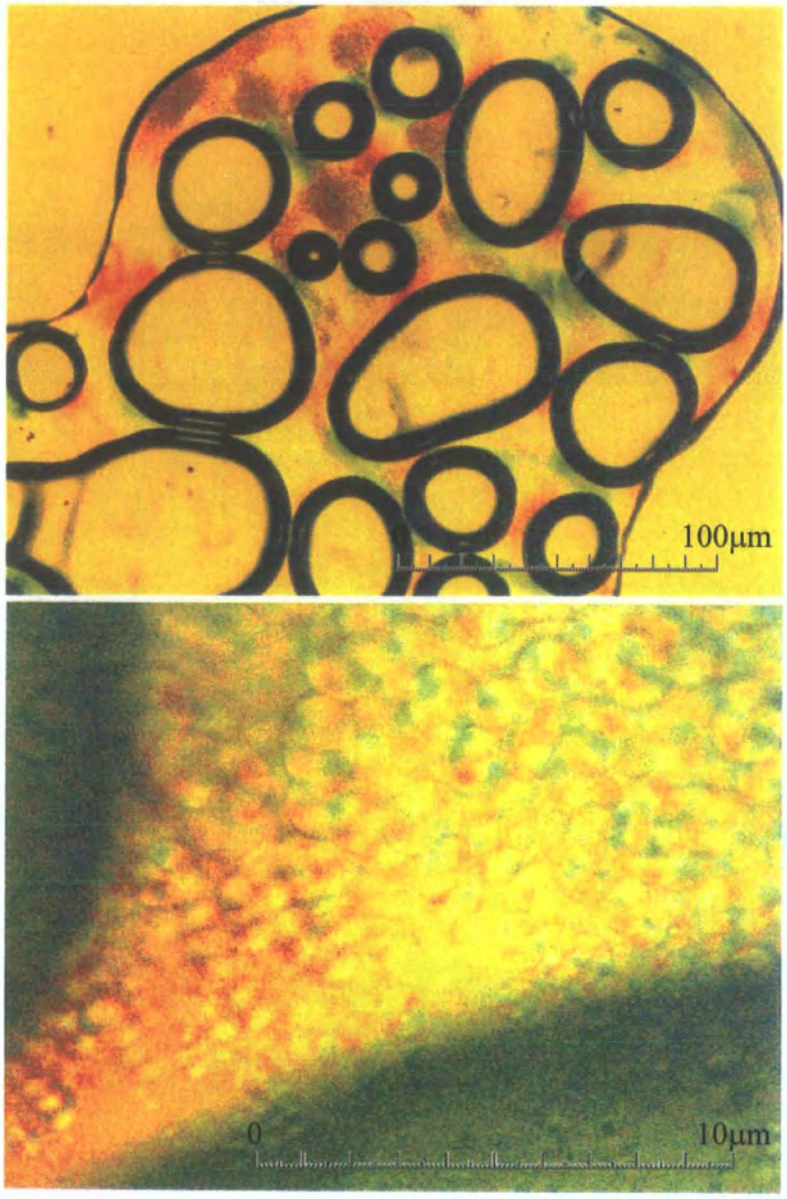

Reaction temperature 280°C
Reaction time 15 minutes

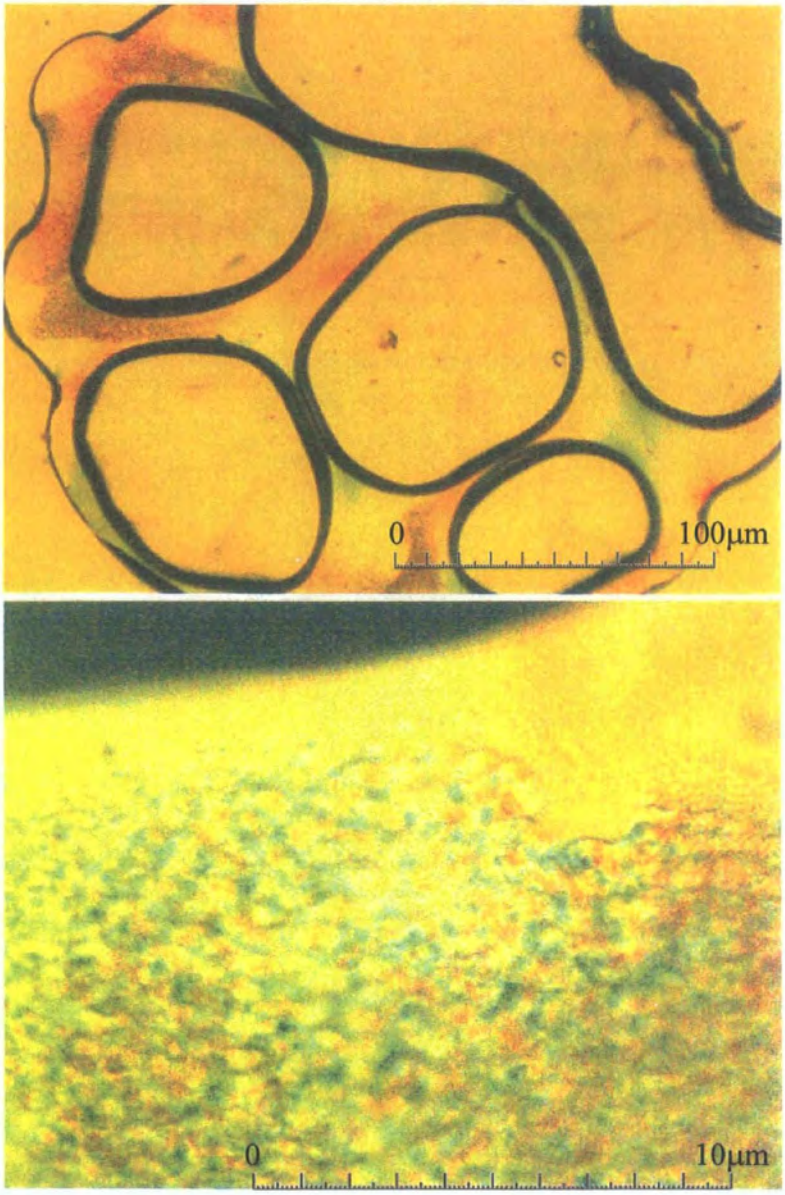

Reaction temperature 280°C
Reaction time 30 minutes

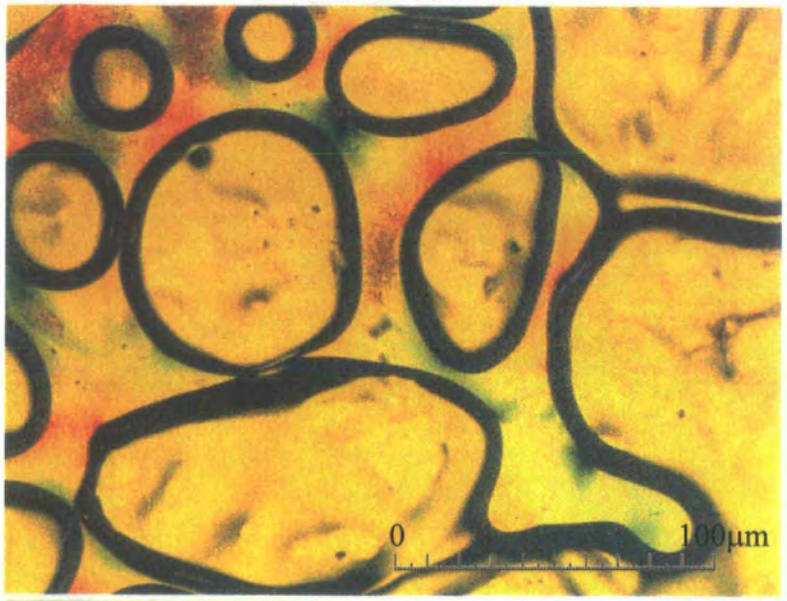

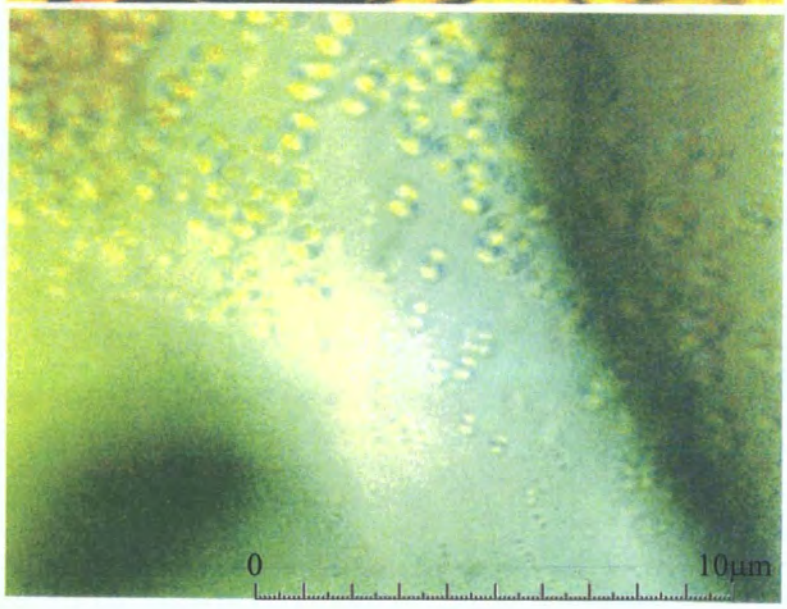

Reaction temperature 280°C
Reaction time 60 minutes

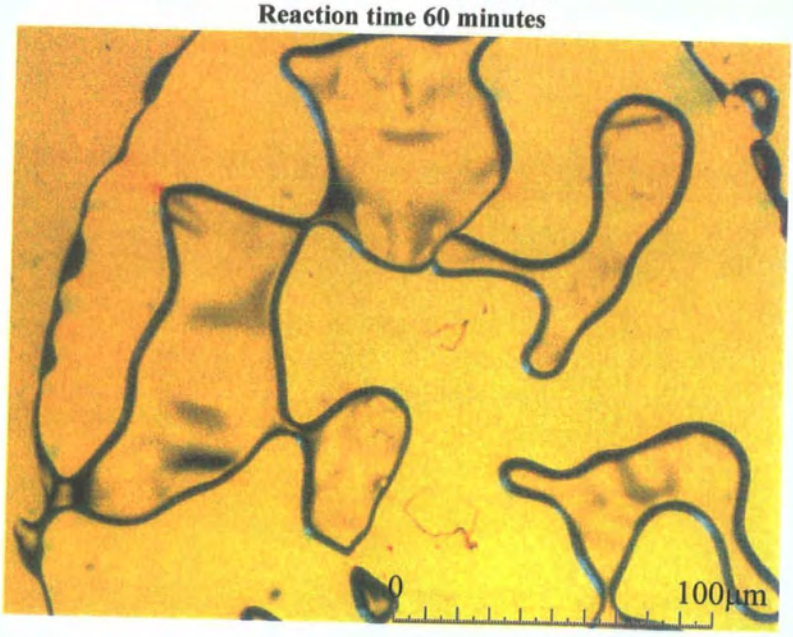

Reaction temperature 290°C
Reaction time 5 minutes

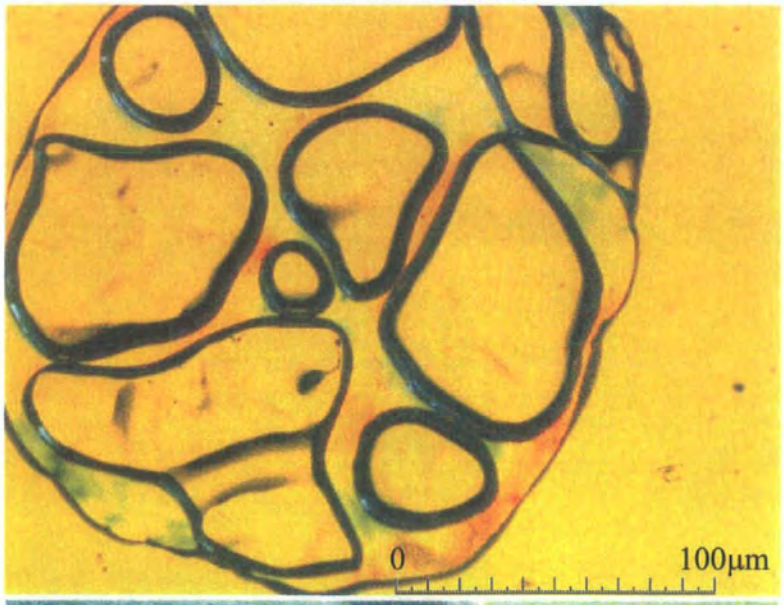

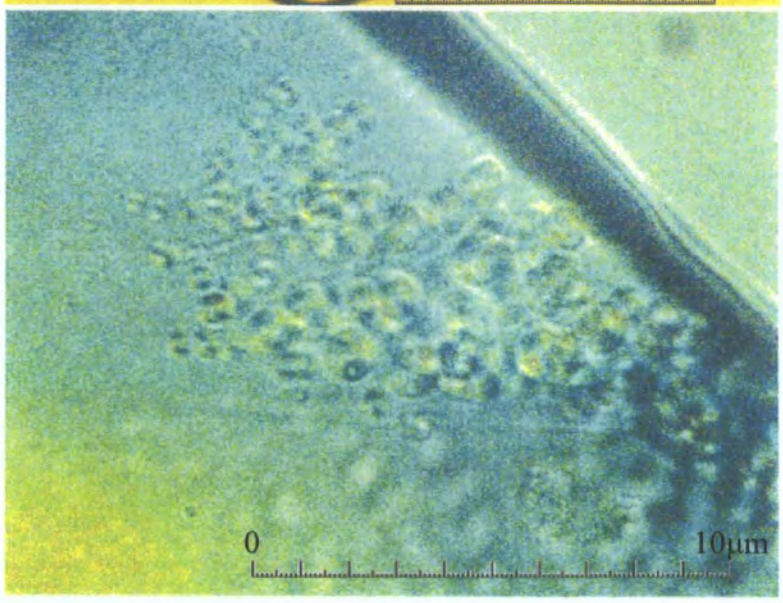

Reaction temperature 290°C
Reaction time 10 minutes

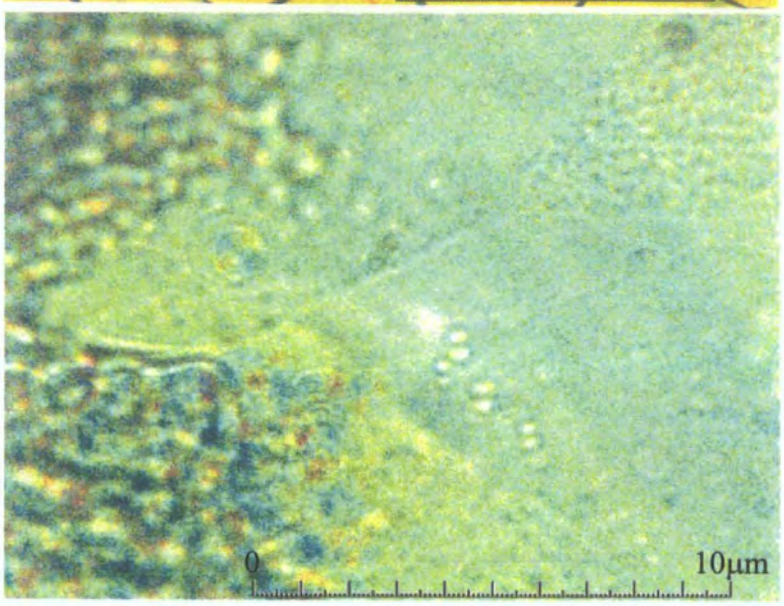

Reaction temperature 290°C
Reaction time 15 minutes

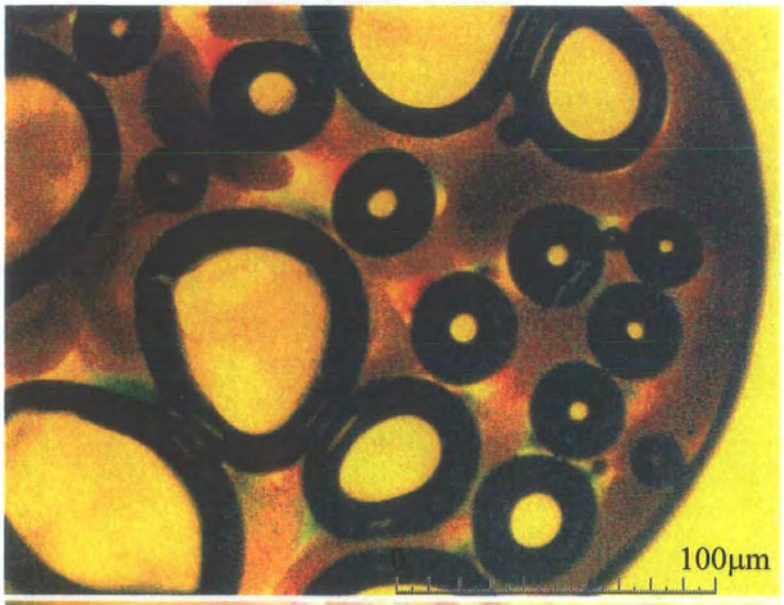

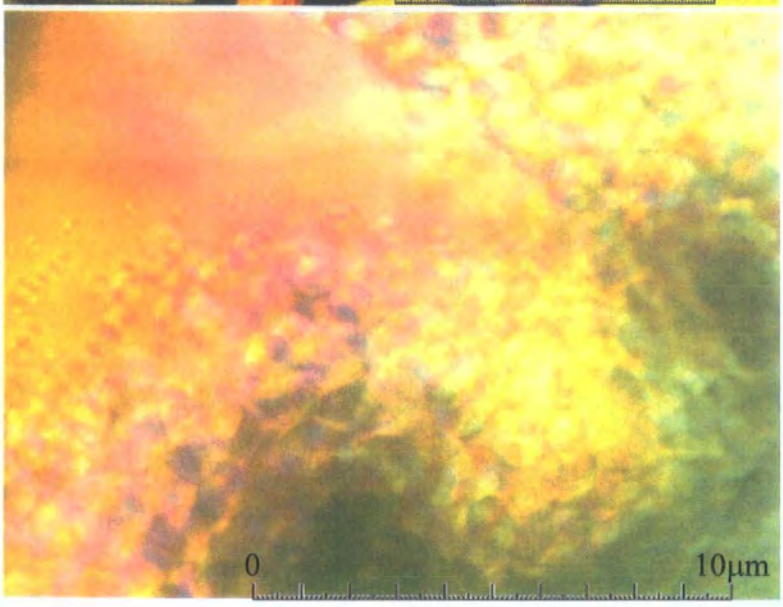

Reaction temperature 290°C
Reaction time 30 minutes

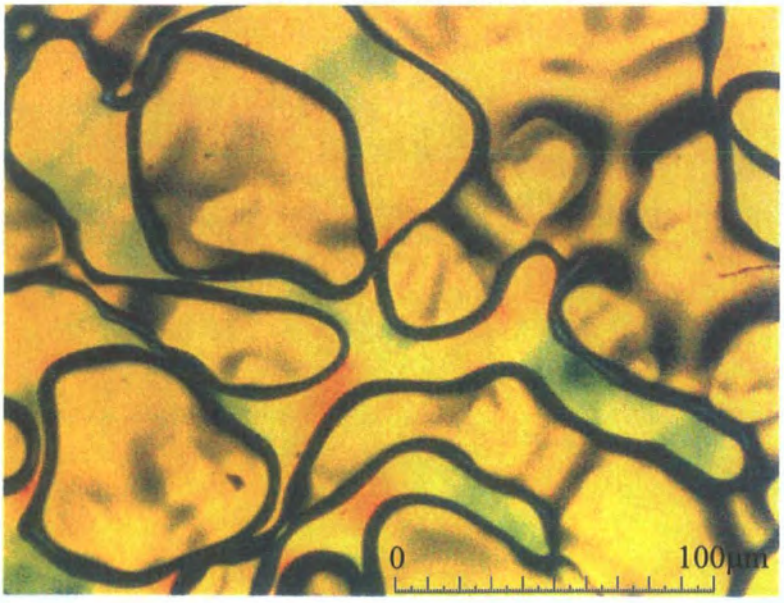

Reaction temperature 290°C
Reaction time 60 minutes

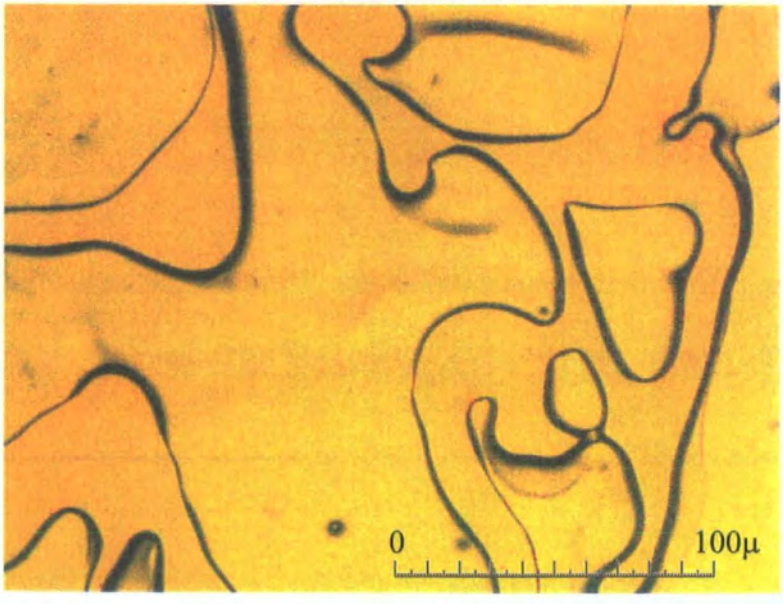

Reaction temperature 300°C
Reaction time 5 minutes

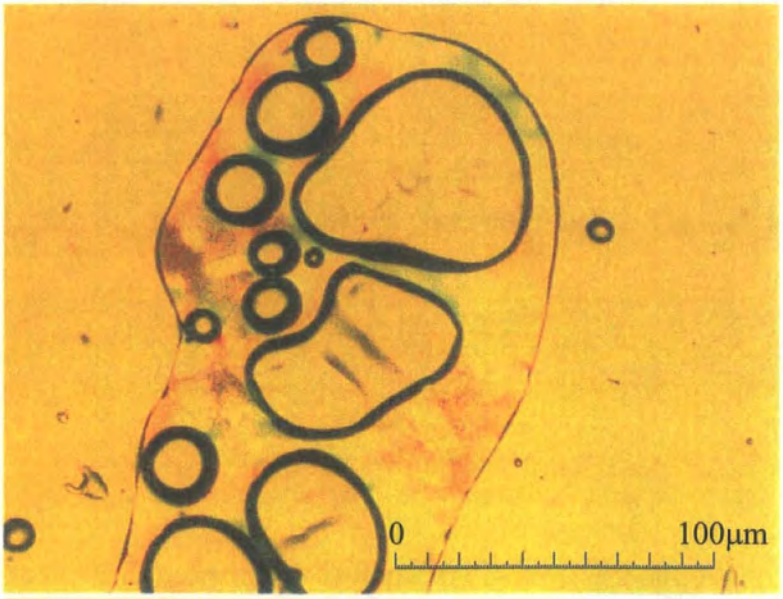

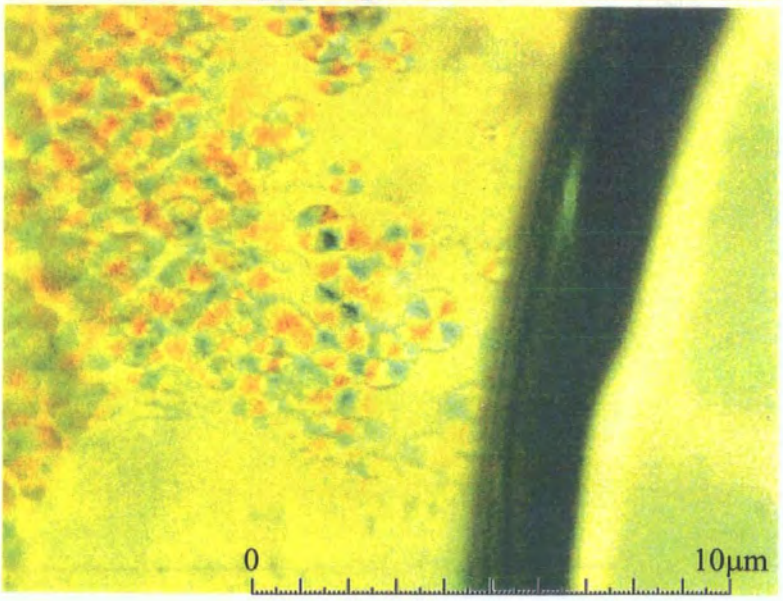

Reaction temperature 300°C
Reaction time 10 minutes

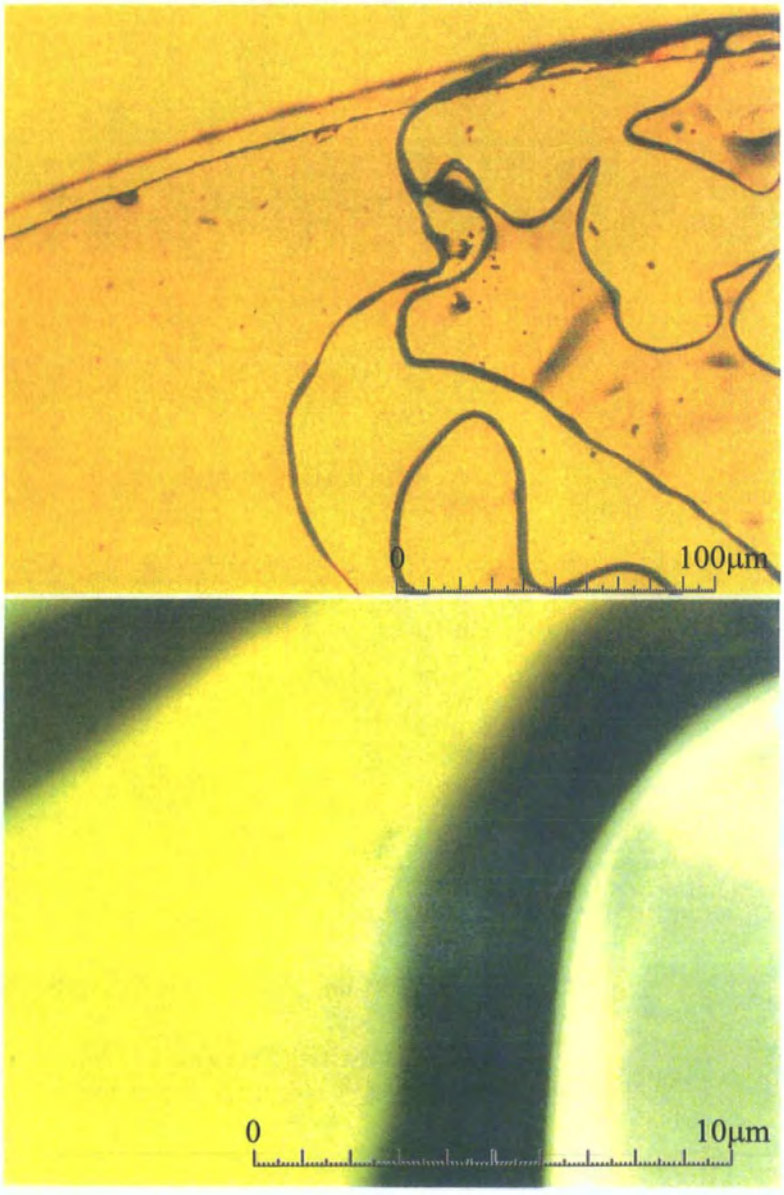

Reaction temperature 300°C
Reaction time 15 minutes

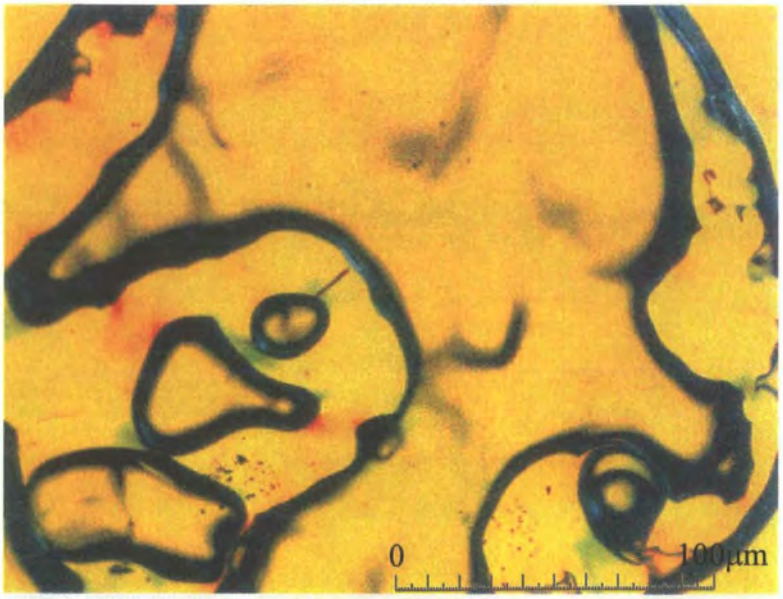

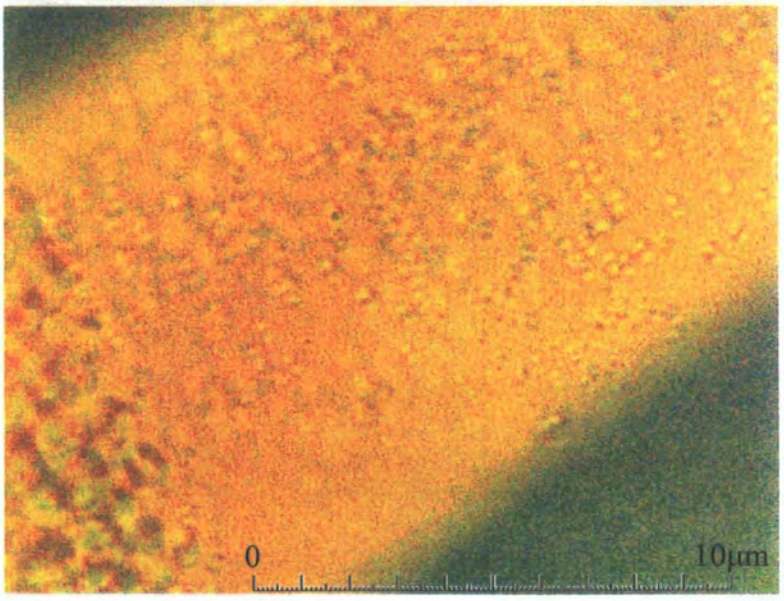

Reaction temperature 300°C
Reaction time 30 minutes

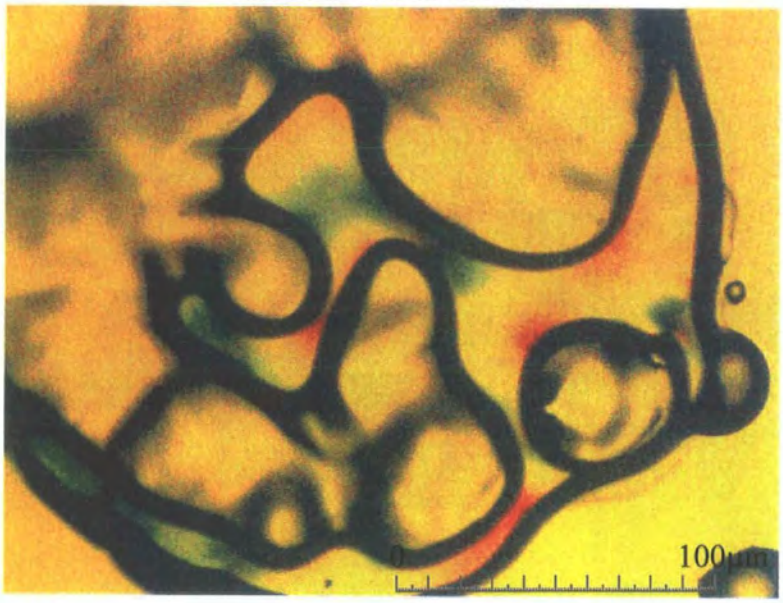

Reaction temperature 300°C
Reaction time 60 minutes